The Development of Alkali-Metal Zincate Chemistry for Application in Synthesis and Catalysis

Stephen Towie

March 2020

The Development of Alkali-Metal Zincate Chemistry for Application in Synthesis and Catalysis

Stephen Towie

A report submitted to the Department of Pure and Applied Chemistry, University of Strathclyde, Glasgow, in part fulfilment of the regulations for the degree of Master of Philosophy in Pure and Applied Chemistry.

I certify that the thesis has been written by me. Any help I have received in my research work and the preparation of the thesis itself has been acknowledged. In addition, I certify that all information sources and literature used are indicated in the thesis.

Signed: S. Towie

September 2019

Acknowledgements

I did not know what to expect when undertaking a postgraduate research position. The one thing that I do know, is that I was not expecting the impact that it had on me. I can speak the truth when I say that it has changed my life in a multitude of ways, some good, some bad. If I was told at the start of the journey that I would have been hiking hills - that felt like mountains, been learning two languages, met a significant other or even developed as much as a person as I have, I would have said that it was unbelievable. Yet, here I am, living the unbelievable.

Firstly, it is paramount to thank my two supervisors, Dr. Stuart Robertson and Prof. Robert Mulvey. Thank you for giving me the opportunity to work in your groups and for the many discussions that we had about my work. I can honestly say that I wouldn't have made it this far and be where I am in my life without your influences. My next thanks must go to the remaining academics that I have had the pleasure of working next to, these being Prof. Eva Hevia and Dr. Charlie O'Hara. If I can ever have a modicum of the knowledge that these four people have, then I will be satisfied.

The last thing I want to do, is miss someone out. So, I would like to give one big collective thank you to everyone that I have worked with. I could go through you all individually and thank you personally for everything you have done for me, but that would require a thesis on its own. I have created memories with you all that I will cherish for the rest of my life.

From all the knowledge and wisdom passed down to me by Ross and Etienne, from the duets with Scott in the lab, to the conversations with Mini in the office, from the conversations with Vicky to listening to the political banter between Richard and Callum and even the daily "Ciao" or "Buongiorno" with Pasquale. I would also like to thank the undergraduate students that I had the pleasure

to mentor. One of my most cherished memories I will take with me, is the feeling of pride that I felt when you achieved the things that you wanted. My aim was to provide you with the tools that you needed to go on and succeed in the laboratory. So, when you done this, I feel that it was moment for us both to enjoy.

I must mention Callum and Michael. There were many days that the highlight, were our conversations. Ranging from the football, to the phonology of other languages and why they have more vowels than English. My friend Bruñi, it is no word of a lie when I say that there hasn't been a person in the laboratory, whose life, you haven't touched. You have always had kind words to share with me and they have always been and will be appreciated.

In my time, I have also formed friendships with people from other countries. Lea, Kaddy, Becky and Lara. You have put up with my butchering of your languages and my incessant questions about them. I hope that you all know that I regard you as good friends of mine. No one could ever replace that gaps that remain when you left.

A special thank you is for the people that keep the lab going. They may not realise it, but without them, the lab would be in chaos. Janie-Anne, whenever something goes wrong, you are always the first person that someone will turn to. I think this speaks volumes about your abilities and how much we all depend on you. NMR Craig, your insight and knowledge of NMR is greatly appreciated, especially when you have to fix our mistakes. The trips to NMR were always great, as we knew that we would always be able to have a bit of banter with you. You would always give as good as you get. Paul and Billy, I think it tells a great deal about people when they will offer their help, so often, without ever expecting as little as a thank you. Finally, but by no means least, Alan. I can only apologise for all the frustration I may have caused you. You never let it show.

Everyone that I have thanked thus far, have all been people from my journey, within the university. However, there are a number of people from outside the university, that have had to put up with my many ups and downs. Kenny, Bob, Corey and Scott. From the many heartfelt conversations during the day, to the not so sober evenings, or even gambling our money away in the casino. You guys have always been there for me and I thank you for that. In those small temporary moments, I was building friendships to last a lifetime.

“Buongiorno Bella”. **You** are the one that breathed life into a hopeless man. It started each morning with this phrase. I cannot tell you how many times, seeing you walk into the office was the highlight of my day. Whenever anyone asks me about my time during this adventure, I will tell them about you. This is just the beginning of our journey together and I pray that it will be a journey to last a lifetime. Ti amo Ale e noi saremo insieme per sempre. Il mio cuore è tuo da questo giorno fino al mio ultimo.

None of this would have been possible without my family. They have been there at every single step of my journey. Not only this research position, but my life journey. One of the greatest things that I have taken from this, is the closer bonds to my family that I have formed. I have always drawn inspiration from my family, from a young age, my mum and dad have always pushed me to be the best I can be. They have always put me above themselves and I am eternally grateful for that. My oldest brother John has always been an inspiration to me, since I can remember. I always wanted to be as smart as you. I wanted to go to university like you did. To me, he was the smartest person I knew. Although, I think I would give him a run for his money these days. My other brother Chris, I have always regarded you as one of the people closest to my heart. You have always been there to put a smile on, not only my face, but of everyone around you. Everyone needs a release, an activity that allows them to relax. Us playing football, was mine. I will always remember and cherish our memories of playing together.

Abstract

The work reported within this thesis focuses on two main projects. With these projects involving the chemistry of the metal zinc. The first of these projects was to investigate the chemistry an unprecedented tetrazincated ferrocene complex (**4**) and the second project was to investigate the primarily interactions in the zincate [{K(HMDS)$_2$ZnBn}$_\infty$]. The first project is a continuation of a previous study that resulted in the formation of a tetrazincated ferrocene complex (**4**), with the intention of using this as an intermediate for the synthesis of tetrasubstituted ferrocenes. These functionalizations were attempted using three different electrophilic reagents, specifically I_2, D_2O and CO_2. The results from this were often confusing and inconclusive. However, when using D_2O for a quench of the tetrazincated ferrocene complex, this did in fact seem to produce the desired D_4-ferrocene product. Furthermore, the reactivity of the tetrazincated ferrocene complex towards aromatic substrates was probed to provide understanding of how this species behaves as a base.

Previous studies had shown that when pyridine is added to compound **4**, a polymeric γ-metallated pyridine species (**6**) is formed. However, this was only acquired in an isolated yield of 5%. Here, the reaction was optimized, improving the crystalline yield to 29%. This study has also revealed that this process is more complicated than originally thought, via electrophilic quenching reactions with I_2, as it seems to also metallate at the β-position of pyridine and not exclusively the γ-position as previously thought.

During the course of this project, an alternative zinc reagent to *t*Bu$_2$Zn was desired in order to avoid safety issues. A synthesis of isomeric *i*Bu$_2$Zn has been successfully developed and was found to be reproducible to a yield of 78%. This compound was then tested in a series of reactions in order to form a comparison with *t*Bu$_2$Zn and its related bimetallic ‘ate’ bases.

The second of these two projects, focuses on a recent publication by Guan *et al.* which has shown that the polymeric potassium zincate [{K(HMDS)$_2$ZnBn}$_\infty$] (**8**) can be used for the direct catalytic functionalization of the benzylic C-H bond of diarylmethanes. One of the main aims of this project was to achieve the isolation and characterisation of the proposed intermediate in the investigation performed by Guan *et al.*, which was the metallated diphenylmethyl system [{KZn(HMDS)$_2$(CHPh$_2$)}$_\infty$]. Despite there being promising signs of achieving this, due to time constraints, this ultimately was not achieved.

The second main aim of this section was to investigate how the potassium atom in [{K(HMDS)$_2$ZnBn}$_\infty$] primarily interacts with the zincate component by disrupting its polymeric nature. This was achieved through the use of the highly effective monomerizing agent Me$_6$TREN which revealed that the monomeric unit should be considered as (HMDS)$_2$ZnBnK rather than K(HMDS)$_2$ZnBn as suggested by Guan. This can be rationalized due to the π-philicity of the heavier alkali metal which preferentially coordinates to the delocalised charge within the aryl ring rather than the localised charge of the amido nitrogen centres of the HMDS ligands when the hemisolvating Me$_6$TREN ligand forces it to choose only one.

List of Common Abbreviations

AM	Alkali Metal
AMMAl	Alkali-Metal-Mediated Alumination
AMMMg	Alkali-Metal-Mediated Magnesiation
AMMZn	Alkali-Metal-Mediated Zincation
Ar	Aryl
Bn	Benzyl, CH_2Ph
*i*Bu	*iso*-butyl
*n*Bu	*n*-butyl
*n*BuLi	*n*-butyl lithium
*t*Bu	*tert*-butyl
*t*BuLi	*tert*-butyl lithium
*t*BuOK	Potassium *tert*-butoxide
*t*BuONa	Sodium *tert*-butoxide
CCDB	Cambridge Crystallographic Database
C_6D_6	Deuterated benzene
$CDCl_3$	Deuterated chloroform
C_6D_{12}	Deuterated cyclohexane
DCM	Dichloromethane
DFT	Density Functional Theory
DMG	Direct Metallating Group
Et_2O	Diethyl Ether
D*o*M	Directed *ortho*-metallation
DOSY	Diffusion Ordered Spectroscopy

Et	Ethyl
Fc	Ferrocene
g	grams
h	hours
HMDS	1,1,1,3,3,3-hexamethyldisilazide
HMDS(H)	1,1,1,3,3,3-hexamethyldisilazane
HSQC	Heteronuclear Single Quantum Correlation
LiCKOR	Alkyllithium/potassium alkoxide superbase
M	Molar
Me	Methyl
Me_6TREN	tris[2-(dimethylamino)ethyl]amine
MHz	Megahertz
ml	Millilitres
mmol	Millimoles
MW	Molecular weight
NMR	Nuclear Magnetic Resonance
	s – singlet
	d – doublet
	t – triplet
	q – quartet
	mult – multiplet
	br – broad
OMOM	Methoxymethoxy
Ph	Phenyl

PMDETA	*N*,*N*,*N'*,*N"*,*N"* –pentamethyldiethylenetriamine
ppm	parts per million
*i*Pr	*iso*-propyl
R	Generic alkyl group
RT	Room Temperature
RLi	Generic alkyl lithium reagent
RMgX	Generic Grignard reagent
THF	Tetrahydrofuran
TMEDA	*N,N,N',N'*-tetramethylethylenediamine
TMP	2,2,6,6-tetramethylpiperidide
TMP(H)	2,2,6,6-tetramethylpiperidine
TMS	Trimethylsilyl
TMT	Trans-Metal Trap
Tol	Toluene
TREN	Tris(2-aminoethyl)amine
X^-	Halide

Numbered Compounds

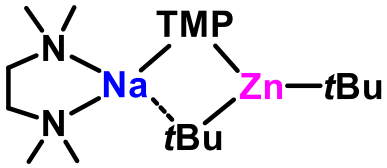

1

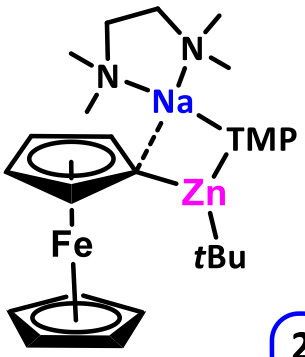

2

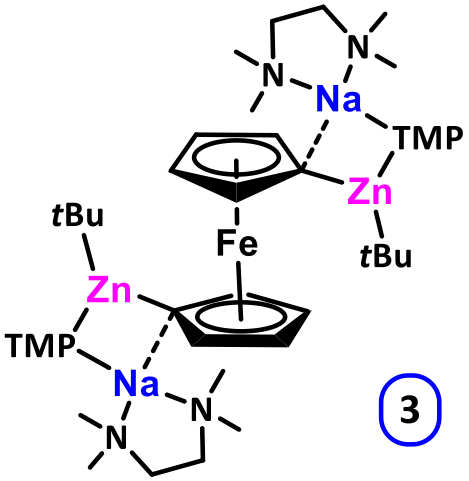

3

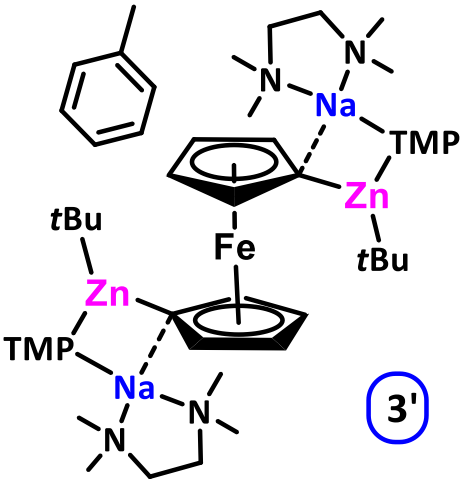

3'

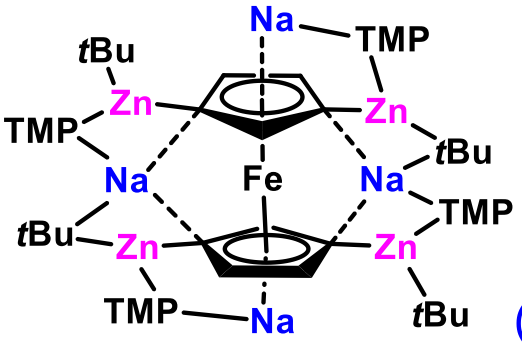

4

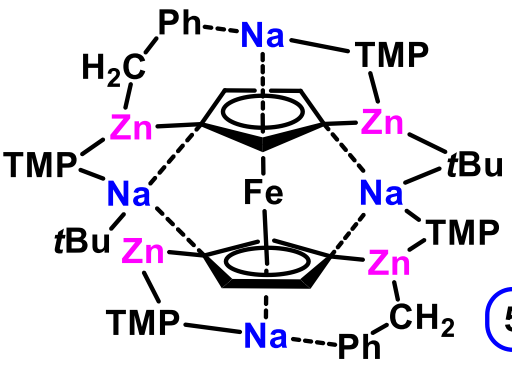

5

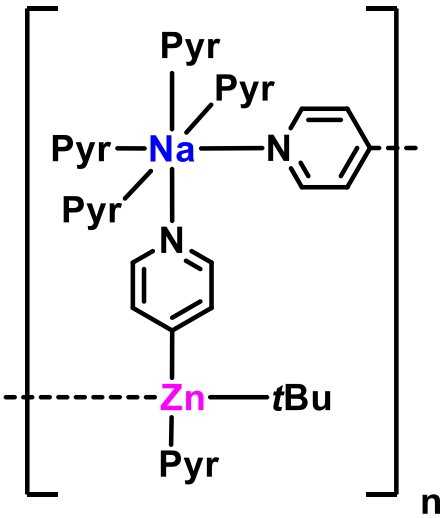

6

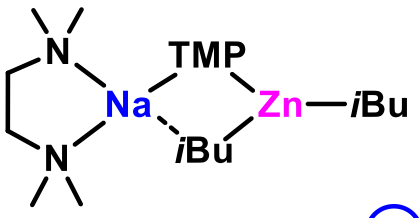

7

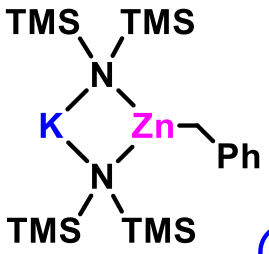

8

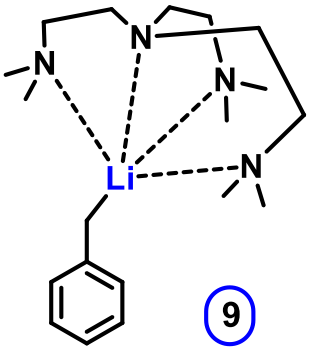

9

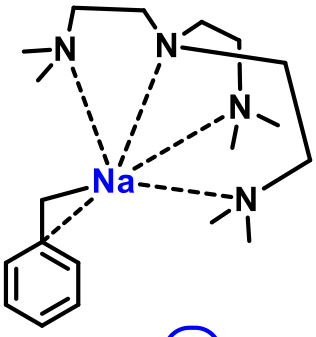

10

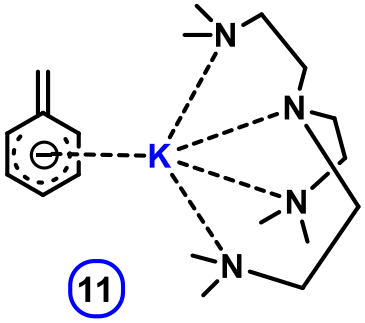

11

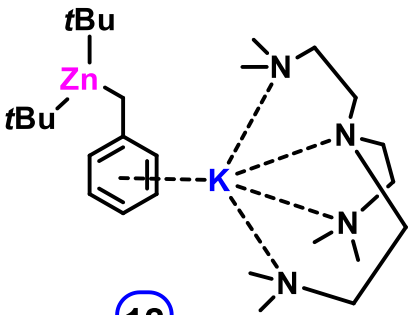

12

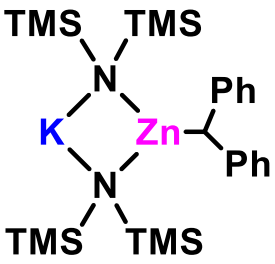

13

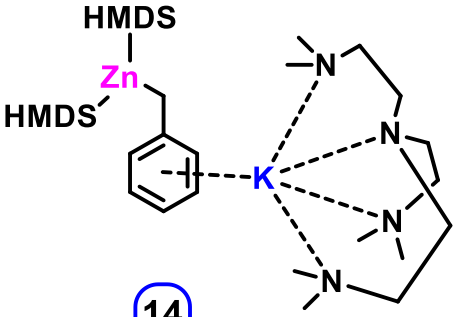

14

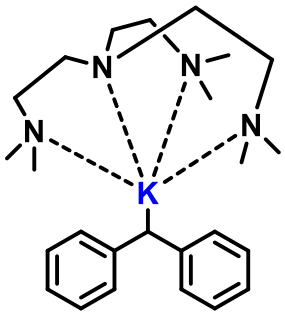

15

Table of Contents

Chapter 1: Introduction to Organometallic Chemistry

The field of organometallic chemistry has become a behemoth in chemistry, with importance in a variety of areas ranging from pharmaceuticals, agrochemical, dyes and many other research areas. Therefore, to cover the entirety of the field of organometallic chemistry would be outwith the scope of this thesis. However, some of the more major landmarks will be discussed, such as the discovery of organolithium compounds and their use in metallation.[1] The second-generation 'ate' compounds and the synergistic chemistry these provide will also be discussed as these have been prevalent in the work performed within this thesis.

1.1 Organolithium Chemistry

The year 1917 is undoubtedly an important year within the history of organometallic chemistry. This was the year that the German chemist, Wilhelm Schlenk, reported the breakthrough of the synthesis of the first organolithium compounds, specifically methyllithium, ethyllithium and phenyllithium, as well as their sodium counterparts. Schlenk himself gives an adequate description "… the numerous yellow-glowing sparks thrown out by the red flame make the burning of methyllithium a magnificent sight".[1] This breakthrough was noted within the scientific community, resulting in a nomination for the Nobel Prize for this work. However, he did not win the Nobel Prize due to the high reactivity of these compounds, since at the time, it was thought that these compounds would not have a useful place within chemistry, due to such high reactivity.[2]

However, skip ahead one hundred years and Schlenk's name is known worldwide. Today, the use of Schlenk apparatus and Schlenk techniques are commonplace within the laboratory. The use of these innovative pieces of glassware and techniques allow the chemist to overcome the reactivity of these pyrophoric compounds, allowing for them to be used in a safe manner, under an inert atmosphere. Once these reagents had been tamed and could be used safely, their true potential could be realised. They have become

indispensable for synthesis and are some of the most commonly used organometallic reagents.[3–7] This becomes even more apparent with Collum highlighting that around 95% of syntheses of natural products will utilise organolithium reagents at some stage.[8]

1.1.1 Organolithium Reagents

Throughout the years, there have been many studies performed, which have advanced the knowledge and understanding of these reagents. It is generally accepted that there is a correlation between their structure and their reactivity. Usually, it is the case that as the aggregation size decreases, the reactivity of the reagent increases.[9–11] The first of these structural studies was conducted by Dietrich *et al.*, which revealed the first characterisation of ethyllithium as a tetrameric aggregate.[12,13] Sterics of the alkyl group play a key role in aggregation state, with an increase of sterics causing a lower aggregation state. An example that displays this perfectly is butyllithium. In the solid state, *n*butyllithium is a hexamer (shown left, figure 1.1), whereas its *t*butyllithium isomer is a tetramer (shown right, figure 1.1).[14]

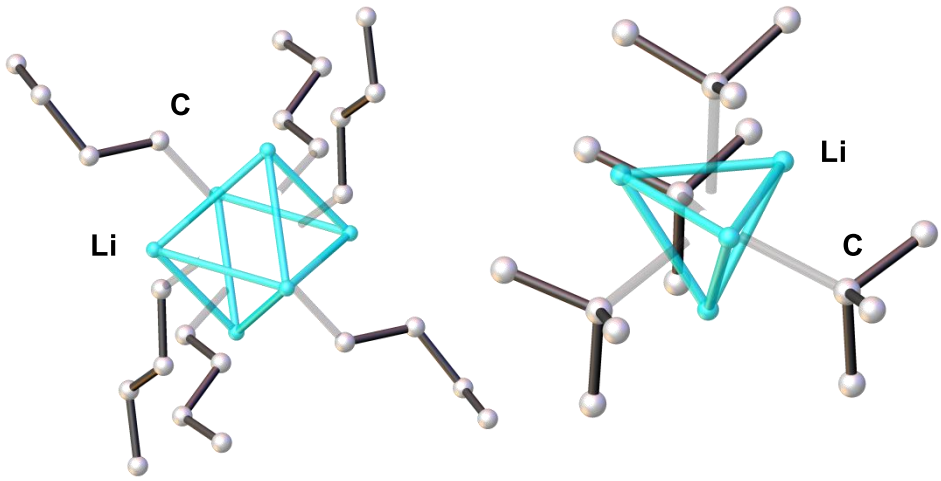

Figure 1.1 – Solid-state structures of *n*BuLi (left) and *t*BuLi (right)

The presence of these steric influences in these systems coupled with the relatively small size of the lithium cation prevents polymerization and thus

allows them to exhibit solubility in hydrocarbon solvents. This is not the case however for methyllithium or phenyllithium. A suspension is observed in non-polar solvent in these cases as a polymeric organolithium reagent forms. This is due to the smaller degree of steric hindrance in the case of methyllithium (which induces polymerization via interactions between tetrameric $[MeLi]_4$ units) and the intermolecular π-interactions present in phenyllithium (figure 1.2), which are not available to alkyllithium reagents.[15]

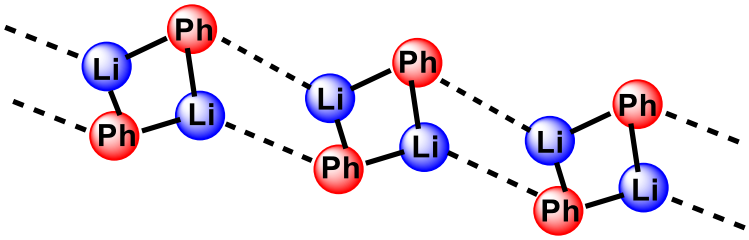

Figure 1.2 – Illustration showing the polymeric nature of phenyl lithium by the formation of intermolecular π-interactions

This leads to a need for Lewis donor molecules to be added to the mixture, in order to deaggregate the polymer (or oligomer), making it more soluble and also more reactive.[15,16] This can be seen when *n*butyllithium is in combination with bidentate *N,N,N',N'*-tetramethylethylenediamine (TMEDA). This results in the deaggregation of *n*butyllithium changing from a hexamer to a dimeric complex $(n\text{BuLi}\cdot\text{TMEDA})_2$.[17] This newly formed dimer displays an enhanced reactivity, when compared to the hexamer.[18] For example, if the reaction between *n*BuLi and benzene is considered, in the absence of any donors, *n*BuLi cannot deprotonate benzene to any significant degree. However, when *N,N,N',N'*-tetramethylethylenediamine (TMEDA) is added, *n*BuLi is capable of deprotonating benzene to a near quantitative yield (scheme 1.1).[19]

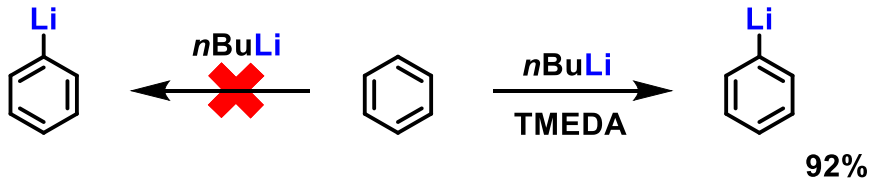

Scheme 1.1 – Scheme illustrating the importance of Lewis donors with respect to the reactivity of alkyllithium reagents

It has been shown to be possible to use Nuclear Magnetic Resonance (NMR) techniques, including Diffusion Ordered Spectroscopy (DOSY) experiments to determine the aggregation of these structures in the solution state.[20] These studies have contributed to the understanding of the reactivity and mechanisms of action of these compounds.[21,22]

The reactivity of organoalkali metal complexes arises from the polarity present within the M(δ^+)-C(δ^-) bond. This is due to the high degree of electropositivity of the alkali metal. This contribution increases as the group is descended.[23] Naturally, as the group is descended and a higher degree of polarity is present within the C-M bond, the degree of reactivity will increase. This can lead to difficulties in manipulating and storing these heavier alkali metal compounds.[17,24,25] Due to the smaller size of the central metal in organolithium complexes, they often will form smaller, discrete aggregation states as mentioned earlier and because of this, are usually more soluble than their sodium and potassium counterparts.

1.1.2 Synthesis of Organolithium Reagents

Due to how versatile and powerful these reagents are, it is no surprise that companies have decided to market them and make them commercially available. These companies include Sigma Aldrich and BOC Sciences amongst others. Perhaps, the most useful of all the organolithium reagents, is *n*BuLi. This is an incredibly powerful reagent as it has the reactivity of the M-C

bond, whilst also having the *n*butyl group which provides a middle ground between *t*butyl and *s*butyl, in terms of reactivity. The *n*butyl is not as reactive and thus, safer than the *t*butyl variant. Whereas, the *n*butyl is more reactive than the *s*butyl. This butyl group is lost as butane gas during the deprotonation reaction, preventing the possibility of the reverse reaction occurring in equilibrium. This reagent is synthesised by the reaction between the parent organohalide and lithium metal (equation 1.1).

Equation 1.1 – Simplification of *n*BuLi synthesis

This is the typical synthesis for the simpler organolithium compounds. When it comes to the synthesis of more complex compounds, it is common that *n*BuLi is employed in various reactions, such as deprotonative metallation or metal-halogen exchange.

1.1.2.1 Deprotonative Metallation

One of the most common reactions of organolithium reagents is deprotonative metallation. This is a reaction in which a R-H bond (R is typically C, N or O) is manipulated to result in the formation of a new R-Li bond, by reaction of the organic species with a simple organolithium reagent.

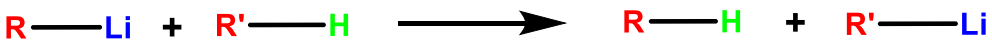

Scheme 1.2 – A general deprotonative metallation reaction

For this reaction to proceed, the hydrogen atom to be replaced must be more acidic than the conjugate acid of the organolithium reagent. The high pK_a of an alkyl lithium reagent, coupled with the volatility of the alkane generated, is what

makes simple short chain alkyl lithium reagents so effective. If the conjugate acid is not lost to the system then an equilibrium can occur in the reaction depicted in scheme 1.2, particularly if the pK_a of the two lithium containing components are similar. In reality, the pK_a of alkanes is too high for this to be an issue, even if lower volatility liquid alkanes are generated (for example hexane from hexyllithium).

1.1.2.2 Directed *ortho* Metallation

A specific subcategory of deprotonative metallation, which must be mentioned, is Directed *ortho* Metallation (D*o*M). The metal that is most commonly used in these reactions is lithium.[26,27] The major difference of this process is the presence of a functional group in the aromatic molecule to be deprotonated. The introduction of this functional group leads to an inductive acidification of the *ortho* - with respect to the directing group – protons. This is due to the electronegativity of the directing group causing a polarisation of the covalent bonds. This then leads to the β-hydrogen becoming more acidic. The directing group forms a complex with the organolithium reagent and this causes metallation to be directed towards the *ortho* position of aromatic ring systems. This process is called the complex induced proximity effect (CIPE, scheme 1.3).[28]

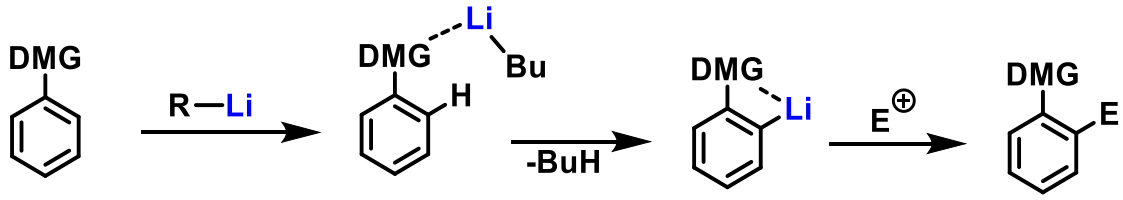

Scheme 1.3 – Simplified scheme illustrating how a donating group can influence the metallation of an aromatic ring

This process of D*o*M was recognized in the years 1939 and 1940, independently, by both Gilman and Wittig.[29,30] The more classical approach of electrophilic aromatic substitution will yield a mixture of *ortho* and *para* substitution products, whereas this D*o*M method allows for selectivity to be

obtained and yields only the *ortho* product, with respect to the directing metallating group (DMG). Figure 1.3 shows a selection of different *ortho* directing groups ordered from the weakest directors to the strongest.

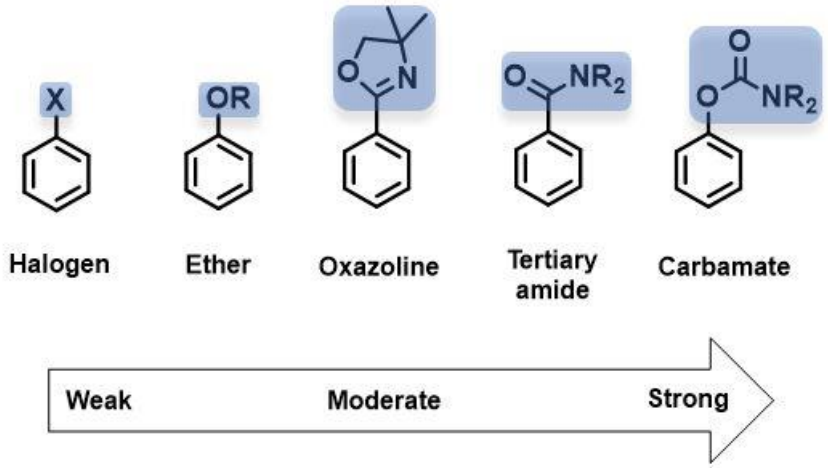

Figure 1.3 – Most common directing groups ranked by directing ability

1.1.2.3 Metal-Halogen Exchange

Another method of generating an organolithium reagent, is by means of metal-halogen exchange. Generally speaking, for this process to occur to a significant degree, the resulting carbanion should be better able to facilitate the negative charge than the starting carbanion. A general example of this process can be seen in scheme 1.4.

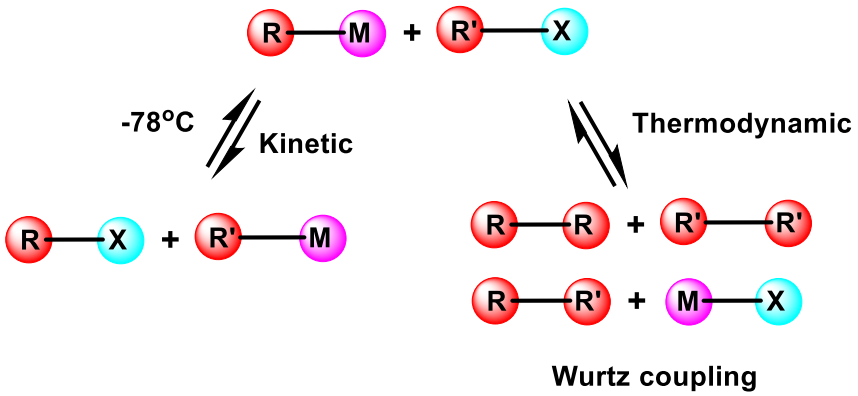

Scheme 1.4 – A simplified illustration of a typical metal-halogen exchange reaction

The major advantage to this reaction method is that regioselectivity is obtained since the metal will occupy the position previously occupied by the halogen. However, the lithium reagent can still react with the halogenated compound in competing processes, such as nucleophilic addition. If these competing side reactions can be avoided, then metal-halogen exchange can be a powerful alternative to deprotonative metallation, as the C-H bonds would be left untouched. It should also be noted that there is a competing side reaction of this process, where it is possible to obtain the kinetic products or the thermodynamic products. The thermodynamic process involves Wurtz coupling and this results in homocoupling occurring as well as the formation of R-R' alongside formation of the corresponding metal halide.[31] It is possible to circumvent the formation of these undesired thermodynamic products by controlling the temperature. If the reaction is carried out at sub-ambient temperatures, then the kinetic products are observed due to the speed of the metal-halogen exchange process. It is also easier to form the kinetic products through the careful selection of the halogen. The smaller more electronegative halogens (Cl or F) result in shorter and stronger C-X bonds. However, when larger halogens (Br or I) are used, these compounds have longer and weaker C-X bonds and thus, make it easier for the kinetic products to be obtained. Alternatively, a second equivalent of the R-M reagent can help the prevent Wurtz coupling from occurring.

1.1.3 The Lithium Amides

Lithium amides are a class of compounds which are formed as derivatives of secondary amines. These reagents have proven to be useful for important organic reactions, including deprotonations, generating enolates and condensation reactions.[32] These alkali metal amides have proven to be extremely useful due to two factors, sterics and electronics. These compounds display a strong basicity, due to the presence of the nitrogen-alkali metal bond, whilst maintaining a low degree of nucleophilicity due to the bulkiness of the typically employed compounds. A large number of these compounds have been studied. However, there are three compounds that stand above the

others, these being lithium diisopropylamide (LDA), lithium 2,2,6,6-tetramethylpiperidide (LiTMP) and lithium 1,1,1,3,3,3-hexamethyldisilazide (LiHMDS), collectively known as the “utility amides” (figure 1.4).[33]

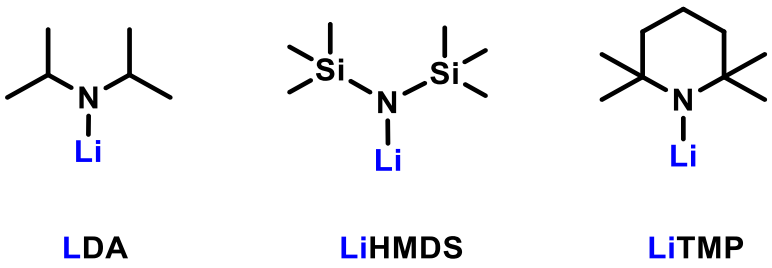

Figure 1.4 – The three empirically formulated utility amides LDA, LiHMDS and LiTMP

It is possible to commercially purchase some of the more common alkali metal amides, but for some of the more reactive or sensitive compounds, the reaction pathway follows the aforementioned deprotonative metallation reaction. Most commonly, this is achieved through deprotonation of the N-H of the parent amine by an alkylithium, such as *n*BuLi. This results in the production of the lithium amide and butane gas, which is lost to the atmosphere, providing a thermodynamic driving force for the reaction. These compounds are typically used *in-situ*, but there have been studies performed where these lithiated amides have been isolated and analysed.[33–36] These formed lithium amides can then even be used in the generation of other metal amides. For example, it is possible to utilise LiTMP in a salt metathesis reaction to yield the zinc bis(amide), $Zn(TMP)_2$, shown in scheme 1.5.[37]

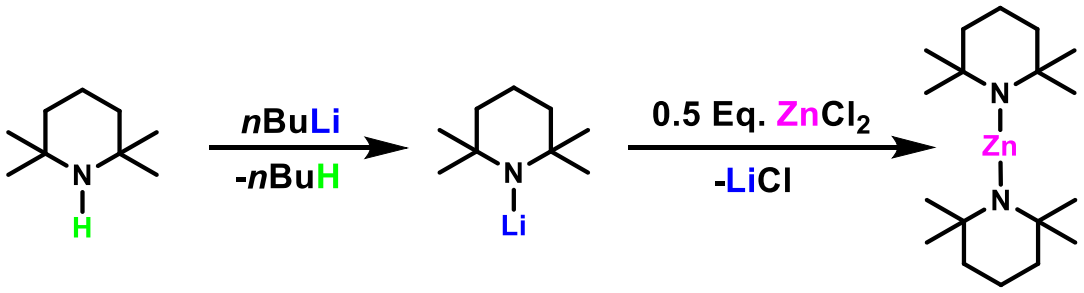

Scheme 1.5 – Preparation of $Zn(TMP)_2$ from LiTMP

The electronics of these compounds allow them to undergo similar reactions, when compared to organolithium reagents. However, the steric bulk of these compounds prevents them from displaying the same degree of reactivity as organolithium reagents. More specifically, organolithium reagents will often undergo a competing nucleophilic addition reaction. Whereas the bulkiness of the utility amides succeeds in preventing this from occurring and only allowing the desired deprotonation. This is clearly demonstrated in scheme 1.6 by the contrasting reactivity of 2-fluoropyridine with LDA[38] and *n*BuLi.[39]

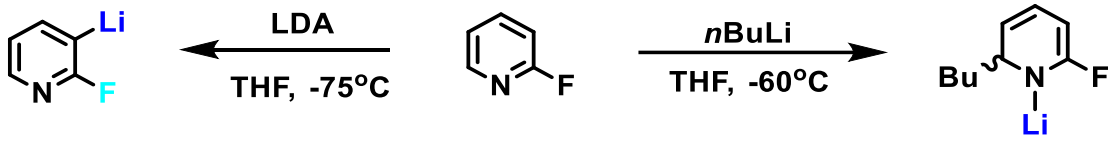

Scheme 1.6 – Reactivity of LDA versus *n*BuLi

As well as boasting a range of reactivity advantages over the more traditional alkyl reagents, such as butyl lithium reagents, these amide reagents are much safer in terms of handling. They can also help prevent issues with the use of certain solvents, which are observed with lithium reagents. For instance, alkyl lithium reagents can undergo attack of the solvent, for example when tetrahydrofuran (THF) is employed, this is illustrated below, in scheme 1.7. [40–42]

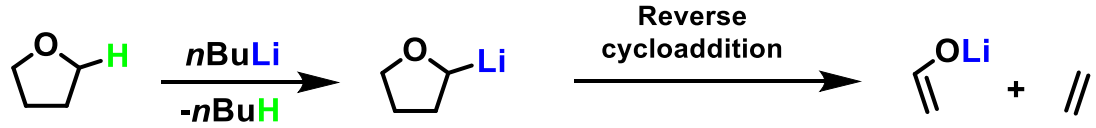

Scheme 1.7 – *n*BuLi induced ring opening of THF

Given the uniqueness of these compounds and their potential as useful reagents for a synthetic chemist, as well as their disadvantages, it is understandable that studies have been performed to determine their structures, in both solid and solution states. One such study was performed by

Mulvey and Robertson.[43] This study provides a thorough discussion about the structures of lithium, sodium and potassium amides in the solid state and in differing solvent states. For instance, it is seen that without any solvent present, LiHMDS exists as a cyclic trimer.[44] However, addition of THF results in partial deaggregation and yields a symmetrical cyclodimer, with each lithium atom being solvated by one THF molecule.[45] Finally, when the diamine TMEDA is added, this results in a mononuclear alkali-metal amide being obtained with the TMEDA being sufficient to provide enough steric protection and electronic stabilisation for the lithium atom.[46] Another example of the changing structures of metal-amides in differing environments can be observed with NaTMP. In the unsolvated state, NaTMP is seen to be a Na_3N_3 cyclotrimer species.[47] Upon the addition of THF, a deaggreation occurs to yield a cyclodimer species where each metal atom is saturated by one molecule of THF.[48] Finally, when TMEDA is added with NaTMP, the common doubly solvated cyclodimer structure in the solid state.[49] For the solution state, the lithium salts of the metal-amides are most commonly used for two reasons. Firstly, the lithium salts are generally more soluble than their heavier sodium and potassium counterparts. Secondly, lithium provides NMR active nuclei for studies. When investigating the solution state of LiHMDS in hydrocarbon solvents a dimer-tetramer equilibrium is observed. Alternatively, when in ethereal solvents, a monomer-dimer equilibrium is observed.[50]

1.2 Cooperative Mixed-Metal Chemistry

1.2.1 Superbases

The Lochmann-Schlosser superbase is more commonly written as LiCKOR because of its composition, specifically alkyllithium (LiC) and potassium alkoxide (KOR).[51–53] This class of compounds has been coined ‘superbase’ due to the enhancement of the deprotonative capabilities and the regioselectivity of the species that is formed from mixing *n*butyllithium and potassium *t*butoxide. The combination of the lithium and potassium metals in this species results in an intermediate reactivity. The reactivity of the LiCKOR

superbase can be seen to be more reactive than the alkyllithium, but less reactive than the corresponding alkylpotassium.

The enhancement of the metallating ability of the LiCKOR superbase can be demonstrated by the metallation of benzene.[54] Normally, *n*BuLi requires the presence of Lewis base donors to metallate benzene. However, when *n*BuLi is mixed with KO*t*Bu and forms the superbase species, this is able to metallate benzene even in the absence of a Lewis donor. There has been no definitive proof to determine the structure of the LiCKOR superbase. However, there have been some suggested models of potential structures.[55–57] The first substantial piece of evidence to the possible structure of the LiCKOR superbase was provided from the reaction of *n*BuLi, KO*t*Bu with an excess of benzene, in THF at -78 ^{o}C [58] This resulted in the formation, isolation and characterisation of a species that contained fragments of LiCKOR superbase and the metallated benzene in $[(PhK)_4(PhLi)(tBuOLi)(THF)_6(C_6H_6)_2]$, as shown in figure 1.5.

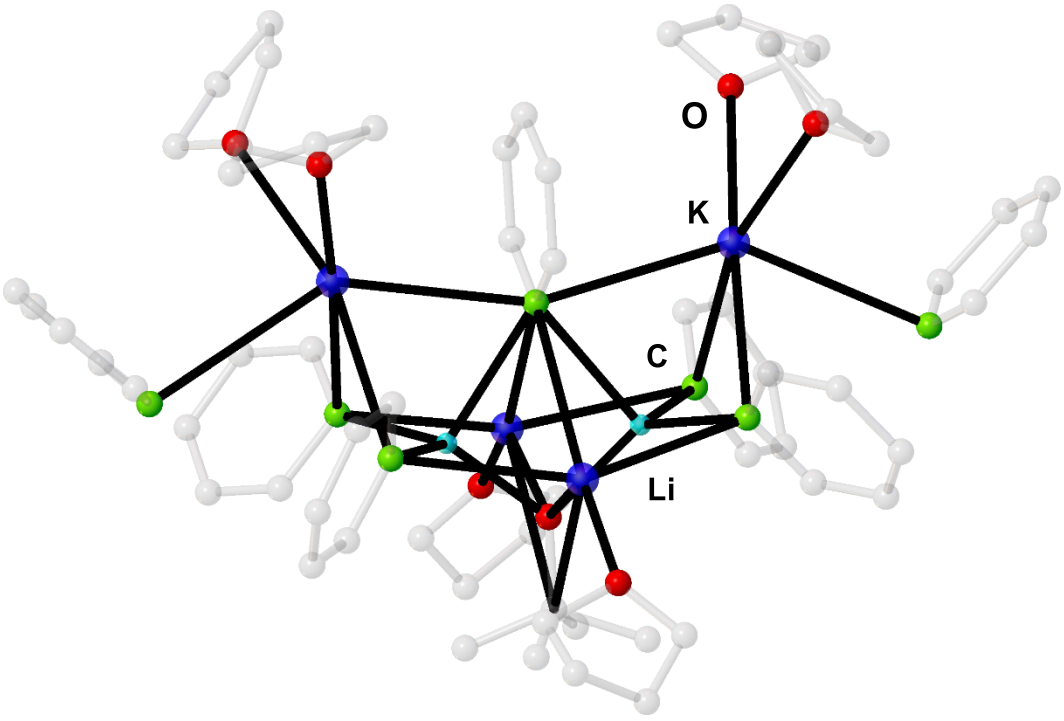

Figure 1.5 – Molecular structure of the complex $[(PhK)_4(PhLi)(tBuOLi)(THF)_6(C_6H_6)_2]$, formed by LiCKOR superbase metallation of benzene, with the core highlighted

Without the presence of the butyl anions, from the organolithium used, it cannot be said that this is the true representation of the LiCKOR superbase. However, further efforts in attempts to unlock this mystery have been made. One such investigation is that of Klett *et al*., which utilises a neopentyl variant of the LiCKOR superbase.[59] Within this study, the difficulty in isolating X-Ray quality crystals is reported and that the crystallographic data that was collected, was not of sufficient quality to allow for an in-depth analysis of the compounds. However, the data does confirm the connectivity of the atoms within the structure of the neopentyl variant, $Li_4K_3Np_3(OtBu)_4$. In this structure, the formation of a ring is observed that displays connectivity between the lithium and oxygen atoms. In the lower portion of this complex, the potassium atoms are part of a six-membered ring with two neopentyl ligands and one *tert*butoxide ligand with the remaining neo-pentyl ligand capping this ring. The structure of this is shown in figure 1.6.

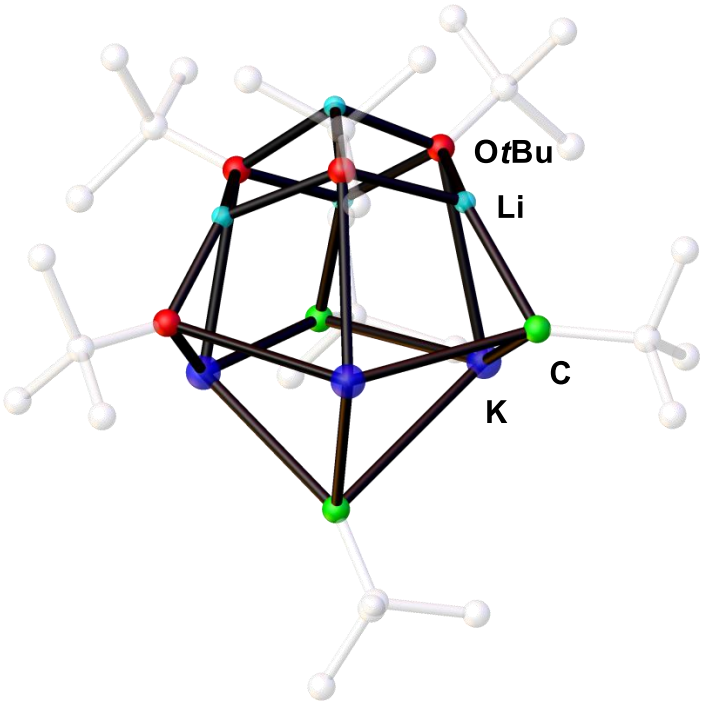

Figure 1.6 – Molecular structure of the neopentyl variant - $Li_4K_3Np_3(OtBu)_4$ - of the Lochmann-Schlosser superbase

This class of organometallic compound has been continually investigated and developed and has resulted in the generation of what can be considered a second generation of the LiCKOR superbase. A TMP(H) variant of the LiCKOR superbase has been investigated by O'Shea.[60] This second generation utilises the secondary amine TMP(H) with a mixture of *n*BuLi and KO*t*Bu and is commonly referred to in an abbreviated form of LiNK. Much like the LiCKOR superbase, the structure of this LiNK superbase is also still to be determined. This second-generation LiNK superbase shows a differing reactivity, when compared to that of the LiCKOR superbase.[61] When the reactivity of these two bases was compared when metallating methoxymethoxy (OMOM) substituted toluene compounds, it was seen that these two bases metallated the substrate in different ways. The LiCKOR superbase gave metallation *ortho* to the OMOM group, whereas when the LiNK superbase was employed, selective metallation of the benzyl species was possible, by means of a controlled anion migration, which is attributed to the presence of the TMP amide fragment. The comparison is shown in scheme 1.7.

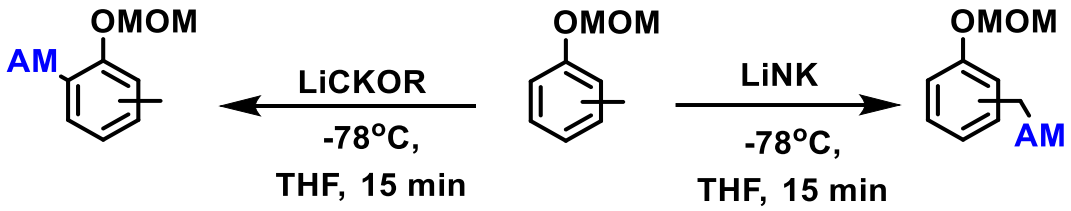

Scheme 1.7 – Comparison of the LiCKOR and LiNK metallating capabilities

In the study conducted by O'Shea *et al*. it was seen that when the LiCKOR superbase is employed in these conditions, that the strong OMOM directing groups leads to almost exclusive *o*-metallation. However, during this study it was also found that during the LiNK metallation process, initially a mixture of *o*- and benzylic metallation was observed. After a period of 60 minutes, analysis of the same mixtures then showed almost exclusive benzylic metallation. This was rationalised by means of a C_{aryl} to C_{benzyl} anion migration.

1.2.2 Ate Compounds

Although this is a field of inorganic chemistry that has only gathered much attention in recent years, the existence of ate compounds can be traced back to 1858, when the first zincate, $NaZnEt_3$, was synthesised by Wanklyn.[62] Originally, these compounds were not known as ate compounds. This term wouldn't be used for almost one hundred years, until Wittig synthesised [$LiMgPh_3$] and [$LiZnPh_3$] and he coined them "ates".[63] An ate complex is usually a bimetallic complex that contains two moieties, one of which is formally cationic and the other is anionic. They can either be contacted or non-contacted.[64] Often, these complexes consist of an organoalkali-metal fragment (such as lithium, sodium or potassium) and an organometallic fragment of a different, less polar metal (such as magnesium or zinc) as described schematically in scheme 1.8.

Scheme 1.8 – Simplistic representation of the formation of an alkali metal metallate

The unique synergistic effect that is witnessed from ate compounds arises from the cooperative effects of the two metal components. This label of ates, was made according to their arrangement. The negative charge will lie towards the softer, less electropositive metal (Zn χ - 1.6, Mg χ - 1.2 and Li χ - 1.0), yielding an anionic fragment, such as $[ZnPh_3]^-$ and an alkali metal fragment, such as Li^+.[65]

Different reactivity is evident when comparing a monometallic species with a bimetallic species. This is attributed to the presence of the secondary, less

electropositive metal, which offers its selectivity to the bimetallic species. However, the bimetallic species still retains the reactivity from the alkali metal. This is particularly evident when considering toluene as a substrate. It can be seen when using a monometallic species, that toluene will be deprotonated at the most acidic methyl site. This is as expected since the anion that is formed is stabilised by resonance with the ring system.[66–68] However, a different reactivity is observed when the bimetallic species [(TMEDA)Na(μ-Bu)(μ-TMP)Mg(TMP)] is employed.[69] This bimetallic species leads to the selective *meta* deprotonation of the toluene ring, as shown in scheme 1.9.

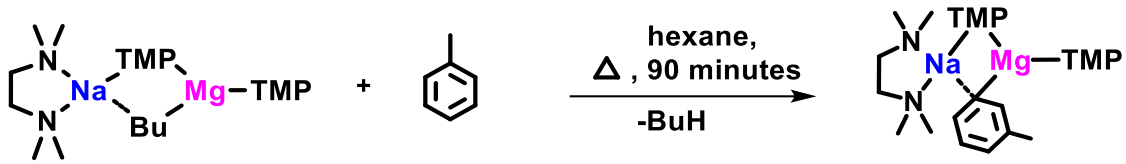

Scheme 1.9 – Selective *meta* deprotonation of toluene using a bimetallic species

Another example of a bimetallic ate base in operation is in the metallation of THF with sedation of the resulting anion. Traditional bases - such as *n*butyllithium - will deprotonate THF at the α position. This then results in a large amount of electron density adjacent to the electron rich oxygen atom, causing a rapid ring opening process to occur that results in the production of ethene and the acetaldehyde enolate (discussed in section **1.1.3)**. However, when the sodium zincate TMEDA·Na(μ-TMP)(μ-CH_2SiMe_3)Zn(CH_2SiMe_3) is utilised, this cleaves the same C−H bond - adjacent to the oxygen atom - and also captures the sensitive THF anion before it can undergo the ring opening process (scheme 1.10).[70]

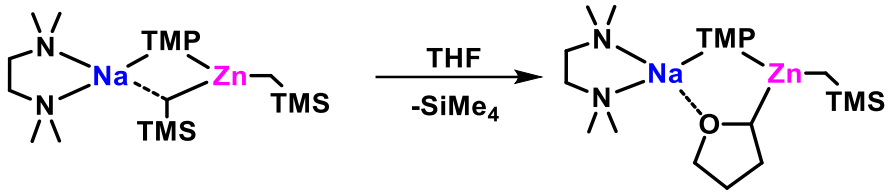

Scheme 1.10 – The deprotonation of THF by a sodium zincate species

When an equimolar mixture of *n*butylsodium, *t*Bu$_2$Zn, TMP(H), and TMEDA is utilized, a bimetallic synergistic effect is witnessed.[71] Deprotonation of the TMP(H) by the strong base *n*butylsodium was expected. This would have been followed by the co-complexation of the resulting NaTMP with *t*Bu$_2$Zn and TMEDA, to give the homoalkyl sodium zincate TMEDA·Na(*μ*-TMP)(*μ*-*t*Bu)Zn(*t*Bu), (**1**). However, it seems that an intermediate sodium zincate species TMEDA·Na(*n*Bu)(*t*Bu)Zn(*t*Bu) is formed and the deprotonation of the TMP(H) was performed by the basic *t*butyl group to give the heteroalkyl sodium zincate TMEDA·Na(*μ*-TMP)(*μ*-*n*Bu)Zn(*t*Bu) as shown in scheme 1.11, based on a two-step mechanism investigation performed by Hevia *et al.*[72]

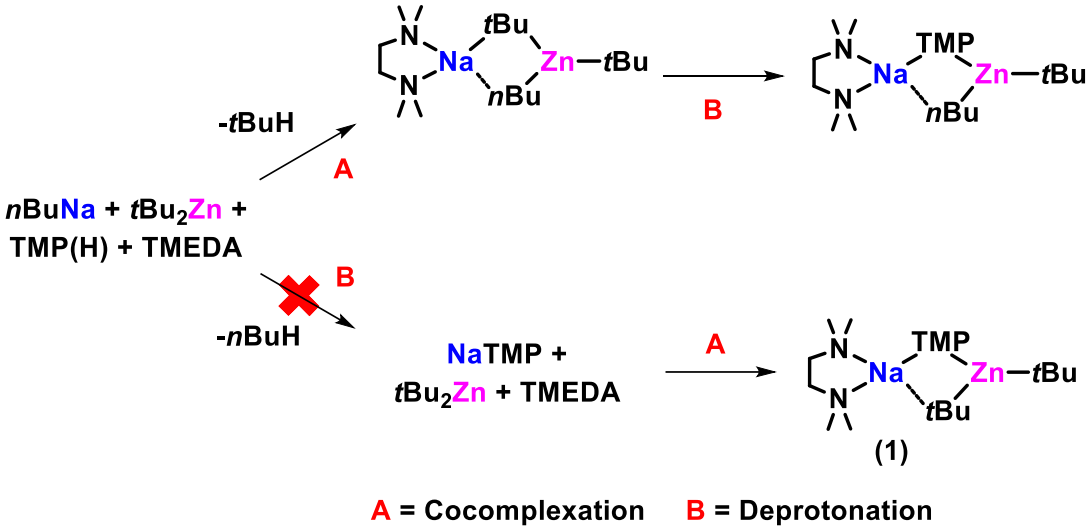

Scheme 1.11 – Formation of the intermediate zincate [(TMEDA)Na(*μ*-*n*Bu)(*μ*-*t*Bu)Zn(*t*Bu)] by co-complexation en route to the heteroalkyl complex [(TMEDA)Na(*μ*-TMP)(*μ*-*n*Bu)Zn(*t*Bu)]

It should also be noted that the co-complexation of isolated NaTMP, *t*Bu$_2$Zn and TMEDA does occur to form compound 1. (which was formed by the co-complexation of *t*Bu$_2$Zn, BuNa, TMP(H) and TMEDA), meaning that reactivity must have originated from the TMP anion. The synthesis of complex **1** is shown in scheme 1.12.

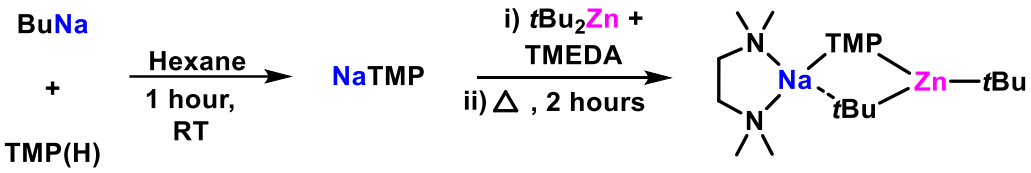

Scheme 1.12 – Synthesis of complex **1**

It is clear that both metals are required for this synergistic effect to occur. However, it is normally the formally less reactive metal that actually performs the deprotonative metallation step. It is generally seen that the individual components cannot replicate this metallation process independently. They must be partnered together for the synergistic effect to occur and metallate the substrate. This phenomenon is observed when complex **1** is considered.[73] It can be seen here that benzene cannot be metallated by the individual NaTMP or *t*Bu$_2$Zn. However, when they are joined into one species - forming TMEDA·Na(μ-TMP)(μ-*t*Bu)Zn(*t*Bu) – metallation of benzene does occur (scheme 1.13). This synergistic effect and need for the alkali metal to be present, has led to this type of process being known as an Alkali-Metal-Mediated Metallation (AMM*M*) reaction.

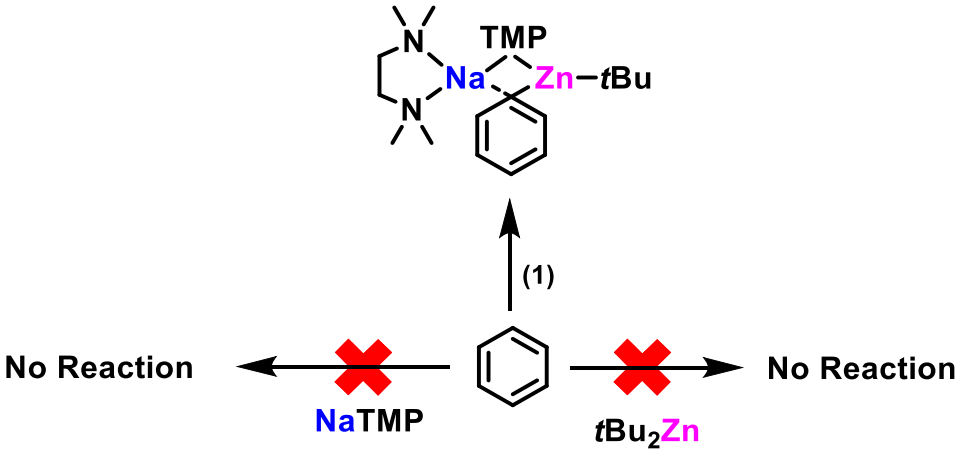

Scheme 1.13 – Reactivities of benzene with the monometallic components versus the bimetallic combination

When the sodium zincate [TMEDA·Na(*μ*-TMP)(*μ*-*n*Bu)Zn(*t*Bu)] is compared to its di-*t*butyl variant, **1**, it can be seen that it is a less powerful base. Unlike the di-*t*butyl variant, it failed to react with toluene, anisole, or *N,N*-dimethylbenzamide. However, it actually performs a double deprotonation of benzene to yield [1,4-{TMEDA·Na(*μ*-TMP)Zn(*t*Bu)}$_2$C$_6$H$_4$].[74]

Owing to the unique reactivity that they can display, these synergistic bimetallic systems have attracted widespread attention.[64,75–78] Their typical conformation corresponds to the formula [AM*M*R$_x$], where AM is an alkali metal, *M* is either a divalent or trivalent metal, R is an anionic ligand (usually alkyl or amido) and x is the number of anionic ligands that are required in order to balance the charge of the complex. Of course, as there is the possibility of having more than one type of anionic ligand, this gives rise to homoleptic and heteroleptic complexes, dependant on whether or not all the anionic ligands are the same. Also, it is possible to have a differing ratio between AM and *M*. This gives rise to ates which can be described as having a lower order, when the ratio is 1:1 or a higher order, when the ratio is 2:1 or greater. The varying structures of higher and lower order complexes can be seen in figure 1.7.

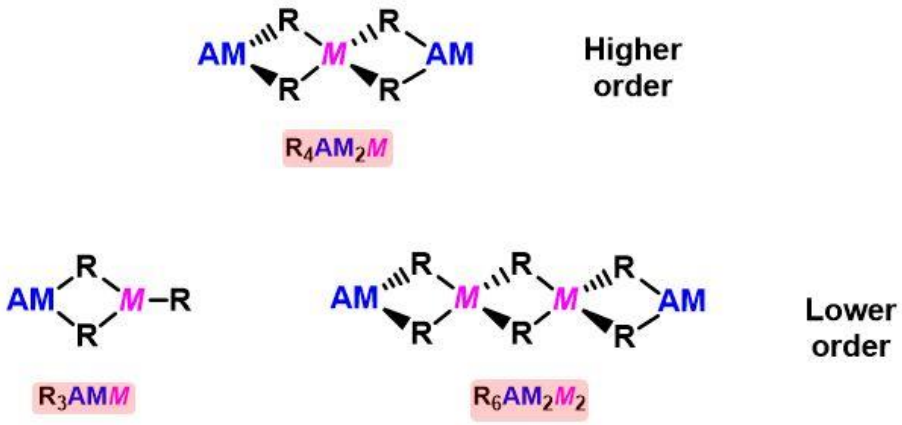

Figure 1.7 – Examples of higher and lower order complexes

The first structural characterisation of a zincate, [Li_2ZnMe_4], was published in 1968, by Weiss.[79] Weiss has performed many X-Ray crystallographic studies on various organometallic compounds.[80] Later, studies performed by Kondo and Uchiyama revealed the reactivity of the lithium zincate LiZn(TMP)(*t*Bu)$_2$.[81,82] However, the molecular structure of this complex was actually determined by Mulvey and was found to also have a molecule of THF present, solvating and capping the Li atom.[83] This study was then followed by one on the sodium derivative and led to the characterisation of complex **1**. This complex was found to be versatile in that it displays an affinity for a multitude of various reactions, summarised in scheme 1.14. This sodium zincate was found to be effective in metallation reactions (shown in scheme 1.14, highlighted as red),[84–87] nucleophilic addition (shown in scheme 1.14, highlighted as blue)[88,89] and even single electron transfer processes (shown in scheme 1.14, highlighted as green).[90]

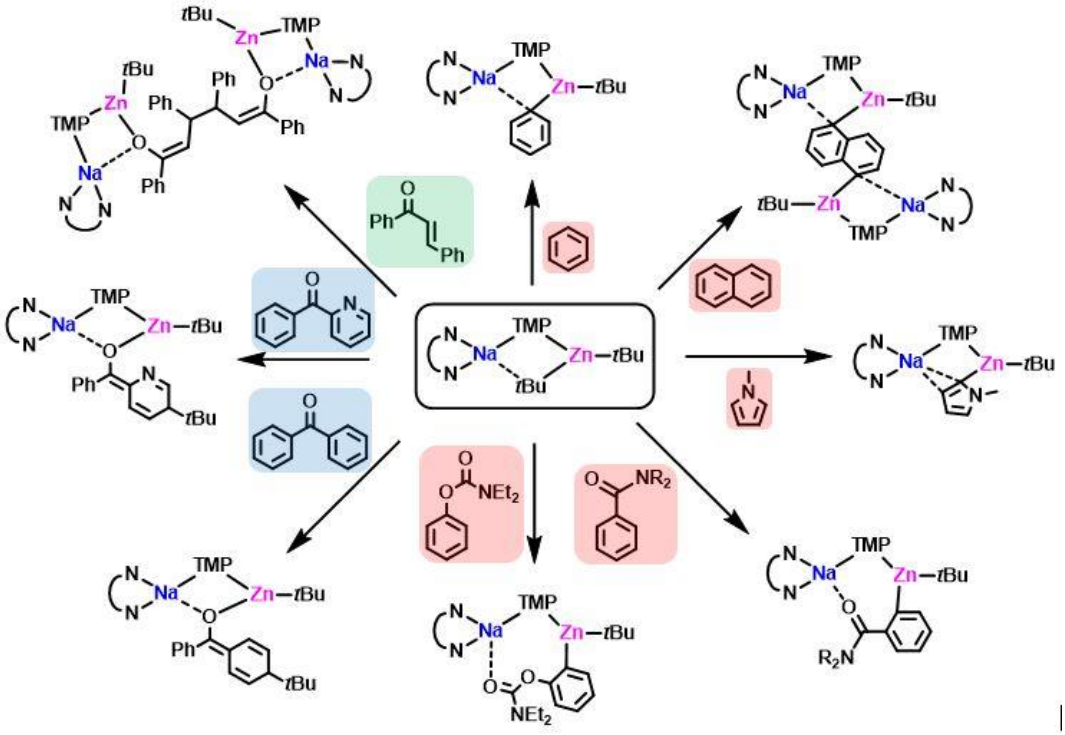

Scheme 1.14 – Simplistic representation of the various reactivity that is displayed by complex **1**

This type of metallation utilising zinc, is known as Alkali-Metal-Mediated Zincation (AMM*Zn*). Other metals have also shown that they can be utilised in these types of systems to great effect, for example, when magnesium and manganese were used in bimetallic systems with alkali metals to show the controlled fragmentation of THF.[91]

A possible mechanism for the metalation mechanism of **1** was investigated by Uchiyama and Nobuto via DFT calculations.[92] It was suggested that this metalation process actually occurs via a two-step mechanism. In the first step, **1** acts as an amide base, deprotonating the substrate, resulting in a bisalkyl intermediate and TMP(H). In the following step, the intermediate then reacts with the TMP(H) that was generated in the previous deprotonation step, yielding the final zincated substrate and also *t*Bu(H) gas, as shown in scheme 1.15.

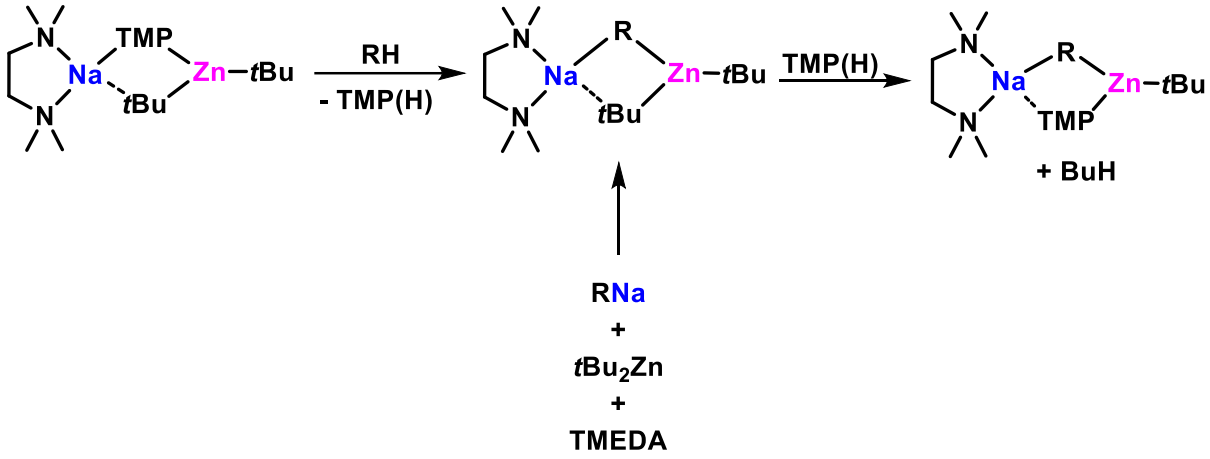

Scheme 1.15 – 2-step mechanism for deprotonation of a substrate with complex **1** showing overall alkyl basicity and protocol for proving this by directly preparing intermediate complex by co-complexation

This two-step mechanism has been investigated further by Hevia and Mulvey who provided evidence in support of this two-step process.[72,93] This study was aimed towards developing an understanding of intermediates involved in the two-step mechanism and yielded the bis(alkyl)-aryl sodium zincate, $[\{(TMEDA)_2Na\}^+\{Zn(C_6H_4\text{-}CF_3)(t\text{Bu})_2\}^-]$, from the reaction of complex **1** and trifluoromethyl benzene at 0 ^oC. This was the first example of an intermediate of an AMMZn reaction of an aromatic molecule being isolated and structurally defined. This structure contained both *t*Butyl groups from the starting material **1**. The isolation of this structure is proof that these deprotonations must proceed via a two-step mechanism.

Mixed-metal complexes have also gained prominence in what is known as template metallation. This is another example of a process which utilises a bimetallic complex to display a reactivity that cannot be replicated by its monometallic fragments. This is observed in the dimagnesiation of *N*,*N*-dimethylaniline, as demonstrated by O'Hara and Mulvey.[94] It can be seen that when the mixed-metal $Na_2Mg(TMP)_3Bu$ base is employed to metallate this substrate, unprecedented *meta-meta* metallation occurs (scheme 1.16). The

use of this complex also allows for *ortho-meta'* dimetallation of common arene substrates, such as anisole. This is in contrast to the long established *ortho*-metallation which is normally expected with heterosubstituted aromatic rings. However, it is said within this study by O'Hara and Mulvey[94] that the structure of this complex has not yet been determined; its proposed structure is based on related complexes and NMR studies that were performed in this work.

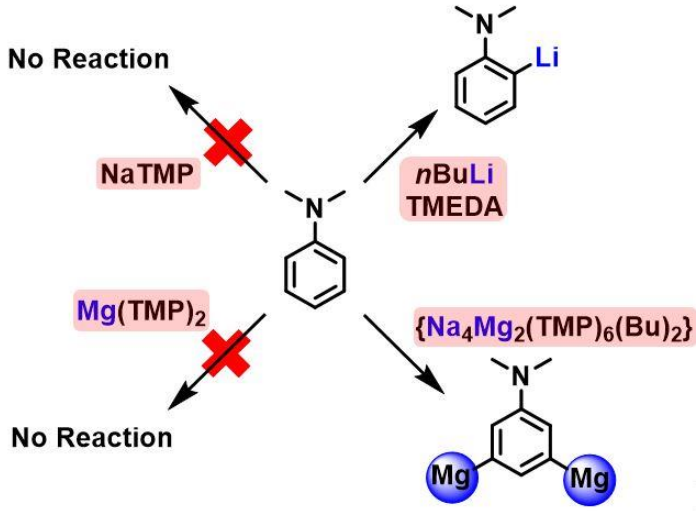

Scheme 1.16 – Dimagnesiation of *N*,*N*-dimethylaniline by $\{Na_4Mg_2(TMP)_6(Bu)_2\}$

Aluminium has been the focus of many studies relating to these mixed metal complexes. For instance, the joint work of Kondo and Uchiyama has proposed the alkali-metal mediated alumination (AMM*Al*) abilities of [THF·Li(*μ*-TMP)(*μ*-*i*Bu)Al(*i*Bu)$_2$], where it was believed to be a potent metallating reagent for aromatic substrates that bore a halogen.[95–97] Mulvey has also participated in this field of work and has introduced a dialkyl-diamido complex, putatively formulated as [LiAl(TMP)$_2$(*i*Bu)$_2$].[98] Further study into the complex reactivity involved in AMM*Al* resulted in the understanding that this metallation process does not proceed via a direct alumination reaction, proposed by Uchiyama, but instead, follows a two-step method which is labelled as *trans-metal-trapping*.[99]

1.2.3 Trans-Metal-Trapping (TMT)

The use of aluminium in metallation chemistry, was briefly touched upon in the previous section. However, this section will go into more depth and describe how a new theory was born out of this chemistry; namely, the theory of *trans-metal trapping*. The theory arose when considering the work of Uchiyama, Kondo and Wheatley, who had been performing studies on species that included the lithium aluminates [LiTMP·Al(*i*Bu)$_3$] and [LiTMP·Al(TMP)(*i*Bu)$_2$].[95–97] The reactions performed by these aluminates were carried out in the Lewis donor solvent, THF. THF is a solvent which can drastically change the aggregation state of organometallic species as discussed earlier. So, this led to the investigation of whether the THF could be changing the state of these aluminates and therefore, changing the mechanism of the metallation. It was hypothesised that instead of a one-step alumination of a C-H bond, that these reactions could be occurring via a two-step process without the two bulky parent organometallic species ever co-complexing into an ate-type complex. The first step is thus a lithiation of the substrate and this is followed by a rapid trapping of the resulting (less bulky) carbanion by the aluminium species.

There have been several investigations performed by the aforementioned authors, regarding the X-Ray crystallographic structures of various motifs containing LiTMP and Al(*i*Bu)$_3$ with differing Lewis donors solvating the lithium atom. Throughout this work, it had been thought that the active species for the alumination reactions, was the crystallographically verified [THF·Li(*μ*-TMP)(*μ*-*i*Bu)Al(*i*Bu)$_2$], grown from hexane. However, these reactions were performed by utilizing the homometallic component parts *in-situ* in THF, a Lewis donor medium. So, the aggregation state and existence of this species in solution could be influenced during the reaction.

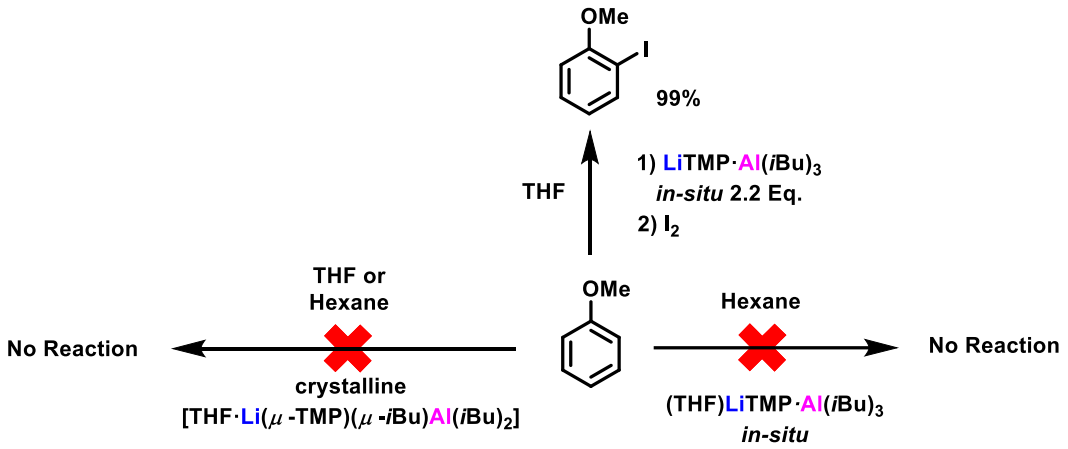

Scheme 1.17 – Reactivity of composition of LiTMP·Al(*i*Bu)$_3$ versus [THF·Li(*μ*-TMP)(*μ*-*i*Bu)Al(*i*Bu)$_2$]

This hypothesis was then tested by Mulvey, where anisole was aluminated and then subsequently quenched with iodine.[99] This was achieved by the use of an *in-situ* generated [LiTMP·Al(*i*Bu)$_3$] in bulk THF. However, it was also seen that the recrystallized "active species" that was proposed by Uchiyama, Kondo and Wheatley, [THF·Li(*μ*-TMP)(*μ*-*i*Bu)Al(*i*Bu)$_2$], displayed no reactivity under the same conditions (scheme 1.17). So, the differing species were all analysed by DOSY analysis in their solution states and it was found that when in THF solution, a total of five species were found to co-exist. So, the proposed active species [THF·Li(*μ*-TMP)(*μ*-*i*Bu)Al(*i*Bu)$_2$] was found not to exist in the solution and it was then found that the active metallating reagent was in fact homometallic LiTMP as summarized in scheme 1.18.

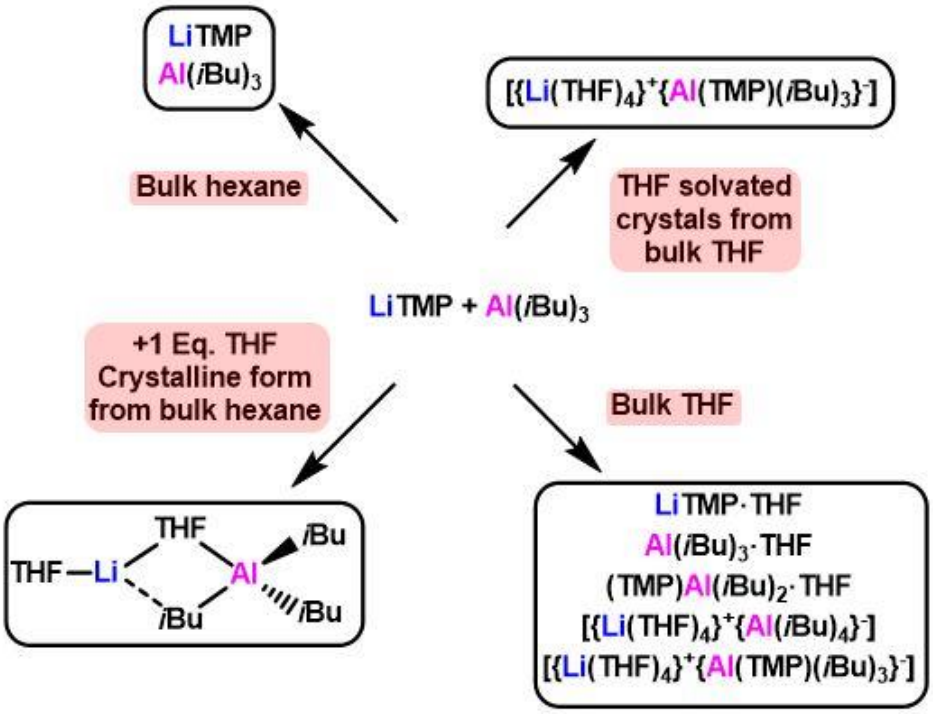

Scheme 1.18 – Summary of the composition of LiTMP and Al(*i*Bu)$_3$ in different media

This investigation was continued by Mulvey and Robertson, with the use of the LiTMP/*i*Bu$_2$Al(TMP) pairing.[99] It was seen from control reactions on anisole, that direct alumination was not possible with this combination of reagents. Instead, a lithiation reaction was occurring first by LiTMP, followed by the trapping of the resulting carbanion by the aluminium fragment (scheme 1.19). The composition of this combination in THF was also investigated and it was found to only exist as two species in solution, these being LiTMP and *i*Bu$_2$Al(TMP). It must also be noted, that the aluminium species plays a pivotal role in this, as it stabilises the carbanion, but there is also a lack of interaction between the aluminium fragment and the LiTMP, due to the increased sterics of both when compared with the alkyl rich example studied by Uchiyama *et al*. The fact that there is no interaction is crucial, as this then prevents the co-complexation of the two monometallic species into a bimetallic species which possesses no metallating power. Furthermore, the trapping step removes

lithiated anisole from the equilibrium meaning that even though it is not a high yielding lithiation it continues to produce lithiated (and ultimately aluminated) product.

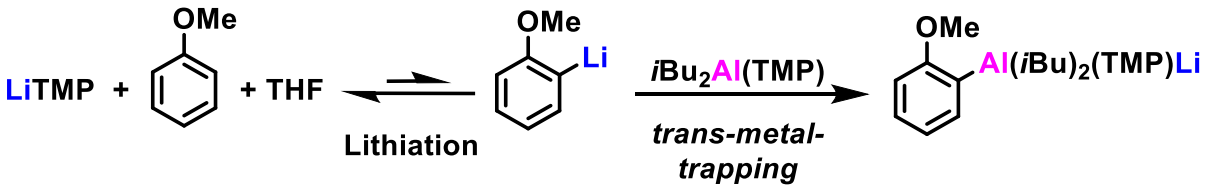

Scheme 1.19 – Proposed *trans-metal trapping* pathway of LiTMP*i*Bu$_2$Al(TMP) using anisole as a test substrate

The impact of the theory of TMT has already been seen; in that it is already starting to influence new approaches to metallation chemistry.[100] Even though this type of chemistry was introduced in aluminium chemistry, it can be applied to other metals, such as gallium, with the use of LiTMP and trialkylgallium species, resulting in the gallation of sensitive substrates.[101] The usefulness and versatility of mixed-metal reagents have long been established. The work performed within this thesis aims to contribute to this field of chemistry and lead to a greater understanding.

Chapter 2: An Investigation into the Reactivity of a Tetrazincated Ferrocene Compound

2.1 Introduction

Monolithioferrocene $(C_5H_5)Fe(C_5H_4Li)$[102] is accessible in high yield by reacting *tert*butyllithium with ferrocene in THF solution.[103] Dilithiation of ferrocene (with a single lithiation occurring on each ring) can be accomplished by increasing the stoichiometry of the alkyllithium base in the presence of a chelating tertiary amine (TMEDA[104] or PMDETA[105]). Several strong metalating agents (a stoichiometric excess of *n*BuLi,[106] or up to 20 equivalents of *n*BuK[107]) will cause the polydeprotonation of ferrocene. However, these methods lead to complex mixtures of little practical use. However, a controlled and efficient method of polydeprotonation of ferrocene had remained elusive. That was until the deprotometallation ability of 'ate' complexes was used in the form of inverse crown bases to achieve tetramagnesiation of ferrocene (scheme 2.1) [108] After successfully tetrametallating ferrocene, this was followed up with an attempt to complete the homologous group 8 series by tetrametallating ruthenocene and osmocene, which proved successful.[109]

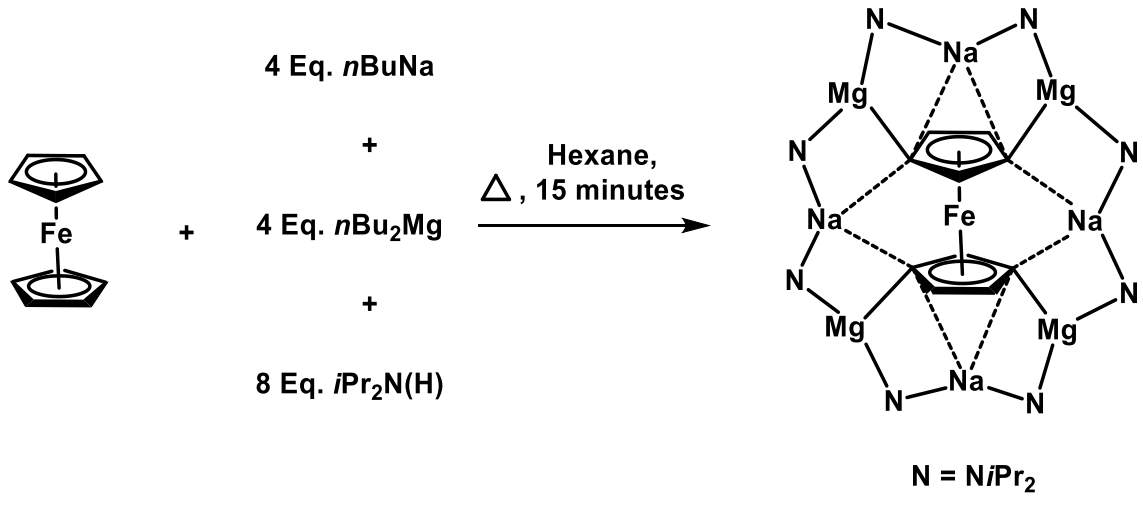

Scheme 2.1 – Simplification of tetrametallation of ferrocene utilising sodium magnesiate chemistry

However, alkali-metal mediated alumination of ferrocene has so far been limited to dimetallation.[110] This was attempted from a synergistic lithium/aluminium mixture generated from LiTMP, *i*Bu_2Al(TMP) and TMEDA. This was initially attempted in a 1:1 ratio of the base mixture to ferrocene and resulted in the expected monoalumination of ferrocene. It was also seen that dialumination of ferrocene could be achieved using a 2:1 ratio of base to ferrocene. These results (mono- and dimetallation) could also be replicated using the sodium zincate base TMEDA·Na(*μ*-TMP)(*μ*-*t*Bu)Zn(*t*Bu) (**1**, scheme 2.2) yielding the complexes **2** and **3** respectively. When trying to replicate the sodium/magnesium pairing to give tetraalumination/tetrazincation of ferrocene, it was seen that this could not be achieved by these reagents and that the dialuminated/dizincated complex was observed (scheme 2.2). In an attempt to circumvent this, the neutral Lewis donor TMEDA was omitted (as no Lewis donor was added in the tetramagnesiation reaction) to allow the inverse crown ring to form around the tetrametallated metallocene guest molecule. For the Li(TMP)/*i*Bu_2Al(TMP) pairing this was unsuccessful as the TMP(H) generated from the deprotonation reaction replaced the TMEDA as a neutral Lewis donor, giving the analogous TMP(H) solvated dealuminated complex. However, the Na(TMP)/*t*Bu_2Zn combination appeared to be successful, with the resulting red powder giving a ^{1}H NMR spectrum whose ferrocenyl region (3.5 – 5.0 ppm) was similar to that of the tetramagnesiated complex.

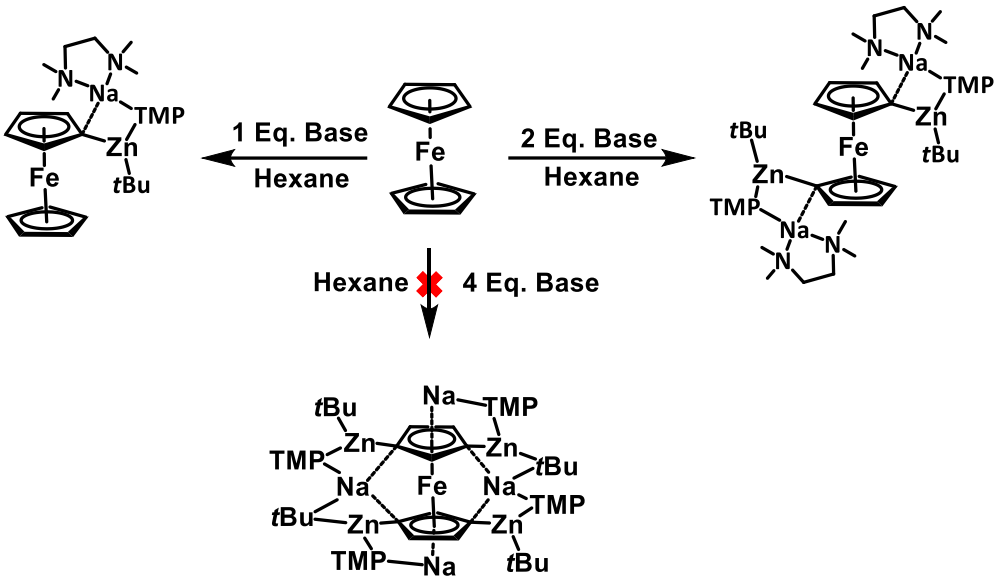

Scheme 2.2 – Simplification of the reactivity of zincate **1** with ferrocene in various ratios

Since that time, the 4:1 reaction has been repeated and upon standing, a small crop of crystals formed, which were determined to be $Na_4(TMP)_4Zn_4(tBu)_4[(C_5H_3)_2Fe]$ (complex **4**, scheme 2.3).[111] Disorder in the resulting crystal structure rules out an in-depth discussion of the data, but the connectivity of the atoms can still be seen.

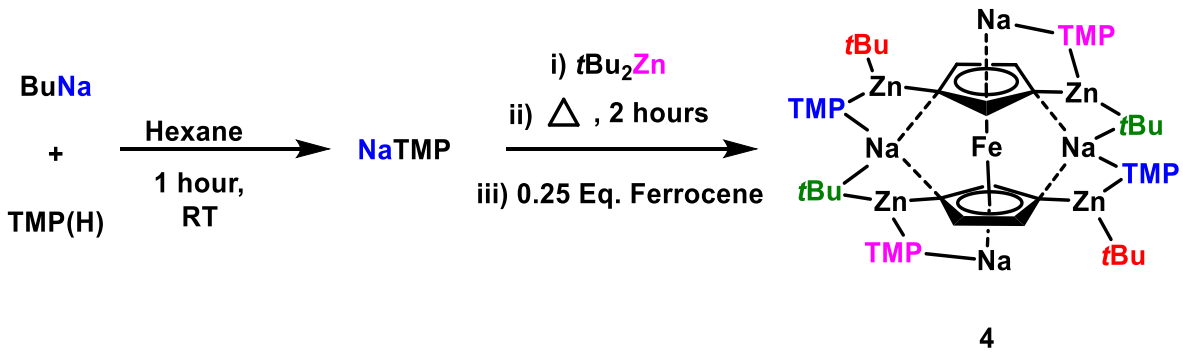

4

Scheme 2.3 – Synthesis of tetrazincated complex **4**

The obtained structure of **4** is unusual, in that the zincate arrangement is retained, but connects with another equivalent of zincate that is attached to the

other ring of the ferrocene, through a bridging sodium atom. It can also be seen that there is a difference between the *t*butyl groups present, with two of these groups bridging between the zinc and sodium atoms (coloured green in scheme 2.3), whereas, the remaining two butyl groups appear terminally bonded to a zinc atom (red in scheme 2.4). A final difference can be seen between the TMP groups of the zincate. Although they all bridge a Zn and Na centre, two of the four TMP molecules lie between the plane of the cyclopentadienyl rings while the other two molecules of TMP lie outwith these planes (blue and pink respectively in scheme 2.4). This is in contrast to the tetramagnesiated example where all anions in the inverse crown ring were identical (N*i*Pr$_2$).

During attempts to analyse this compound, it was dissolved in toluene. This then resulted in the formation of a crop of crystals and X-Ray analysis of these crystals led to the discovery that two equivalents of toluene had been deprotonated - with the expulsion of the terminal *t*butyl groups - at its methyl position and that the resulting benzyl anions had been retained within the structure, giving $Na_4(TMP)_4Zn_4(tBu)_2(CH_2Ph)_2[(C_5H_3)_2Fe]$ (**5**, scheme 2.4).

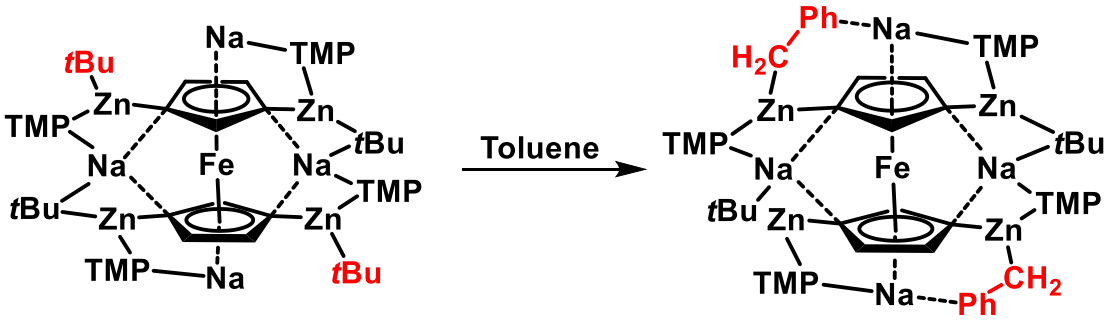

5

Scheme 2.4 – Synthesis of complex **5** through deprotonation of two equivalents of toluene by complex **4**

Following this, the use of a different planar, aromatic was considered. Pyridine was chosen for this, to investigate the potential – if any – for deprotonation of the ring. After dissolving the ferrocenyl complex **4** in pyridine - as opposed to toluene – a crop of crystals was obtained upon cooling. Upon analysing these crystals, it could be seen that the tetradeprotonated ferrocene unit had been lost, in the form of ferrocene, along with the TMP anions [as TMP(H)], but this resulted in a polymer (**6**) which contained pyridine deprotonated at the 4-position, as well as neutral solvating molecules of pyridine (scheme 2.5).

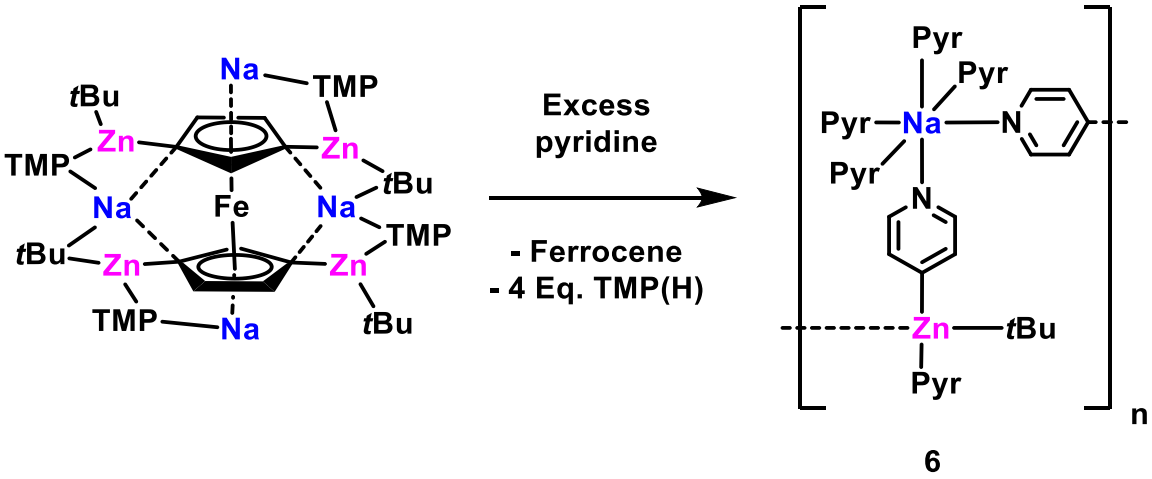

Scheme 2.5 –Synthesis of polymeric complex **6** by reaction of complex **4** with pyridine

2.2 Aims

The main aims of this work were as follows:

- To continue the investigation of an unprecedented tetrazincated ferrocene complex (**4**), with the intention of using this as an intermediate for the synthesis of tetrasubstituted ferrocenes.
- To investigate and develop the understanding of the synthesis of compound **6** from the reaction of **4** and pyridine.
- To investigate the use of *i*Bu_2Zn as an easier and safer to handle zinc reagent than *t*Bu_2Zn and to compare its effectiveness when used as part of a bimetallic base.

2.3 Results and Discussion

One of the first aims of this project was to replicate the synthesis of complex **4** and then obtain a good ^{1}H NMR spectrum of the complex **5** that forms from the reaction between complex **4** and toluene. The toluene molecule had been deprotonated at its most acidic methyl position and the resulting benzyl anion was also retained within the structure, giving complex **5**. Complex **4** was synthesised in hexane, which was then removed under vacuum and the residue dissolved in toluene. This resulted in the formation of complex **5** obtained in a 35% yield. The ferrocene region (3.5 – 5.0 ppm) of the resulting ^{1}H NMR spectrum in toluene is shown in figure 2.2 in section **2.4**.

The ^{1}H NMR spectrum of **5** was acquired from an NMR scale reaction taking place in a J. Young's tube. Compound **4** was dissolved in D_8-toluene and the spectrum appears to be very complicated in the aliphatic region, much like the parent base **4** was. However, the ferrocene region (~3.5 – 5.0 ppm), although still similar to that of the parent base, is indicative of a new species having formed. The resulting NMR spectrum shows two sets of three equal intensity singlets similar to that of **4**, although these new resonances are located at 4.45, 4.24 and 3.74 ppm for the major isomer and 4.43, 4.02 and 3.57 ppm for the minor isomer compared with at 4.40, 4.24 and 3.76 ppm for the major isomer and 4.45, 4.05 and 3.61 ppm for the minor isomer of **4**, in a ratio of 2:1. It must be noted that the change in NMR solvent from benzene to toluene might influence the chemical shifts although the most deshielded resonance of each isomer have exchanged places with the major isomer (4.45 ppm) now more downfield than the minor isomer (4.43 ppm) in **5**.

To further compare the reactivity of the mono- (**2**) and dizincated (**3**) ferrocene compounds to that of **4**, toluene was then added to both **2** and **3** to investigate whether a similar deprotonation of the benzyl position would be seen. While no tangible product was obtained from the reaction involving **2**, a crop of crystalline material had formed from the refluxing of **3** in toluene upon cooling.

Upon X-ray crystallographic analysis of these crystals (**3'**), shown in figure 2.3 in section **2.5.**, it was seen that the dizincated ferrocene compound had remained intact and simply co-crystallized with a molecule of toluene. This confirms that tetrazincated complex **4** displays a greater degree of reactivity than dizincated complex **3**. Unfortunately, the poor quality of the crystallographic data means that no in-depth discussion of the bond parameters can be made.

Previous studies had shown that when pyridine is added to **4**, this results in the formation of a polymeric zincated pyridine species (**6**, Scheme 2.5). However, this product was only obtained in a yield of 5%. So, an attempt was made to improve this yield and also obtain good characterisation of the metallated pyridyl polymer that forms, including ^{1}H and ^{13}C NMR spectra. The synthesis of **6** was successfully completed although the yield only improved marginally to 9%. One possible reason for this low yield could be due to the presence of the polar donor in the form of pyridine, resulting in a low yield of the crystalline material forming. Upon consideration of the ^{1}H NMR spectrum of **6** in D_5-Pyridine, five distinct resonances can be seen in the aromatic region. On comparison with the spectrum of pyridine, it was concluded that the resonances at 8.70, 7.57 and 7.19 ppm were indicative of the α-, γ- and β-carbons of free pyridine respectively. This then left two unassigned resonances at 8.59 and 8.25 ppm which had an integral ratio of 1:1. The resonance at 8.59 was assigned as the α-hydrogen of 4-metallated pyridine and the resonance at 8.25 ppm was assigned as the β-hydrogen of the 4-metallated pyridyl ring. Overall, this NMR spectrum (figure 2.4 in section **2.4**.) is indicative of the successful formation of complex **6**.

As previously mentioned, the yield of product **6** obtained from this process is very low and could only be improved upon slightly. The next step to be attempted was to perform an iodine quench on an *in situ* sample (Scheme 2.7) to investigate whether the low yield could have been a result of the high

solubility of the complex and thus confirm that the solution yield of the reaction was higher. To ensure that the all anionic species were fully quenched, such as the metallated pyridine and the ferrocene anions etc. an excess of 25 mmol of I_2 was used to quench a reaction mixture intended to synthesis 0.5 mmol of compound **5**.

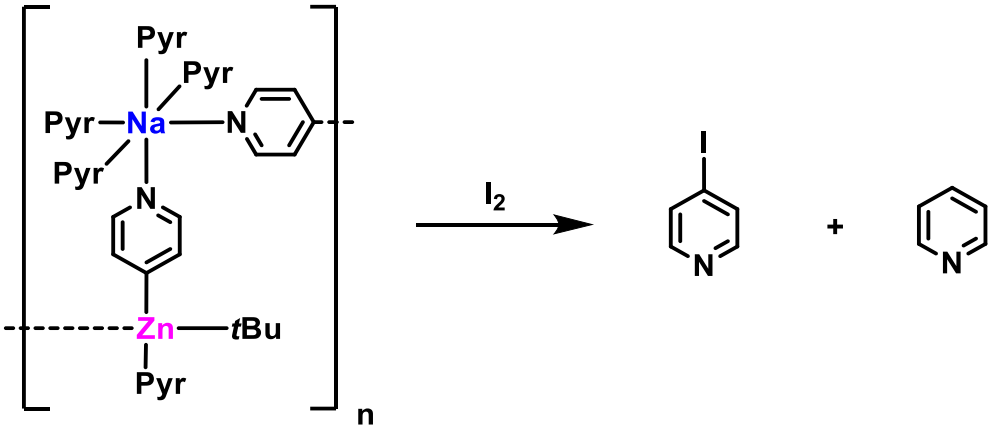

Scheme 2.7 – Scheme illustrating the anticipated products from iodine quench of **6**

However, the ^{1}H NMR spectrum of the products obtained after work-up, shown in figure 2.5 in section **2.4**., indicates a mixture of 3- and 4-deprotonation is occurring and is leading to the generation of both 3-iodopyridine and 4-iodopyridine, with an excess of free pyridine also present, as expected. It can also be determined from the integrations of these resonances in the aromatic region that there is more of the 3-iodopyrine than the 4-iodopyridine, with the ratio being almost 3:2 in favour of 3-iodopyridine.

When revisiting the originally obtained ^{1}H NMR spectrum of **6**, small shoulder resonances on the desired resonances, as well as a small resonance at approximately 9.6 ppm can also be seen, as highlighted in figure 2.6 in section **2.4**.). This could be indicative of another species being present in the sample, which is assumed to be the 3-metallated pyridine unit. It should be noted that these resonances are significantly smaller in this ^{1}H NMR since this spectrum

is of a crystalline sample of **6**. So, these smaller resonances must be of some residual 3-metallated pyridine. Further NMR analysis was performed with the intention of finding the fourth resonance of the 3-metallated species. To this end, a HSQC NMR was obtained and from this, it was seen that the fourth resonance of the 3-metallated species was located under the solvent peak of the pyridine at 7.2 ppm.

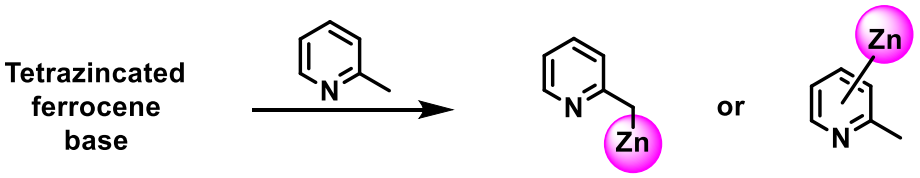

Scheme 2.8 – The possible metallation sites of 2-picoline

Compound **4** was then generated *in-situ* like before. However, the hexane was removed and 2-picoline was used to dissolve the residue. The flask was then placed in a freezer at (-33 ^{o}C) and this resulted in the growth of a crop of crystalline material. However, these crystals were not of sufficient quality for X-ray analysis so a ^{1}H NMR spectrum in d_8-THF was collected.

The obtained ^{1}H NMR spectrum (figure 2.7 in section **2.4**.) seems to indicate the formation of a 2-picolyl species. This can be seen when considering the resonance at ~1.70 ppm (highlighted in green), although it is under a THF solvent resonance, this resonance seems to integrate to 2 with respect to the picolyl aromatic resonances in red. The aromatic pattern of the picolyl species appear similar to those of the free 2-picoline but shifted slightly upfield. Crucially, there appears to be four distinct aromatic environments consistent with retention of all four hydrogen atoms on the ring.

This spectrum can be compared to that of Me_6TREN solvated monometallic picolyl sodium as shown in figure 2.8 in section **2.4**. From this, a clear

difference can be seen in their respective aromatic regions, with the picolyl sodium species adopting the amido resonance form, thus shifting the resonances upfield as this system has lost a degree of its aromaticity and can be thought of as a conjugated olefinic system. Whereas the species obtained from reaction with **2** seems to retain its aromaticity. The resonances are still shifted upfield when compared to 2-picoline, but to a lesser extent than observed in the amido form. An explanation for this could be that the negative charge is localized on the CH_2 carbanion rather than on the nitrogen or being

delocalized across the CCN unit. Alternatively, as sodium has a lower electronegativity than zinc, the M-C bond will be more polarised in the case of sodium. This would cause a greater upfield resonance being observed.

To show that there are only 2 significant species present in the sample, a DOSY NMR was performed which does indicate the presence of 2 species. The first is free 2-picoline, which is expected as an excess of 2-picoline was used in the reaction and the second product is the suspected zincated species, with metallation occurring on the methyl arm. However, as this sample was an isolated crystalline compound, it is possible that there could be some decomposition occurring

Focus was then shifted to a more useful functionalisation of ferrocene from $Na_4(TMP)_4Zn_4(t\text{Bu})_4[(C_5H_3)_2Fe]$, **4**. An attempt was made to quench the system using CO_2. Such a reaction was recently carried out by Klett *et al.* on a tetrapotassiated ferrocene framework obtained through a bimetallic Lochmann-Schlosser superbase approach to metallation of the sandwich complex.[112] This was initially tested on a sample of **4**, in hexane. After bubbling CO_2 through the solution, followed by organic work up, this led to the generation of only a small amount of ferrocenetetracarboxylic acid as evidenced by the ^{1}H NMR spectrum (coloured red in figure 2.9 in section **2.4**.), with the mixture also containing ferrocene (coloured blue), the dicarboxylic-

acid (coloured yellow) and tricarboxylic-acid (coloured green). Table 2.1 contains a summary of the results obtained for this part of the study.

Table 2.1 – The results of the quenching process of compound **4**

Solvent	Ferrocene (%)	Mono-acid (%)	Di-acid (%)	Tri-acid (%)	Tetra-acid (%)
Hexane *	35	0	8	55	2
Hexane	48	0	3	49	*trace*
Toluene	63	0	1	36	*trace*
THF	35	0	2	60	2
Benzene	47	0	8	45	*trace*
Toluene **	56	0	2	40	2

* Compound **4** was generated *in-situ* for this reaction

** A drying tube was used to ensure that dry CO_2 was used for the reaction

It was thought that as this quench was performed on an *in-situ* generated sample, this could be leading to incomplete generation of **4** and thus the mixture of products being obtained. To overcome this issue, it was thought to be best if the quench was repeated on an isolated sample of $Na_4(TMP)_4Zn_4(t\text{Bu})_4[(C_5H_3)_2Fe]$, as this would ensure that the desired compound is being quenched and not an unknown mixture. However, this does not appear to alter the outcome of the reaction to any significant degree. No tetracarboxylic acid can be seen at all, with the majority of the reaction products again being ferrocene and ferrocenedicarboxylic acid.

It was thought that as **4** is insoluble in hexane then this could be interfering with the quenching process. In an attempt to overcome this issue, a series of solvents were then tested, the first of which was toluene, as this would allow for **4** to be fully dissolved. Although the composition of the compound has now been likely altered slightly into **5**, the central tetrametallated ferrocene unit would still be present and so the reaction should still hopefully result in the formation of ferrocenetetracarboxylic acid, as well as benzylic acid. This resulted in no significant change to the outcome of the reaction. There was still trace amounts of ferrocenetetracarboxylic acid observed. The percentage yield of each product from this reaction can be seen in table 2.1. The next solvent to be tried was THF. This does indeed fully dissolve **4**. However, the colour of the solution is noticeably different from the others, with it being an off-orange colour, as opposed to the usual red, which could be indicative of a change occurring to the system due to the presence of the donor. This resulted in no significant change to the outcome of the reaction. Only a 2% yield of ferrocenetetracarboxylic acid was observed. The percentage yield of each product from this reaction can be seen in table 2.1. The final solvent to be tried was benzene as this would hopefully be a middle ground between the toluene and the THF as the benzene would hopefully not alter the structure of **4** like the toluene does and not cause a breakdown of the complex like THF does. Again, this made no significant change to the outcome of the reaction with only trace amounts of ferrocenetetracarboxylic acid being observed.

As none of these solvent alterations seemed to make any significant change to the outcome of the reaction, it was thought that something else could be the determining factor of the reaction. It was thought that this could perhaps be due to the presence of residual moisture from the CO_2, leading to hydrolysis of the starting material. This could provide an explanation for the presence of multiple products (partial hydrolysis of **4**) as well as provide an explanation for the presence of free ferrocene (full hydrolysis). A modification was made to the procedure that would allow for dry CO_2 to be used for the quench of the compound. A drying tube was filled with a drying agent and this was connected

to the Schlenk flask containing CO_2. This should dry the CO_2 as it passes through and at this point pass into another Schlenk, containing **4** dissolved in toluene, via a canula. Again, this did not seem to help improve on the amount of tetracarboxylic acid obtained from the reaction. A noticeable colour change can be seen occurring throughout each of these reactions, from the original red solution to a light orange solution.

A D_2O quench of complex **4** was then performed. A small amount of **4** was taken into a Schlenk flask, to which was added 0.6 mL of D_2O. This was allowed to stir for 10 minutes before C_6D_6 was added. The organic layer was separated and washed with D_2O before obtaining a ^1H NMR spectrum, shown in figure 2.10 in section **2.4**. The obtained spectrum appears to be clean, in that the only resonances that are observed can be attributed to the compounds that were expected to be seen (ferrocene and TMP(D), isobutane would be lost as a gas). Unfortunately, ^1H NMR spectroscopy doesn't resolve separate resonances for D_1-Fc, D_2-Fc, D_3-Fc and D_4-Fc so it could not be determined if only D_4-Fc was being obtained. To ensure that the resonance that was observed for the ferrocene corresponds was that of deuterated ferrocene, a ^2H NMR experiment (figure 2.11 in section **2.4**.) was then performed in an attempt to investigate whether there was a deuterium resonance in the ferrocene region at ~4.00 ppm.

As this is an NMR experiment, the solvent that was used was also deuterated, so the data collection had to be run with no solvent being selected. This causes the appearance of significant resonances corresponding to the solvent. However, a resonance at 4.00 ppm was also clearly observed, indicating the presence of a deuterated ferrocene species. To then investigate this further and following the procedure of previous work that had been done in this area, a GC-MS spectrum was then obtained for the sample, shown in figures 2.12

and 2.13, in order to determine the masses of the reaction products to determine the degree of deuteration of the species.

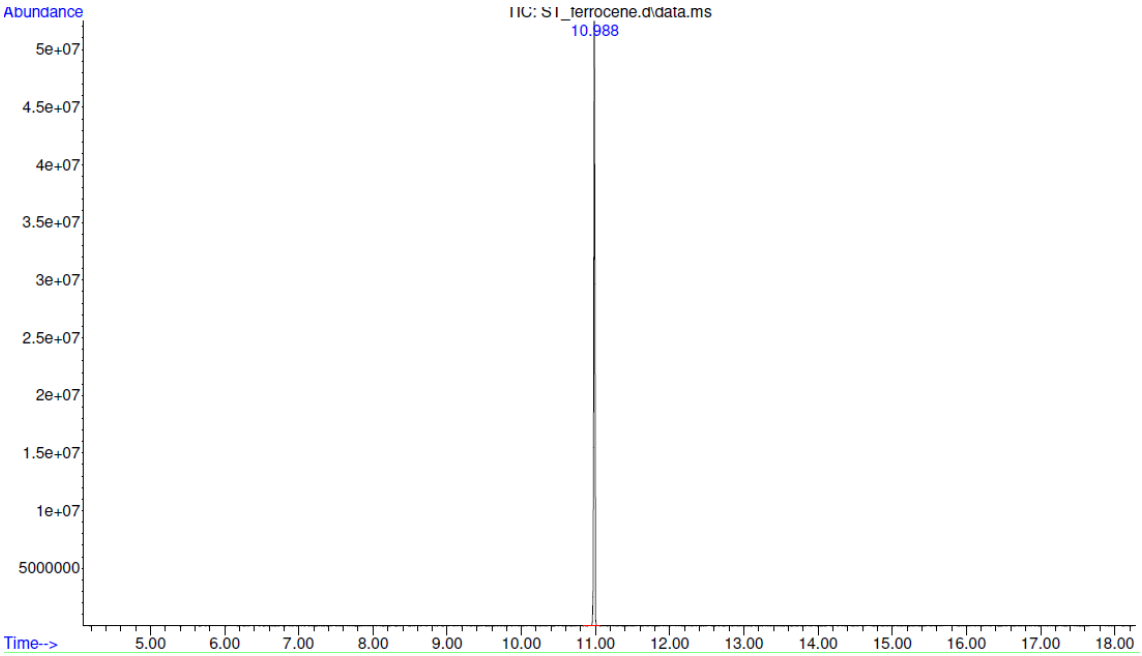

Figure 2.12 – GC-MS spectrum obtained after D_2O quench of **4**

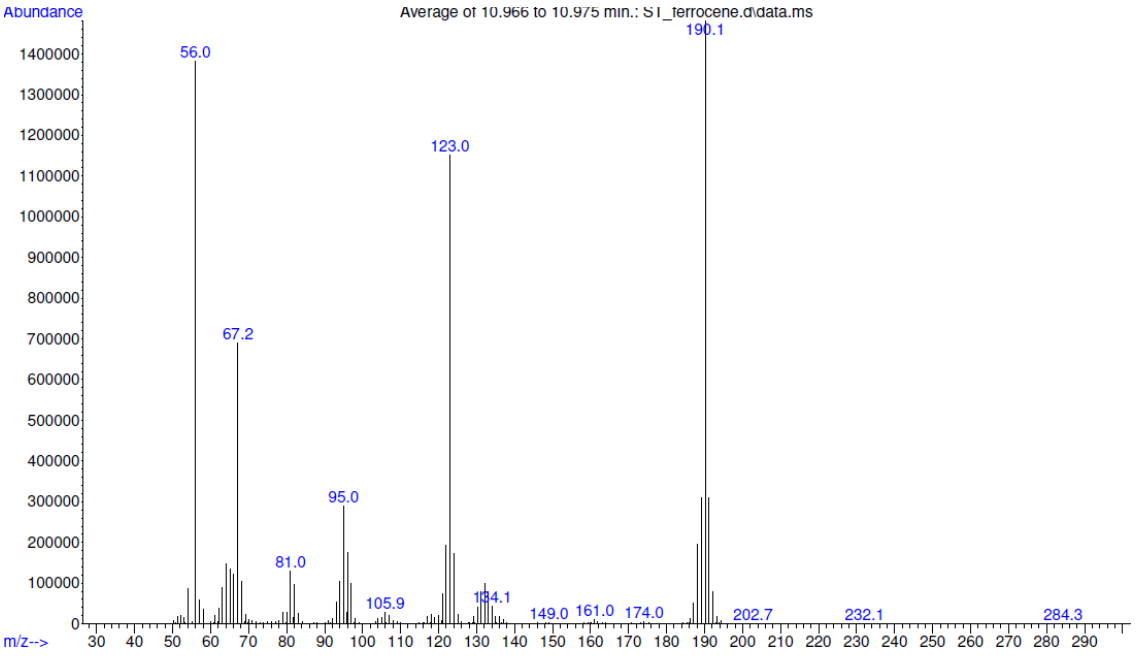

Figure 2.13 – Analysis of GC-MS peak at time 11 minutes, obtained after D_2O quench of **4**

It can be seen from there only being one peak within the timeline that there was only one species that had eluted from the sample. Investigating the masses of the compounds and fragments eluted at this time, a signal with a mass of 190.1 can be seen, which indicates the presence of tetra-deuterated ferrocene, $Fe(C_5H_3D_2)_2$. However, there are also small signals at 189.0 and 188.0, which could be indicative of D_3-ferrocene and D_2-ferrocene respectively.

Figures 2.14 and 2.15 have been generated from a GC-MS predictor and correspond to D_4-ferrocene and D_3-ferrocene respectively. These predictions are in alignment with the suggested conclusions as they match the observed masses from the obtained GC-MS spectrum.

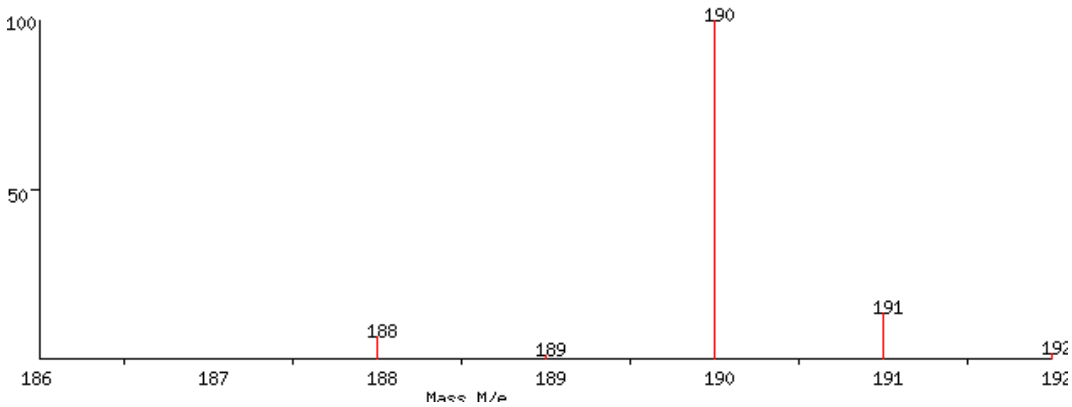

Figure 2.14 – Predicted GC-MS isotope pattern of D_4-ferrocene

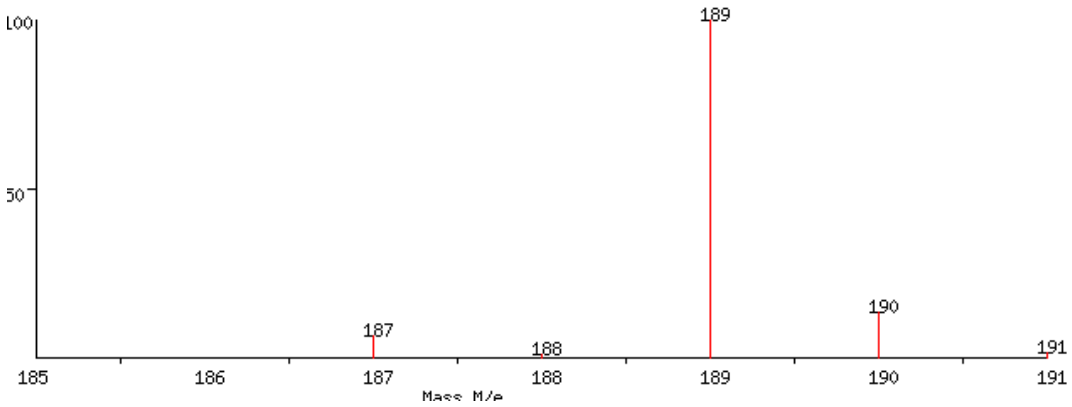

Figure 2.15 – Predicted GC-MS isotope pattern of D_3-ferrocene

The presence of D_2/D_3-ferrocene could have been caused by partial hydrolysis of **4**. However, there is no indication of any monodeuterated ferrocene present. The other major peaks present in the GC-MS spectrum can be rationalised upon consideration of the fragmentation of tetra-deuterated ferrocene. The peak at 56.0 corresponds to Fe, the peak at 67.2 corresponds to a $C_5H_3D_2$ ring and the peak at 123.0 corresponds to a Fe- $C_5H_3D_2$ fragment.

2.4 Synthesising a safer bimetallic base

Due to the danger of using *t*BuLi (which is extremely pyrophoric), the long synthesis and the handling issues of *t*Bu_2Zn (it is a liquid at ambient temperature), it was decided to try and develop the potentially more user friendly *i*Bu_2Zn. This was attempted by employing the same procedure for *t*Bu_2Zn, but using moderately safer *i*BuLi instead of *t*BuLi (scheme 2.9).

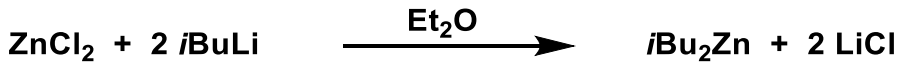

Scheme 2.9 – Equation showing the synthesis of *i*Bu_2Zn

This was successfully achieved and a yield of 95% was obtained after filtration and solvent evaporation. There were some unforeseen issues when synthesising *i*Bu_2Zn, as it remains a liquid when placed under sublimation conditions. Upon inspection of the ^1H and the ^7Li NMR spectra for this compound the ^1H NMR spectrum shows resonances for only the *i*Butyl groups. However, the ^7Li NMR spectrum shows a resonance corresponding to a lithium environment. So, a distillation was performed and a new ^1H NMR spectrum was obtained on the resulting colourless oil. This still displayed the butyl resonances, but this time the ^7Li NMR spectrum had no resonances present, suggesting any residual lithium containing compounds (likely LiCl or *i*BuLi) had been removed.

This product is an oil at room temperature and a solid form of this would be more desirable, as it would be much easier to handle. Also, since it was not possible to crystallise *i*Bu_2Zn, it would be convenient to produce a crystalline form to show beyond doubt the formation of the *i*Bu_2Zn unit. This was attempted using Me_6TREN as a donor since it have been used previously to form the *t*Bu_2Zn adduct.[113] Smaller amines - in the form of TMEDA and PMDETA - were also used as donors. Unfortunately, no crystals formed from these attempts and again only oils were obtained. The ^{1}H NMR spectra of *i*Bu_2Zn and these adduct oils have been included in figures 2.16-2.19 in section **2.4**. In each case the spectrum confirms a 1:1 *i*Bu_2Zn:donor ratio. Note the figures of the PMDETA and Me_6TREN adducts are drawn with the donors behaving as bidentate donors, there is no spectroscopic evidence to confirm this but Me_6TREN has been shown previously to act as a bidentate donor to *t*Bu_2Zn without any spectroscopic evidence distinguishing between free and coordinated arms of the ligand.

These ^{1}H NMR spectra have also been combined into one overlapping image, shown in figure 2.20 in section **2.4**. Shown in black is the original spectrum of donor-free *i*Bu_2Zn. Then above this, shown in blue, is the spectrum of *i*Bu_2Zn·Me_6TREN. The spectrum shown in red, is the spectrum of *i*Bu_2Zn·PMDETA. Finally, the spectrum at the top, shown in purple, is the spectrum of *i*Bu_2Zn·TMEDA.

Previous work that has been performed within the Mulvey and Hevia groups has made use of the sodium zincate species TMEDA·Na(*μ*-TMP)(*μ*-*t*Bu)-Zn(*t*Bu), **1** to great effect. Complex **1** exists as a crystalline material, so, an attempt was made (scheme 2.10) to synthesise the *i*Bu variant of this sodium zincate in an effort to obtain a solid complex containing *i*Bu_2Zn and obtain an X-ray structure of this complex. This would also show indirectly but definitively, the successful synthesis of *i*Bu_2Zn. A secondary aim of this is to investigate

the reactivity differences that could be seen between the two complexes, if any, as a consequence of the change in butyl isomer present.

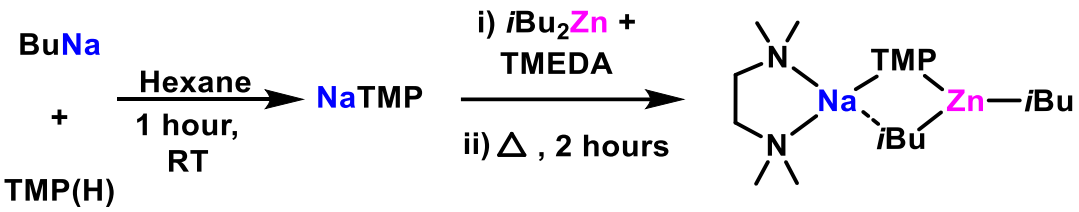

Scheme 2.10 – Synthesis of TMEDA·Na(*μ*-TMP)(*μ*-*i*Bu)Zn(*i*Bu) (**7**)

During the studies of the homoalkyl **1**, it was seen that the sodium atom interacts with the butyl group through a terminal methyl carbon giving a five-membered ZnNNaCC ring.[73] Whereas, studies of the related heteroalkyl TMEDA·Na(*μ*-TMP)(*μ*-*n*Bu)-Zn(*t*Bu) showed that the sodium atom would interact with the butyl group through the CH_2 resulting in a 4-membered ring.[71] Both of these options are clearly available to **7**. The reaction in scheme 2.9 yielded a crop of crystals in a 56% yield, with the resulting crystal structure (figure 2.21 in section **2.5.**) showing that there is an interaction between the sodium atom and the CH_2 carbon. Table 2.2 lists some pertinent bond parameters of **7** alongside those of complex **1** and TMEDA·Na(*μ*-TMP)(*μ*-*n*Bu)Zn(*t*Bu) for comparison.

Table 2.2 - Selected bond lengths (Å) and angles (º) of **7** and related sodium zincates

Solvent	1	7	TMEDA·Na(*μ*-TMP)(*μ*-*n*Bu)Zn(*t*Bu)
$Na\text{-}N_{TMEDA}$	2.528 (6) 2.481 (6)	2.469 (3) 2.464 (3)	2.505 (10) 2.452 (11)
$Na\text{-}N_{TMP}$	2.412 (6)	2.371 (2)	2.3846 (13)
$Na\text{-}C_{br}$	2.412 (6)	2.741 (3)	2.6689 (18)
$Na\text{-}C_{Me}$	2.750 (10)	-	-
$Zn\text{-}N_{TMP}$	2.034 (6)	2.038 (2)	2.0340 (13)
$Zn\text{-}C_{br}$	2.149 (9)	2.048 (3)	2.0635 (15)
$Zn\text{-}C_{ter}$	2.074 (8)	2.063 (5)	2.0461 (15)
$N_{TMP}\text{-}Na\text{-}C_{br}$	97.1 (3)	81.2 (8)	80.93 (5)
$Na\text{-}C_{br}\text{-}Zn$	70.9 (3)	80.4 (8)	82.12 (5)
$Na\text{-}N_{TMP}\text{-}Zn$	98.6 (2)	89.3 (8)	90.28 (5)
$C_{br}\text{-}Zn\text{-}N_{TMP}$	116.9 (3)	108.4 (10)	106.66 (6)
$C_{br}\text{-}Zn\text{-}C_{ter}$	116.8 (3)	129.8 (18)	120.71 (6)
$N_{TMP}\text{-}Zn\text{-}C_{ter}$	126.2 (2)	118.6 (17)	132.62 (6)

One thing that should be noted from Table 2.2. is the Zn-C_{br} bond length of compounds **1**, **7** and TMEDA·Na(*μ*-TMP)(*μ*-*n*Bu)Zn(*t*Bu). It should be noted that compound **1** has a longer bond length, thus should be more reactive than the others. Compound **7** has a bond length that is similar to that of TMEDA·Na(*μ*-TMP)(*μ*-*n*Bu)Zn(*t*Bu), so it could be expected to show a reactivity similar to this complex. This shorter bond length coupled with the less reactive *s*butyl group of complex **7** suggests that it would show a reactivity similar to that of TMEDA·Na(*μ*-TMP)(*μ*-*n*Bu)Zn(*t*Bu).

Included in figure 2.22 in section **2.4.**, is the obtained ^{1}H NMR spectrum of this complex. An interesting phenomenon can be observed within the ^{1}H spectrum, where the methyl peaks of the TMP ring are split into two resonances that integrate to 6 protons each. To the best of my knowledge, this phenomenon has only been observed once before by Mulvey *et al*. when using similar reactions to this work utilising N-Boc pyrrolidine complexes.[114]

In order to compare the reactivity of **7** with **1**, a reaction in which **1** had already been used was employed, but this time using **7**. This reaction was the metallation of napthalene, which has been highlighted previously in section 1.2.2.[84] When **1** was used as the base in this reaction, dizincation of naphthalene was observed. When **7** was used as the base for this reaction, a crop of crystalline material was obtained. However, upon X-Ray analysis of these crystals, the only observed product was unreacted naphthalene. This is indicative that **7** is not as good a base as **1**.

After observing this, an alternative reaction was attempted, in which HMDS(H) was used to test the deprotonation ability of **7** on a substrate which has an easily accessible, relatively acidic proton. The ^{1}H spectrum of this reaction mixture was obtained in D_8-THF and is shown in figure 2.23 in section **2.4**.

The observation of free TMP(H) is indicative of the first step of the two-step mechanism discussed in chapter 1 occurring and then no further reaction (that is the second step) taking place. This is also backed up by the fact that both equivalents of the *i*butyl are still present with the complex. If the second step of the two-step mechanism had occurred, then there would only be one equivalent of *i*butyl present. Overall, this seems to confirm that the *i*Bu ligands are less reactive in **7** than the *t*Bu ligands in **1** and so overall the modification of the base delivers a less useful bimetallic base. Due to the relative pK_a values of the reagents used, it would be expected that the two-step mechanism that is proposed by Kondo and Uchiyama could be expected here. It could also be rationalised that the absence of a TMP product could be due to the bulk of the amine utilised, preventing subsequent reaction with a butyl group.

2.4 NMR Data

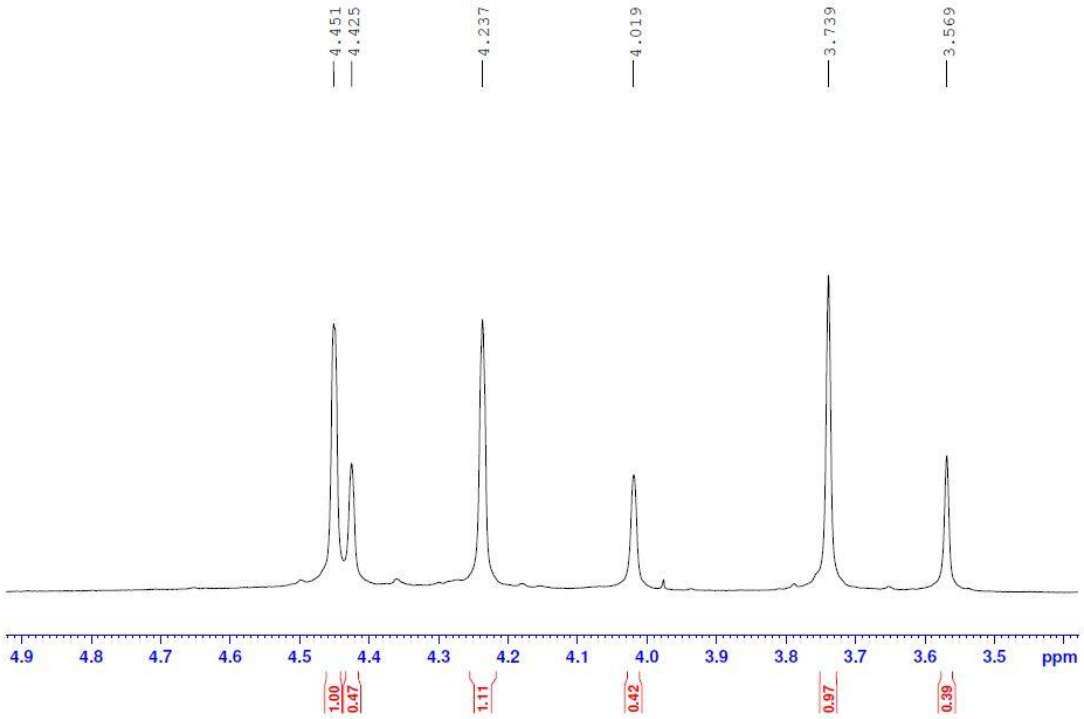

Figure 2.2 – An expansion of the ^{1}H NMR spectrum of complex **5** obtained in D_8-Toluene

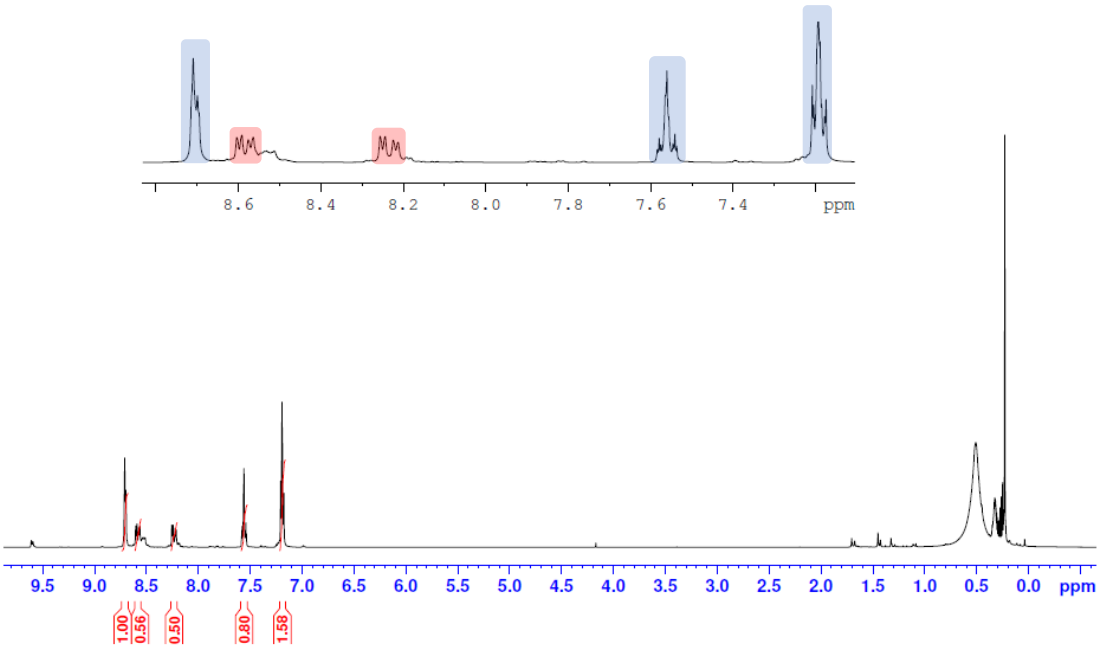

Figure 2.4 – ^{1}H NMR spectrum of a D_5-Pyridine solution of crystalline **6** (Shown in blue – free pyridine and red – 4-zincated pyridine)

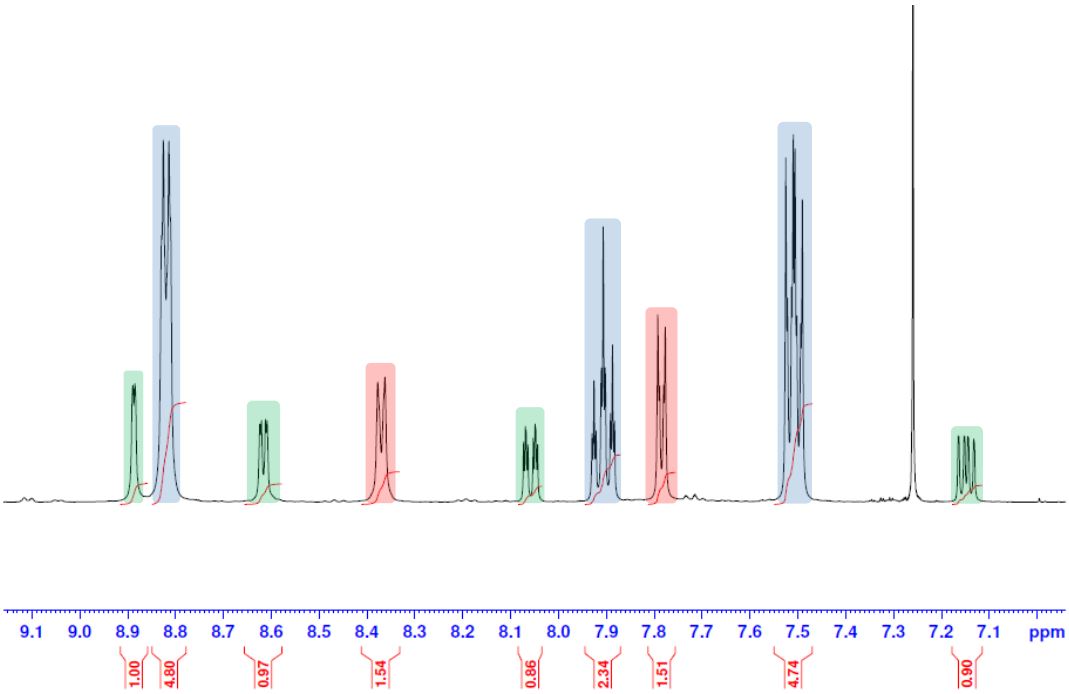

Figure 2.5 – Aromatic region of ^{1}H NMR spectrum of products generated from iodine quench of **6** (Shown in green – 3-iodopyridine, red – 4-iodopyridine and blue – pyridine)

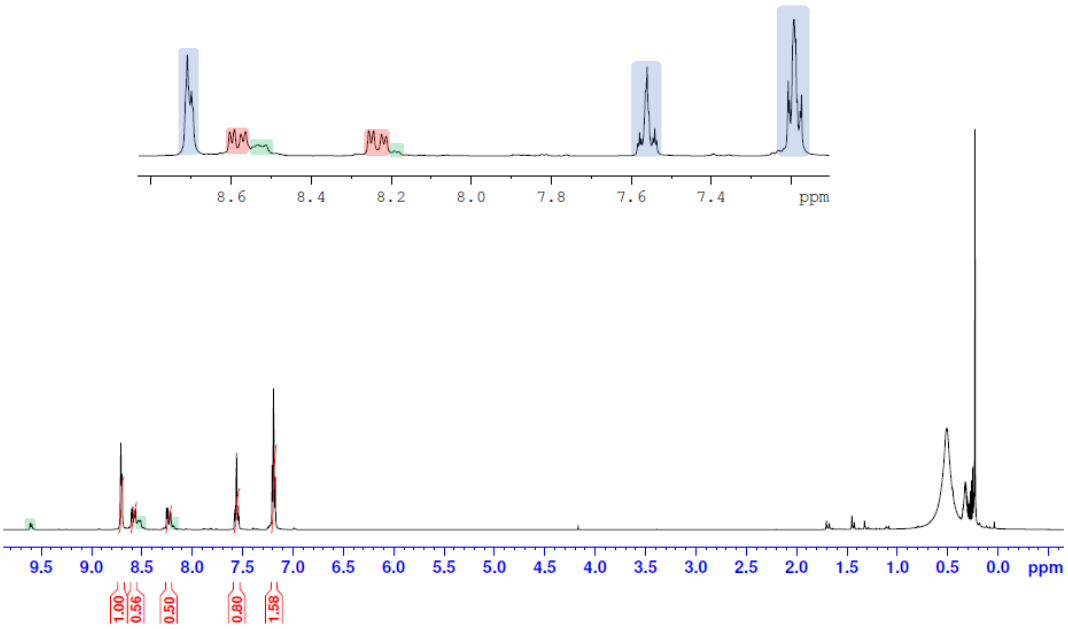

Figure 2.6 – ^{1}H NMR spectrum of crystalline **6** with the shoulders highlighted (Shown in blue – pyridine, red – 4-zincated pyridine green – 3-zincated pyridine)

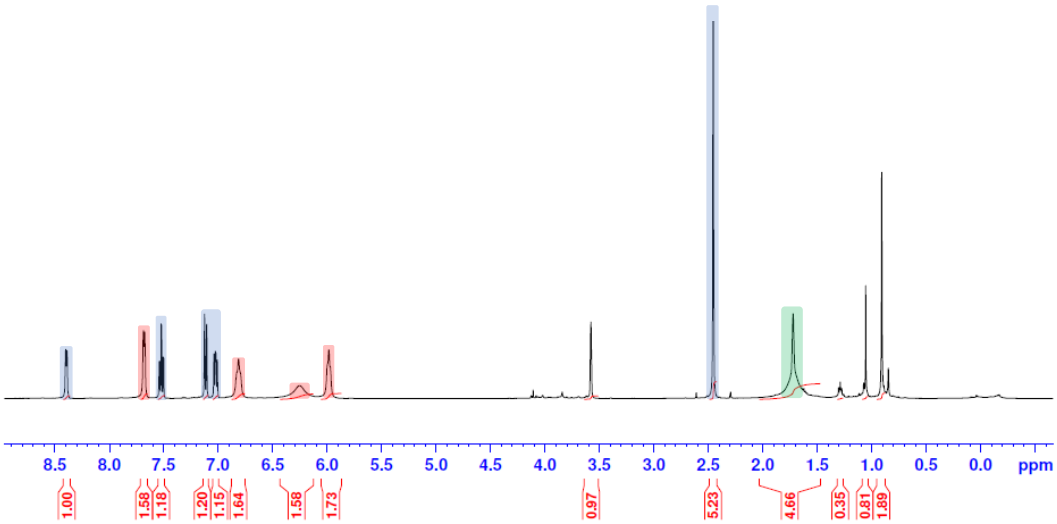

Figure 2.7 – ^{1}H NMR spectrum in d_8-THF of crystals obtained from reaction of **2** with 2-picoline (Shown in blue – 2-picoline, red – 2-picolyl species and green – possible picolyl CH_2)

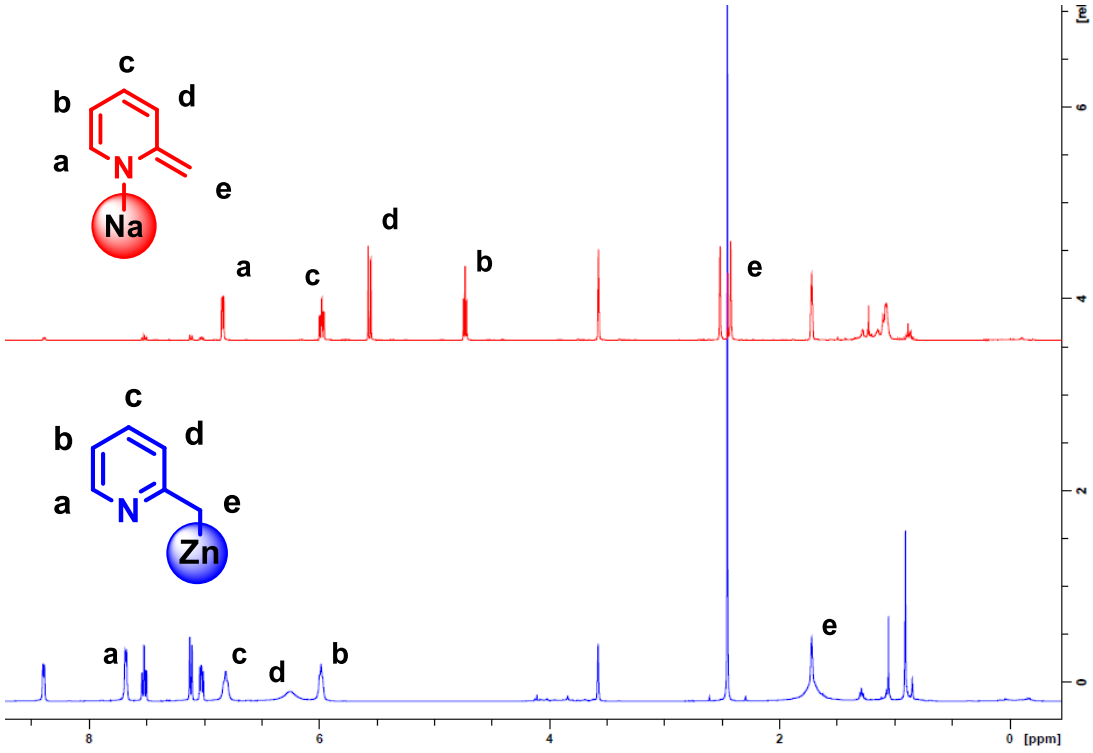

Figure 2.8 – Overlapping ^{1}H NMR spectra of 2-picolylsodium (top) and the unidentified metallated 2-picolyl product (bottom).

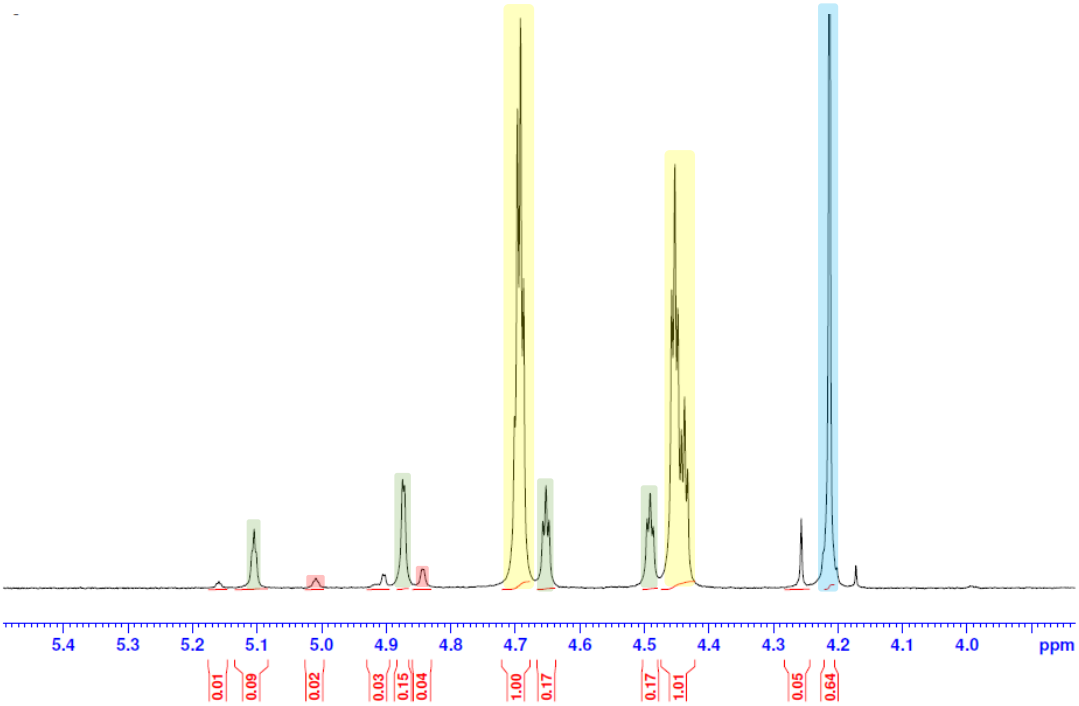

Figure 2.9 – ^{1}H NMR spectrum in DMSO of products generated from a CO_2 quench performed in hexane, on **4** synthesised *in-situ*

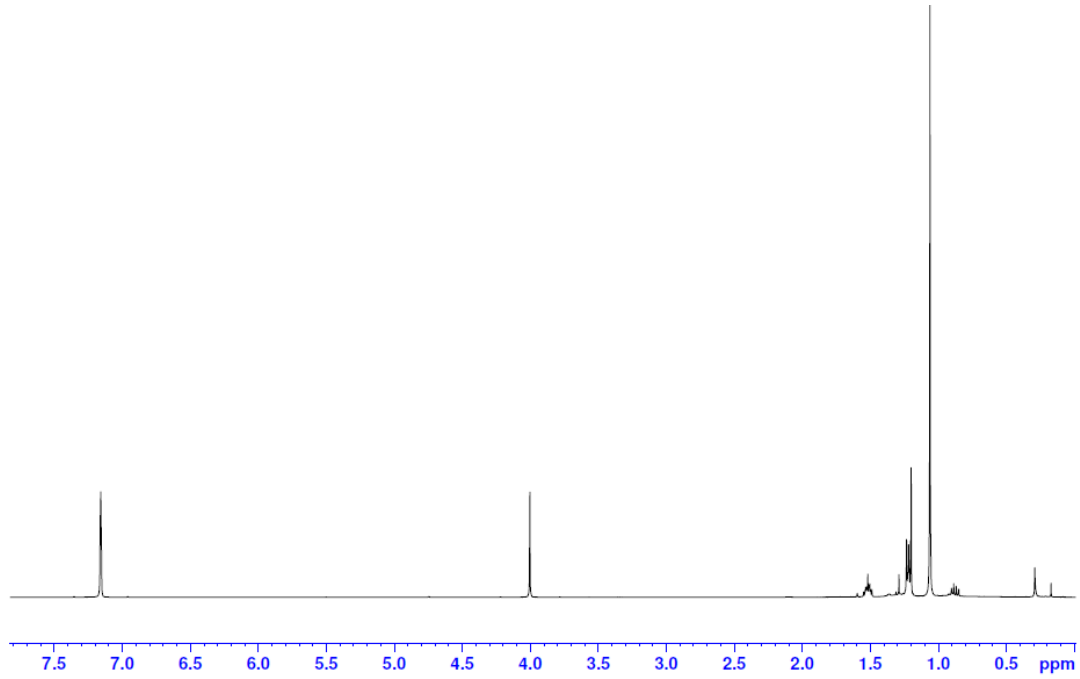

Figure 2.10 – ^{1}H NMR spectrum obtained in C_6D_6 after D_2O quench of **4**

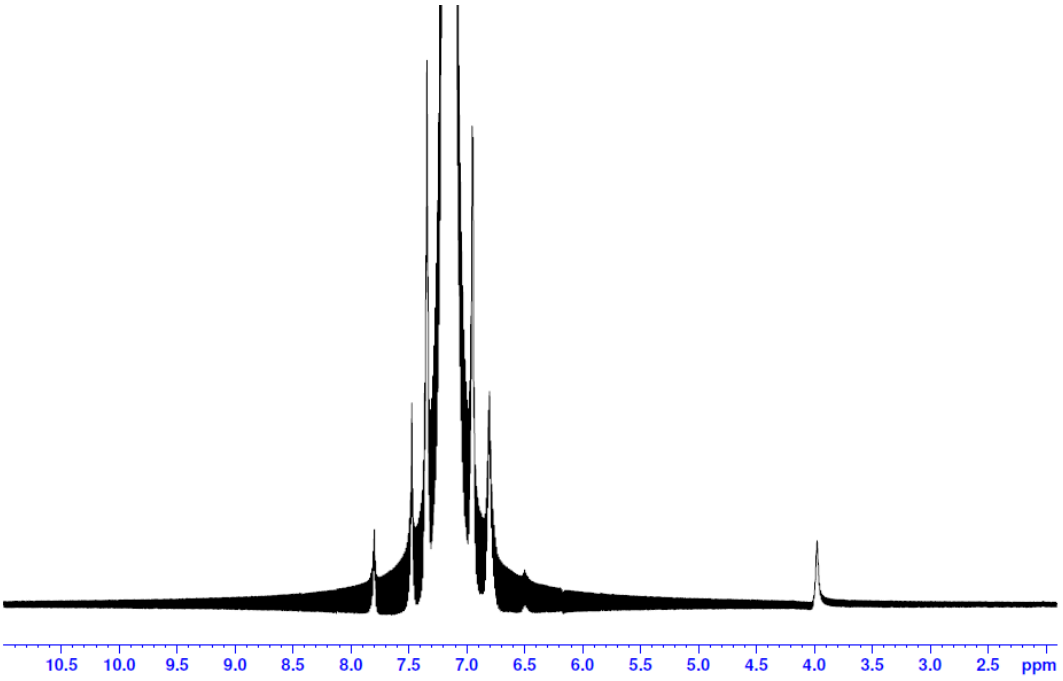

Figure 2.11 – ^{2}H NMR spectrum obtained in C_6D_6 after D_2O quench of **4**

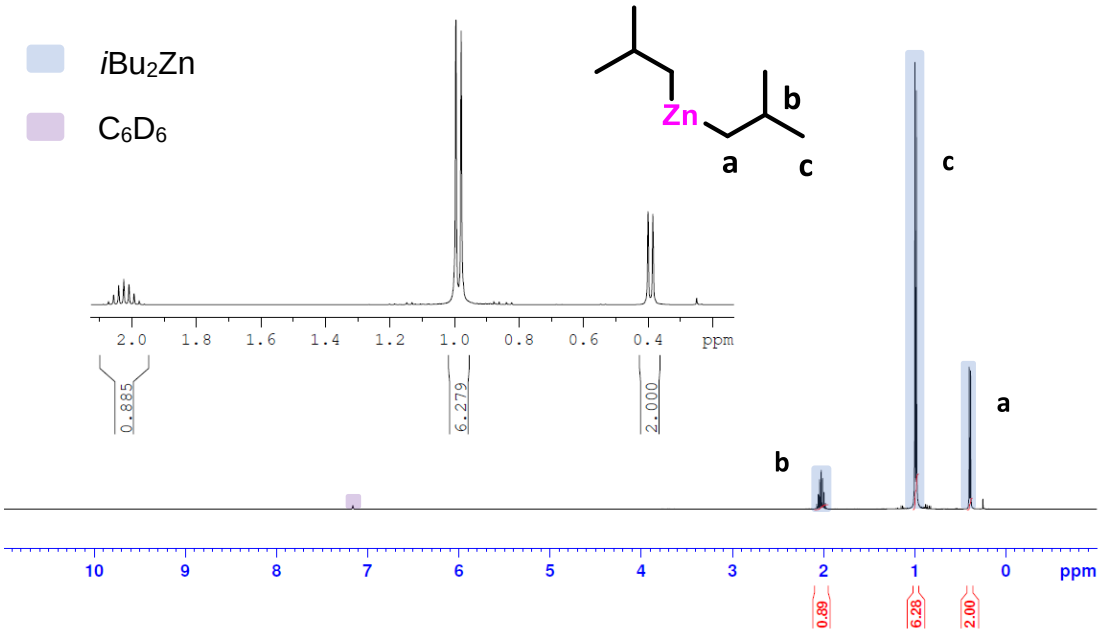

Figure 2.16 – ^{1}H NMR spectrum acquired in C_6D_6 of iBu_2Zn

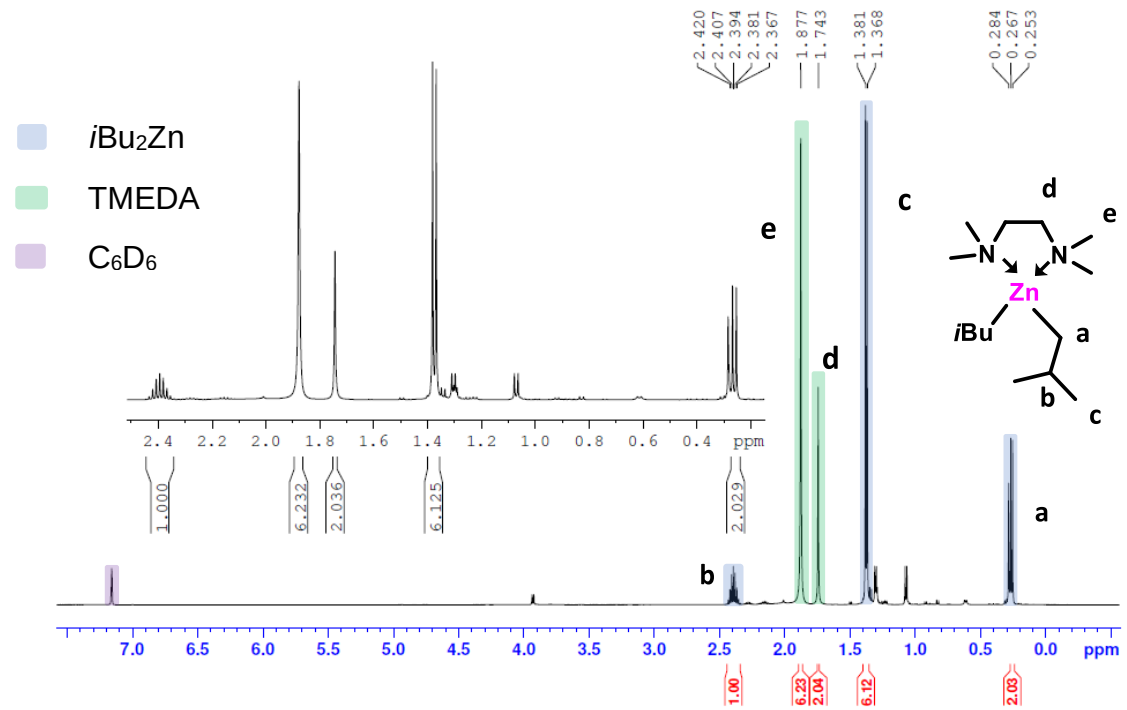

Figure 2.17 – ^{1}H NMR spectrum acquired in C_6D_6 of *i*Bu_2Zn·TMEDA

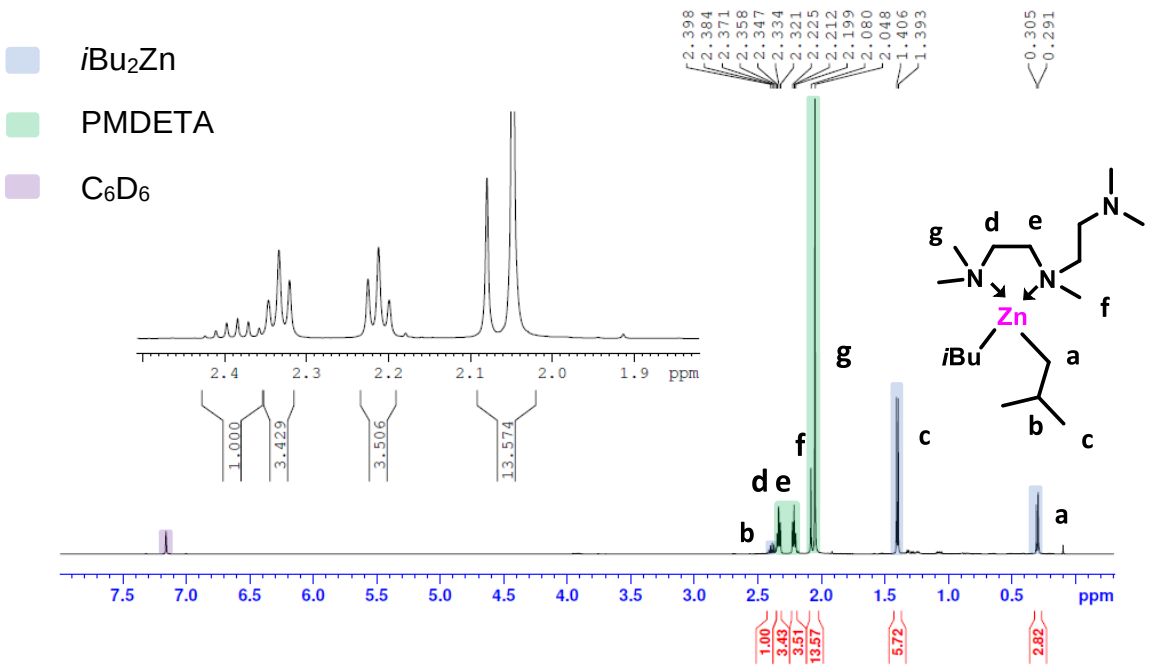

Figure 2.18 – ^{1}H NMR spectrum acquired in C_6D_6 of *i*Bu_2Zn·PMDETA

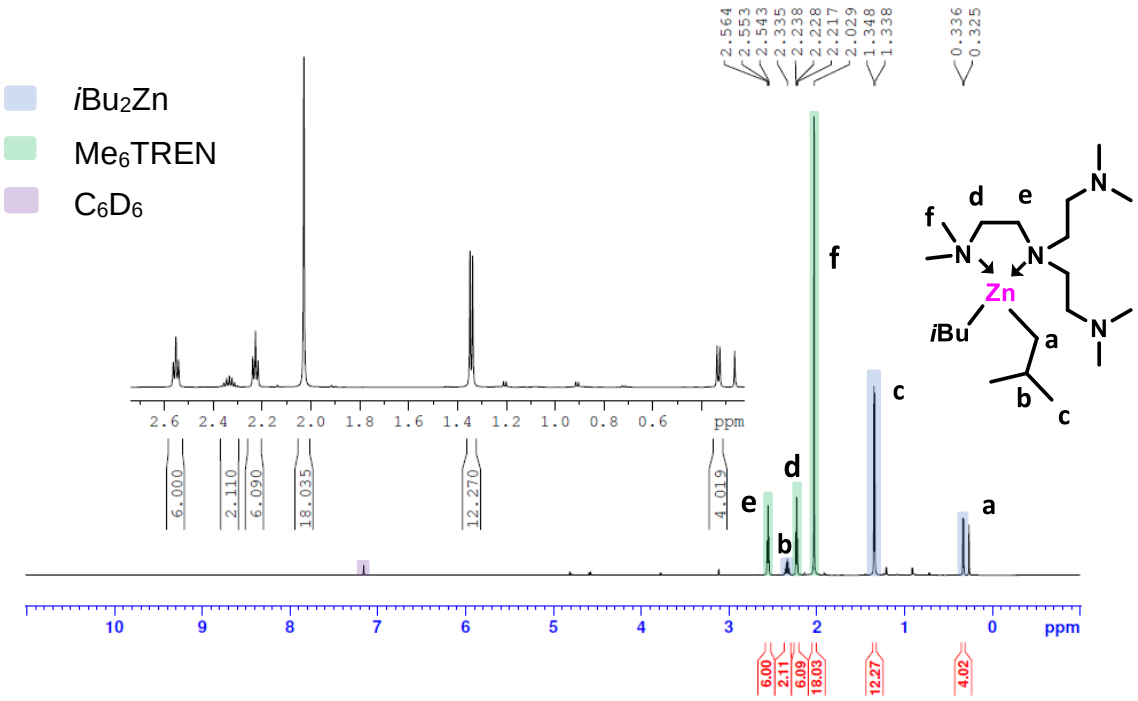

Figure 2.19 – ^{1}H NMR spectrum acquired in C_6D_6 of *i*Bu_2Zn·Me_6TREN

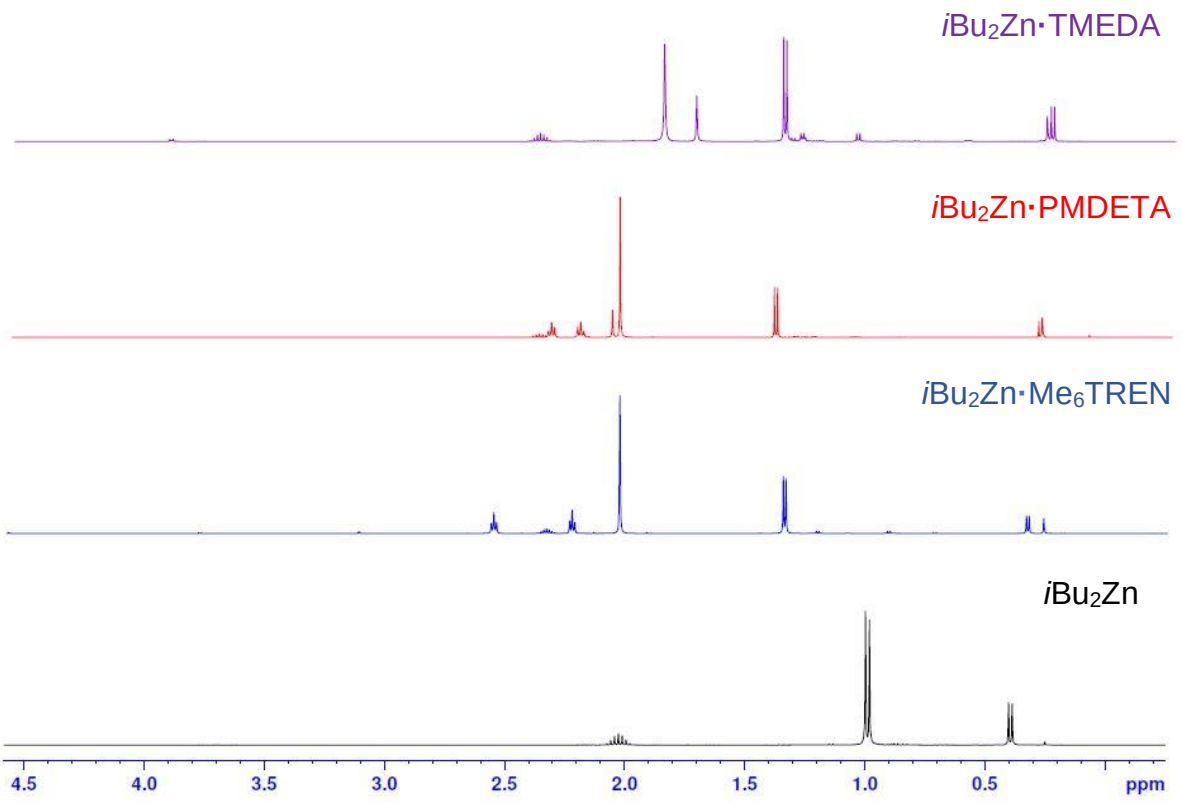

Figure 2.20 – Overlapping ^{1}H NMR spectra of *i*Bu_2Zn·(donor)

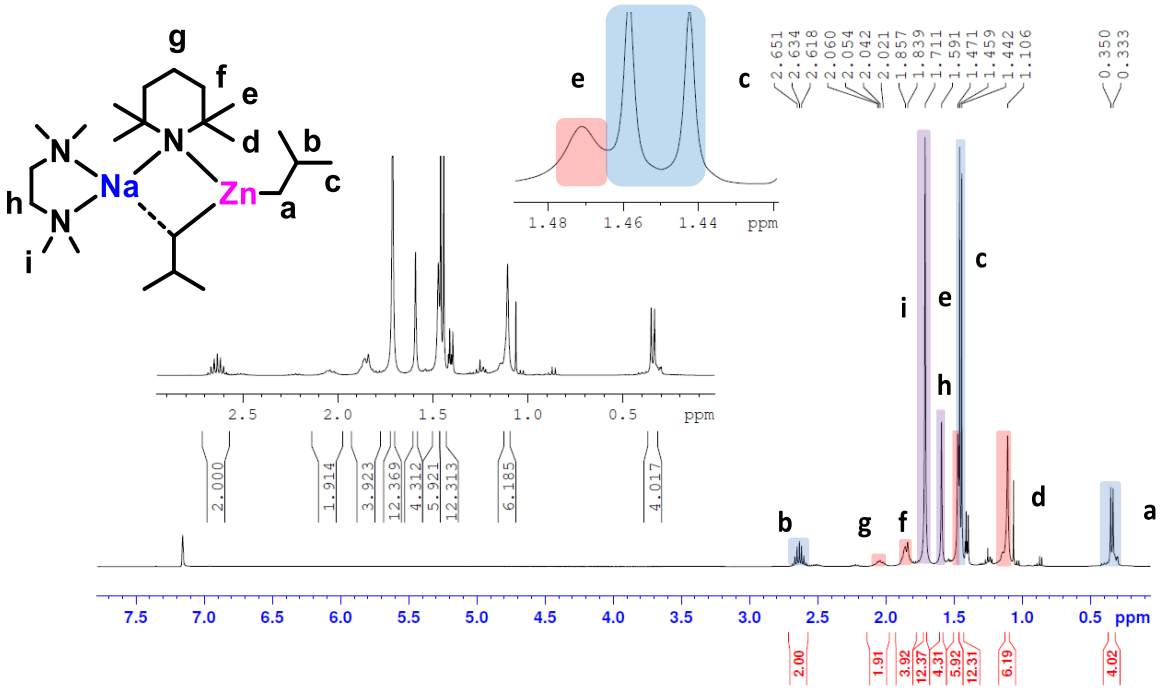

Figure 2.22 – ^{1}H NMR spectrum acquired in C_6D_6 of **7** (Shown in blue – *i*Bu_2Zn, purple – TMEDA and red – TMP)

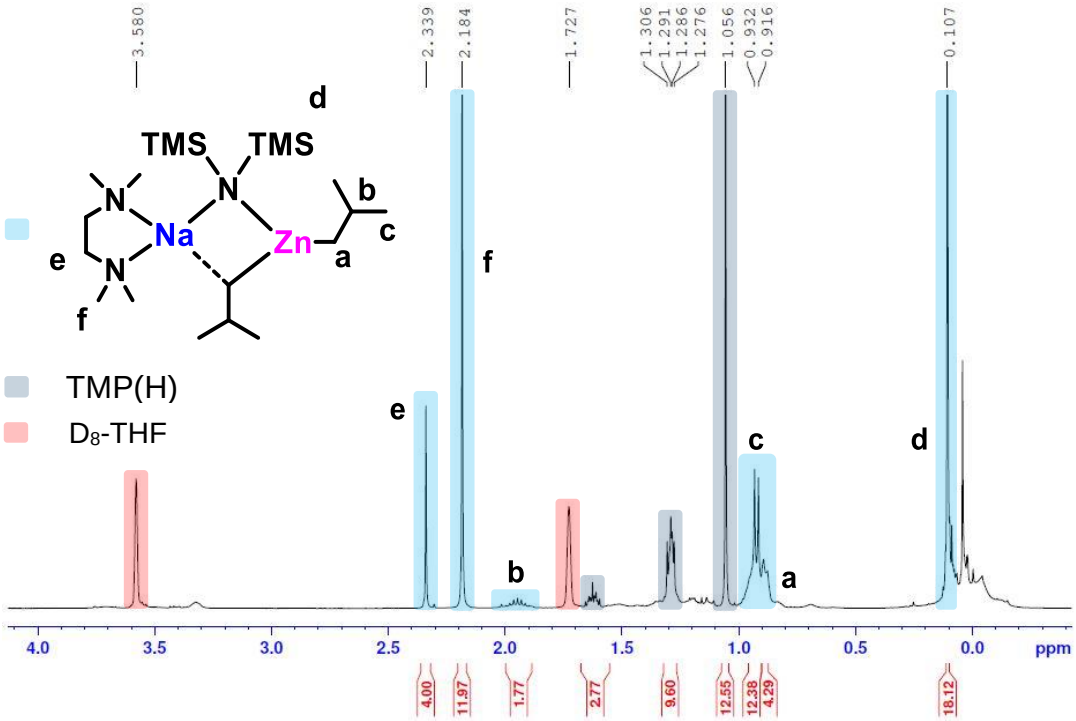

Figure 2.23 – ^{1}H NMR spectrum acquired in D_8-THF obtained from the reaction of **7** with HMDS(H)

2.5 X-Ray Structures

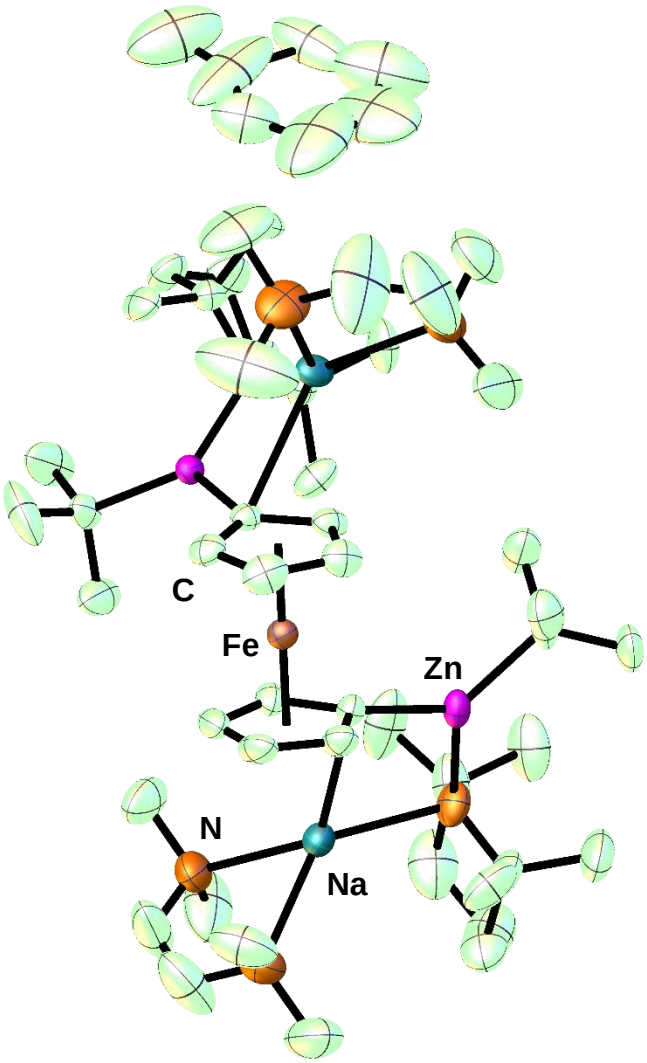

Figure 2.3 – Molecular structure of [TMEDA·Na(*μ*-TMP)Zn(*t*Bu)]$_2$(C_5H_4)$_2$Fe·C_7H_8 (**3'**). Ellipsoids are shown at 50% probability and all hydrogen atoms and minor disordered components have been removed for clarity.

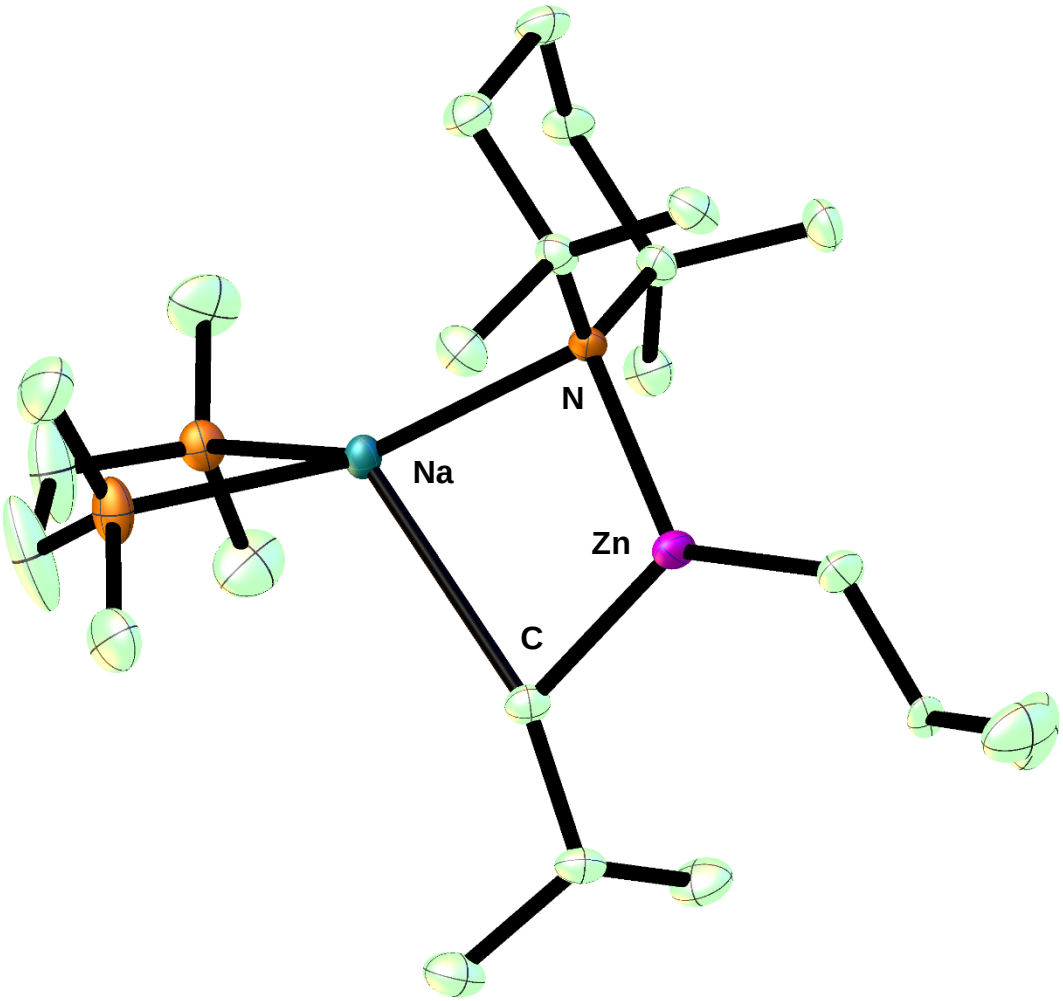

Figure 2.21 – Molecular structure of complex **7**. Ellipsoids are shown at 50% probability and all hydrogen atoms and minor disordered components have been removed for clarity.

2.5 Conclusions

From previous studies it was shown that the NaTMP/*t*Bu_2Zn pairing can perform an unprecedented tetrazincation of ferrocene in the form of $Na_4(TMP)_4Zn_4(tBu)_4[(C_5H_3)_2Fe]$. Attempts to use this compound as an intermediate for the synthesis of tetrasubstituted ferrocenes proved problematic. Attempts to quench this compound using I_2 and CO_2 were made. However, the product mixtures from these reactions proved to be confusing and inconclusive. More success was seen when this compound was quenched with D_2O. Evidence in the form of NMR and GC-MS spectra indicate the formation of the desired D_4-ferrocene. However, this work could be continued through the use of different quenching protocols, where THF and N-Boc pyrrolidine could be used.

Previous studies had also shown that when the tetrametallated ferrocene complex is reacted with pyridine, a polymeric γ-metallated pyridine species is formed via dual TMP/ferrocenyl basicity which is in contrast to its reactivity towards toluene where peripheral *t*Bu basicity is preferred. However, this polymer was only acquired in an initial crystalline yield of 5%. This yield was improved upon, going from 5% to 29%. It was originally thought that this reaction metallates pyridine at exclusively the γ-position. This study has now shown that this process is more complicated than originally thought. I_2 quenching of an *in-situ* reaction of $Na_4(TMP)_4Zn_4(tBu)_4[(C_5H_3)_2Fe]$ with pyridine confirmed that that this reaction does not metallate pyridine exclusively at the γ-position like previously believed, but also metallates the heterocycle at the β-position. Attempts to metallate the related heterocycle 2-picoline were made and while no crystalline material could be obtained, NMR spectroscopic evidence suggests metalation of the methyl group was preferred over ring metalation.

The synthesis of *i*Bu_2Zn has been successfully developed and has been found to be reproducible, with the highest yield obtained of this oil being 95%. The

donors TMEDA, PMDETA and Me_6TREN were employed in an attempt to aid crystallisation of this organozinc species as a Lewis base solvated adduct to no avail. Previous work had shown that the highly useful sodium zincate species TMEDA·Na(*μ*-TMP)(*μ*-*t*Bu)Zn(*t*Bu) can be crystallised and is synthesised using difficult to prepare and handle *t*Bu_2Zn as a starting material. The *i*Bu analogue of this sodium zincate was synthesised and a crystal structure of this obtained, giving the desired TMEDA·Na(*μ*-TMP)(*μ*-*i*Bu)Zn(*i*Bu) in a 56% yield. This compound was then tested in a series of reactions in order to form a comparison with TMEDA·Na(*μ*-TMP)(*μ*-*t*Bu)Zn(*t*Bu), but was found to be less powerful than its *t*Butyl equivalent.

Chapter 3: A Study of a Polymeric Sodium Zincate and its Role in Catalysis

3.1 Introduction

It was recently shown that the potassium zincate $KZn(HMDS)_2Bn$ (**8**) can be used for the direct functionalization of the benzylic C-H bond of diarylmethanes, with the proposed mechanism for this shown in Scheme 3.1. This was reported to be the first catalytic benzylic C-H bond addition of diarylmethanes to styrenes and conjugated dienes. This process makes use of **8**, generated from benzyl potassium and a zinc bis-amide, as a catalyst.[115]

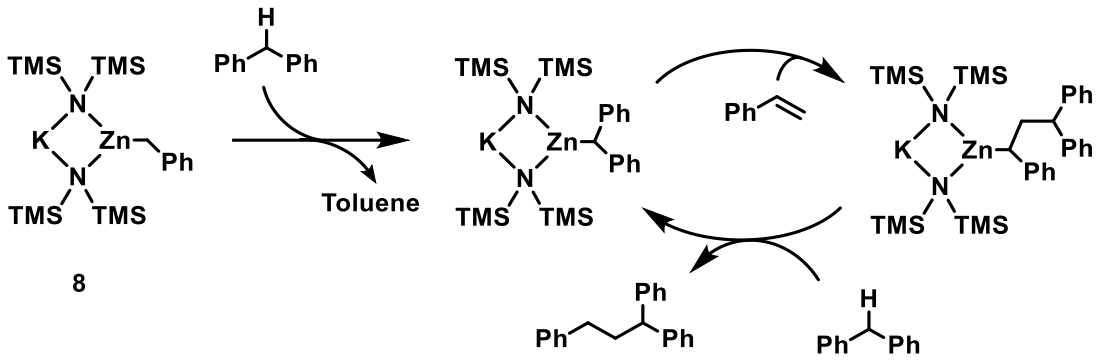

Scheme 3.1 – Simplified representation of the catalytic cycle utilising the potassium zincate **8** as suggested by Guan *et al.*

Surprisingly, when exploring the literature for metallated diphenylmethyl compounds, there were only a few examples.[116–119] Displayed in figure 3.2, are the most relevant structures.

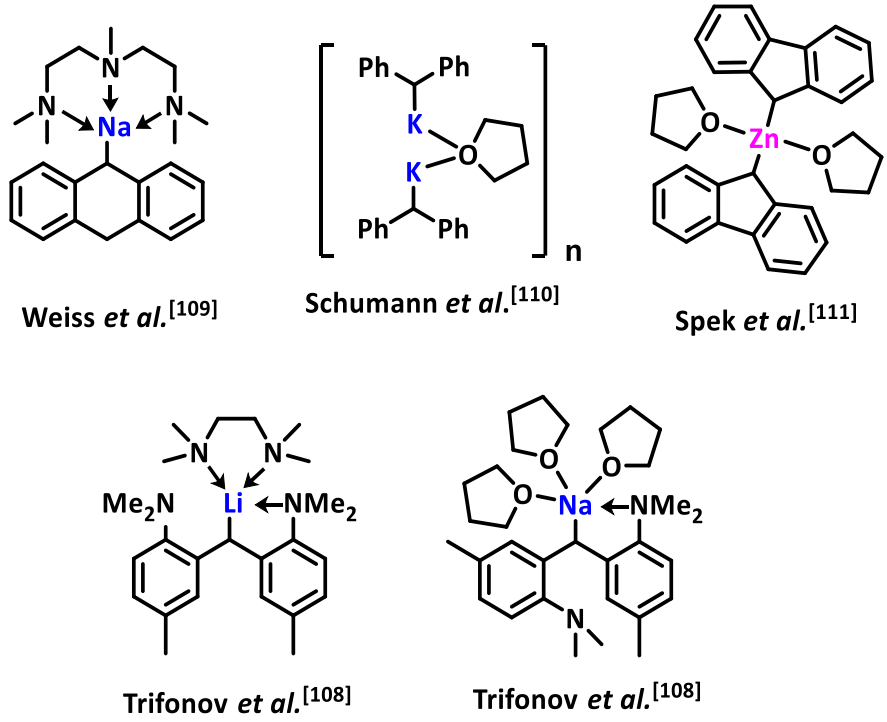

Figure 3.1 – Crystallographically characterized examples of diphenylmethane systems metallated at the benzyl position by an alkali metal

Studies performed by Mulvey *et al.* had previously found that **8** is actually a polymeric species [120] and not a monomer as depicted in scheme 3.1. It was shown that the potassium centre exhibits π bonding to the phenyl ring of another equivalent of zincate, creating a polymeric species, shown in figure 3.2.

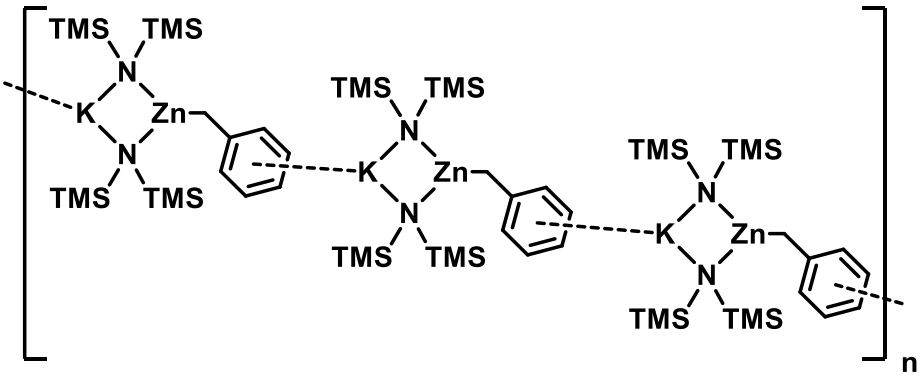

Figure 3.2 – True representation of **8** as a polymeric complex

Previous studies that were conducted within the groups of Mulvey and Robertson have shown that tris[2-(dimethylamino)ethyl]amine (Me_6TREN) can be employed as a useful donor when investigating the relationship between alkali metals and their σ and π modes of bonding.[121–124] Me_6TREN was used due to its versatile denticity, meaning it could encapsulate a range of alkali metals, but leaving space for coordination of the anion.[122] This study focused on the metallation of toluene using the organometallic compounds of the alkali metals to give benzyl-Li (**9**), -Na (**10**) and -K (**11**), with Me_6TREN capping the metal centre (shown in figure 3.3). The solid-state structure shows that complex **9** is a discrete monomeric unit. However, the lithium centre adopts an unusual five-coordinate environment. The structure contains a Li-C σ bond and importantly shows no significant interactions between the metal and the phenyl ring. Similarly, to **9**, the molecular structure of **10** is monomeric with a five-coordinate trigonal-bipyramidal metal centre. The principal difference however, is that although the sodium cation appears to be σ-bonded to the carbanionic centre, it has started to migrate towards the aromatic ring. This is clearly supported by the alteration in the benzyl carbon-metal bond (103.3(1)^o in **10**, vs 133.4(2)^o in **9**), which brings the metal into much closer proximity of the ipso-carbon atom and to a position where π-bonding interactions could participate.

The molecular structure of **11** proved the metal-ligand bonding interaction to be different in comparison to compounds **9** and **10**. Mimicking **9** and **10**, the Me_6TREN ligand in **11** coordinates to the metal centre in a η^4 manner by means of its four nitrogen lone pairs. Surprisingly, the potassium cation shows no interaction with the CH_2 arm, but rather has migrated to bind exclusively to the delocalized π system of the aromatic ring, leaving a “naked” CH_2 head. In a further investigation, performed by Robertson *et. al.* it was found that when a secondary metal is introduced to compound **11** (*t*Bu_2Zn was used in this example), the zinc is bonded to the methyl arm, resulting in the formation of *t*$Bu_2ZnCH_2PhK{\cdot}Me_6$TREN (**12**). This results in a relocalisation of the electron

density from the ring system to the now sp^3 methylene carbon, whilst also leaving the K-Ar interaction intact (although longer), meaning the resulting complex can be considered a true potassium zincate since the zinc is now surrounded by three alkyl anions.[125]

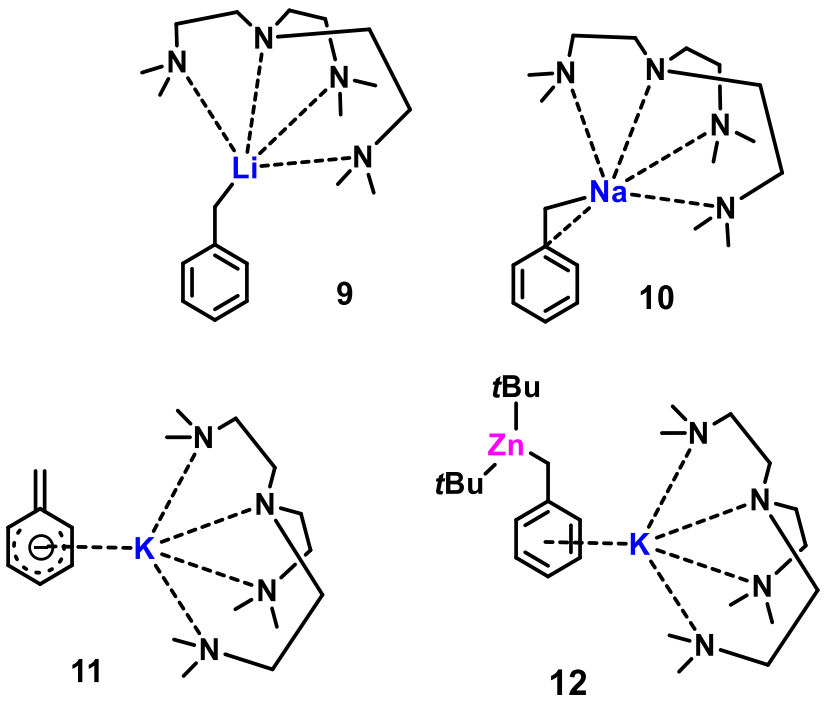

Figure 3.3 – Simplistic representation of the "slipping" of the alkali metal in a benzylic system in the presence of Me_6TREN

3.2 Aims

The main aims of this work were as follows:

- To isolate and characterise the metallated diphenylmethyl system - $[\{KZn(HMDS)_2(CHPh_2)\}_\infty]$ - proposed to be the intermediate in the investigations performed by Guan *et al.*
- To investigate how the potassium atom in $[\{K(HMDS)_2ZnBn\}_\infty]$ primarily interacts with the zincate component when its polymeric nature is disrupted.

3.3 Results and Discussion

One of the main aims of this project was to isolate and characterize the diphenylmethyl potassium zincate intermediate complex suggested in the paper by Guan *et al*. This structure is shown in figure 3.4. One potential method of achieving this was to mix compound **8** with diphenylmethane as shown in the suggested mechanism shown by Guan. This was done by mixing the aforementioned compounds in a J. Young's tube followed by addition of d_8-THF. The reason for the use of d_8-THF was to ensure that the compounds were fully dissolved for the reaction. The aim was for the reaction to stop at the generation of $KZn(HMDS)_2(CHPh_2)$ **13**, and yield the suggested intermediate compound.

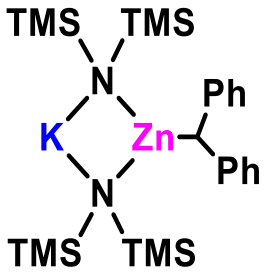

13

Figure 3.4 – The structure of the intermediate compound proposed by Guan *et al.*

A ^{1}H NMR spectrum was then obtained and it shows that there was no reaction. The conditions that Guan *et al*. had used included heat, so heat was then applied to the J. Young's tube and another ^{1}H NMR spectrum obtained. However, again there appeared to be no reaction taking place. This spectrum is shown in figure 3.5 in section **3.4**.

There was no indication that compound **13** was actually isolated during their investigation. So, the exact conditions used by Guan were then employed. This included changing the solvent from THF to benzene and heat was applied to this system throughout the reaction. This was left heating overnight before obtaining a ^{1}H NMR spectrum, shown in figure 3.6 in section **3.4**. Focusing on the region between 2-4 ppm of this spectrum suggested that the desired reaction could be taking place.

Following this observation, the J. Young's tube was left to heat for another night, before another ^{1}H spectrum was obtained, shown in figure 3.7 in section **3.4**. There was an unexpected situation in the 2-4 ppm region. The resonance thought to correspond to the C-H bridge of compound **13,** had all but disappeared.

Upon inspection of the Young's tube at this point, a crystalline material could be seen present in the tube, as well as a large amount of a yellow/orange solid. It was speculated that the crystalline material that was observed could have been the diphenylmethyl potassium zincate intermediate complex suggested in the paper by Guan *et al*. Unfortunately, this sample decomposed before X-ray analysis of the crystals could be attempted and due to time constraints, this could not be repeated. This decomposition could have resulted from hydrolysis of the sample as it was waiting for analysis.

Me_6TREN would then be introduced to **8** as previously mentioned, with the aim of investigating whether the tetradentate donor would encapsulate the potassium centre with the potassium remaining σ-bonded to the nitrogen atoms or bonding to the π-system, thus leading to a similar structure to **11**. The synthesis of **8** was achieved by the canula transferral of a toluene solution of $Zn(HMDS)_2$ into a toluene suspension of benzyl potassium,[2] which was confirmed by ^{1}H NMR spectroscopy of the resulting white precipitate. 1 equivalent of Me_6TREN was then slowly introduced to this compound until a

dark solution was obtained. This was found to crystallise at -33ºC and the structure of this compound was determined using X-ray diffraction and shown to be that of the desired compound $(HMDS)_2ZnCH_2PhK{\cdot}Me_6TREN$ (**14**), shown in figure 3.8 in section **3.5**.

Firstly, it should be noted that the obtained structure is rather similar to that of **11** and **12**, with a molecule of $(HMDS)_2Zn$ bound to the methylene arm. A slight degree of disorder is present on the benzyl ring, which was also seen for **11**. However, there appears to be no disorder shown throughout the rest of the compound. The Me_6TREN ligand ligates to the potassium in a η^4 manner through the four nitrogen lone pairs. This saturation of the metal centre successfully prevents polymerisation of this molecule, as seen in previous studies. Similarly, to **11**, the Me_6TREN solvated potassium cation shows no interaction with the CH_2 anion but binds exclusively to the delocalized π system (C-K distance = 3.097(4) - 3.250(4) Å, average 3.156 Å).

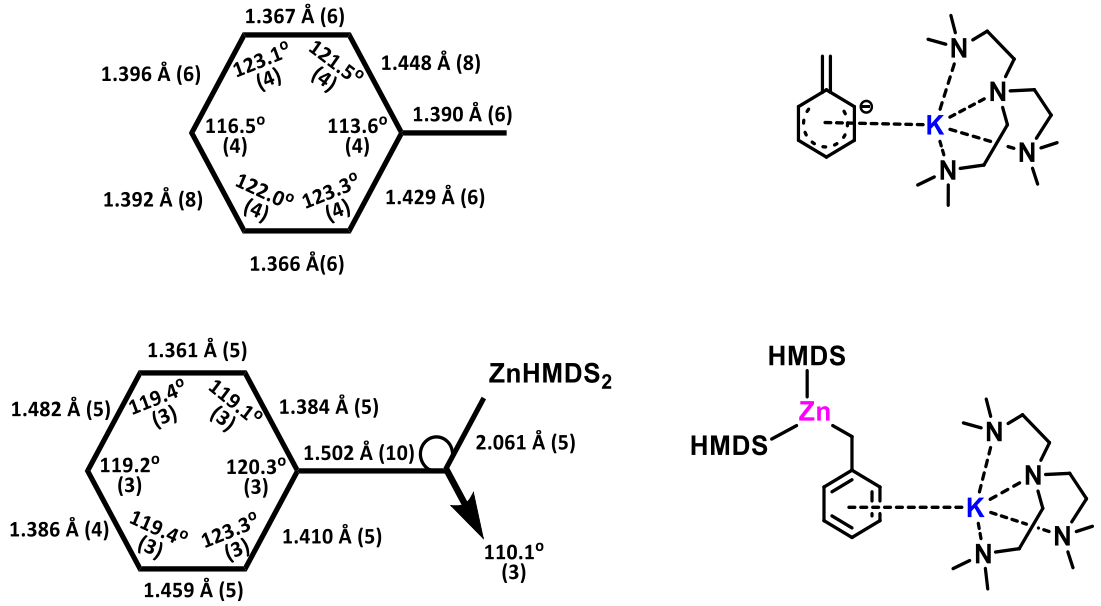

Figure 3.9 – Comparison of the bond lengths and angles between compounds **11** and **14**

The bond distances of compounds **11** and **14** are compared in figure 3.9. These distances can be seen in table 3.1.

Table 3.1 – Selected bond lengths between three similar compounds containing a $Me_6TREN{\cdot}KPhCH_2$ unit

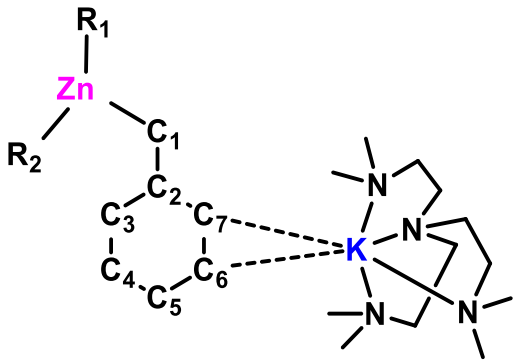

	Bond lengths of 11 (Å)	Bond lengths of 12 (Å)	Bond lengths of 14 (Å)
K-C1	3.893 (4)	3.767 (4)	4.146 (1)
K-C2	3.098 (4)	3.044 (3)	3.202 (1)
C1-C2	1.390 (6)	1.469 (5)	1.502 (10)
K-N1	2.815 (3)	2.848 (2)	2.830 (9)
K-N2	2.838 (3)	2.798 (3)	2.779 (10)
K-N3	2.822 (3)	2.826 (3)	2.794 (10)
K-N4	2.919 (3)	2.806 (3)	2.786 (10)
K-Ar	2.830 (1)	2.868 (1)	2.840 (1)
Zn-C1	-	2.109 (4)	2.060 (5)
Zn-R1	-	2.044 (3)	1.980 (8)
Zn-R2	-	2.045 (3)	1.947 (8)

It can be seen that there is an elongation of the C1-C2 bond upon coordination of the CH_2 unit to zinc. This could in part be due to the presence of the zinc within the compound helping to localize the electron density away from the ring system and back on to the methylene carbon atom altering this bond from sp^2 to a sp^3 hybridisation. This withdrawal of electron density away from the ring and back to the C2 atom then has an effect on the K-Ar bond distances. This can be seen as a slight elongation of the distance between the potassium atom to the centre of the aromatic ring, going from 2.830(1) Å in **11**, compared to 2.840(1) Å in **14**.

Table 3.2 – A comparison of the NMR shifts of the aromatic protons and the CH_2 protons between complexes **11**, **12** and **14**

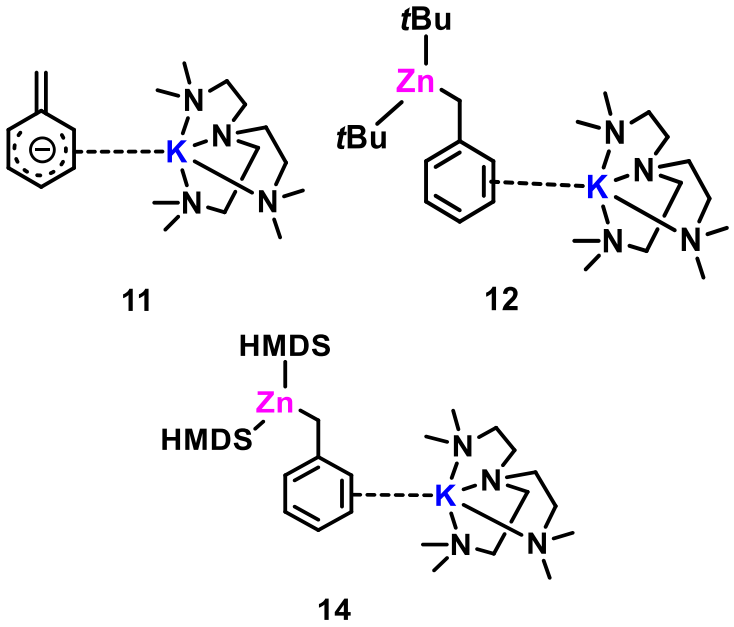

11 12 14

	11	12	14
Ortho	6.16	7.05	7.22
Meta	6.56	6.85	6.92
Para	5.24	6.29	6.48
CH_2	3.21	2.32	2.08

Shown in table 3.2 is some selected ^{1}H NMR chemical shift data in C_6D_6. There are two main trends that can be observed from the data shown. Firstly, it can be seen that the *ortho*, *meta* and *para* resonances shift further downfield towards the aromatic region in the zinc containing compounds. Secondly, it is observed that the resonance that corresponds to the CH_2^- shifts further upfield towards the alkyl region of the spectrum in the zinc containing compounds. These values are all consistent with re-localization of the negative charge onto the methylene group as part of a zincate complex, resulting in a more typical benzyl anion. One conclusion that can be drawn from obtaining this structure and observing the connectivity of the atoms is that the preference of the potassium to be bonded to the π-system should be shown in the polymeric species.

This study was concluded with the synthesis of diphenylmethyl potassium. This was achieved by LiCKOR superbase deprotonation of diphenylmethane and utilising Me_6TREN to cap the potassium atom. This reaction yielded a batch of crystals, which were of sufficient quality for X-ray analysis. The structure obtained was of $Ph_2CHK{\cdot}Me_6TREN$ (**15**), shown in figure 3.10 in section **3.5**.

This structure is very similar to the aforementioned structure in the introduction reported by Schumann *et al*., $[(Ph_2CHK)\{THF\}_{0.5}]_\infty$. A selection of bond lengths and angles have been summarised in table 3.3.

Table 3.3 – Selected bond lengths (Å) and angles (°) of **15** and the $(Ph_2CHK)_2 \cdot THF$

	$[(Ph_2CHK)_2 \cdot THF]_n$	**15**
K-C_1	3.003 (5)	2.948 (7)
C_1-C_2	1.441 (7)	1.432 (12)
C_1-C_3	1.429 (8)	1.448 (12)
C_2-C_1-K	86.4 (3)	87.2 (4)
C_3-C_1-K	101.1 (1)	79.3 (4)
C_2-C_1-C_3	132.1 (5)	131.5 (9)

In general, the bond lengths and angles between these two compounds are in good agreement, with the exception of the C_3-C_1-K angle. In the THF-solvated polymeric potassiated diphenylmethyl complex, this angle was 101.1(1)° as compared to **15** where it is 79.3(4)°. This is potentially a consequence of the monomerization occurring in **15** since the presence of adjacent diphenylmethyl ligands in the THF-solvated polymer prevents the potassium from adopting its preferred position with a similar interaction to each aromatic ring. The structure of **15** suggests that the negative charge of the ligand is likely delocalized through both rings.

3.4 NMR Data

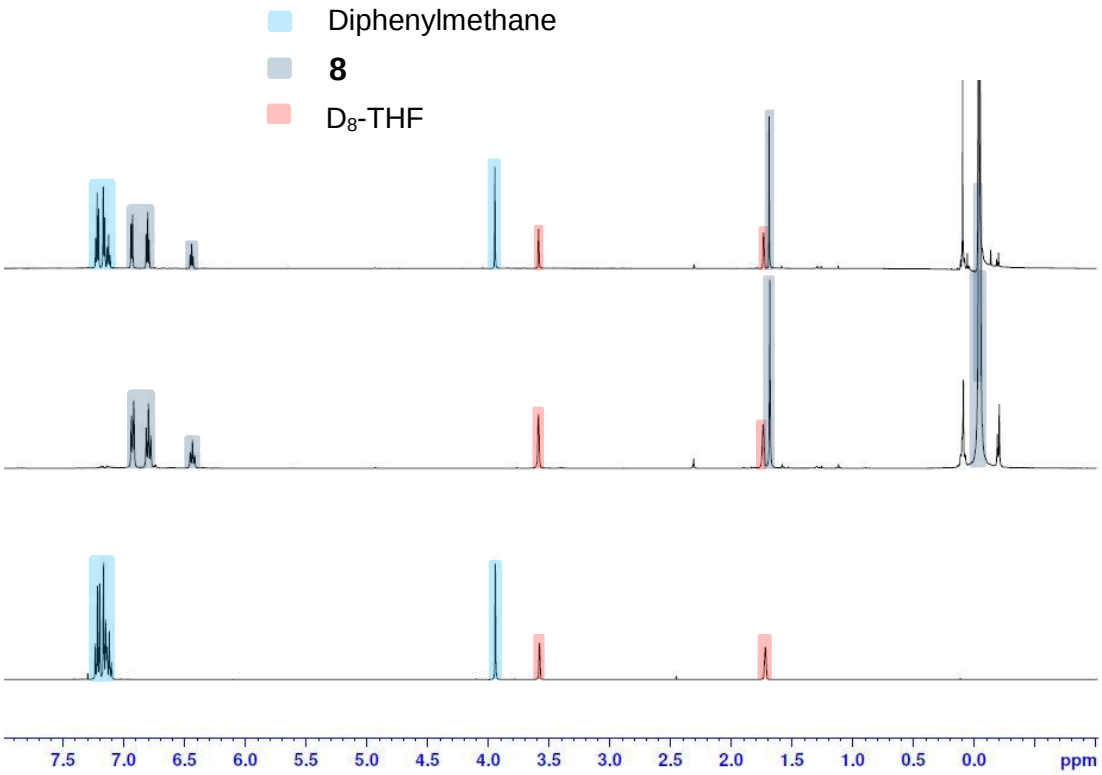

Figure 3.5 – Overlapping ^{1}H NMR spectra obtained in D_8-THF displaying the reaction mixture (top), a standard of **8** (middle) and a standard of diphenylmethane (bottom)

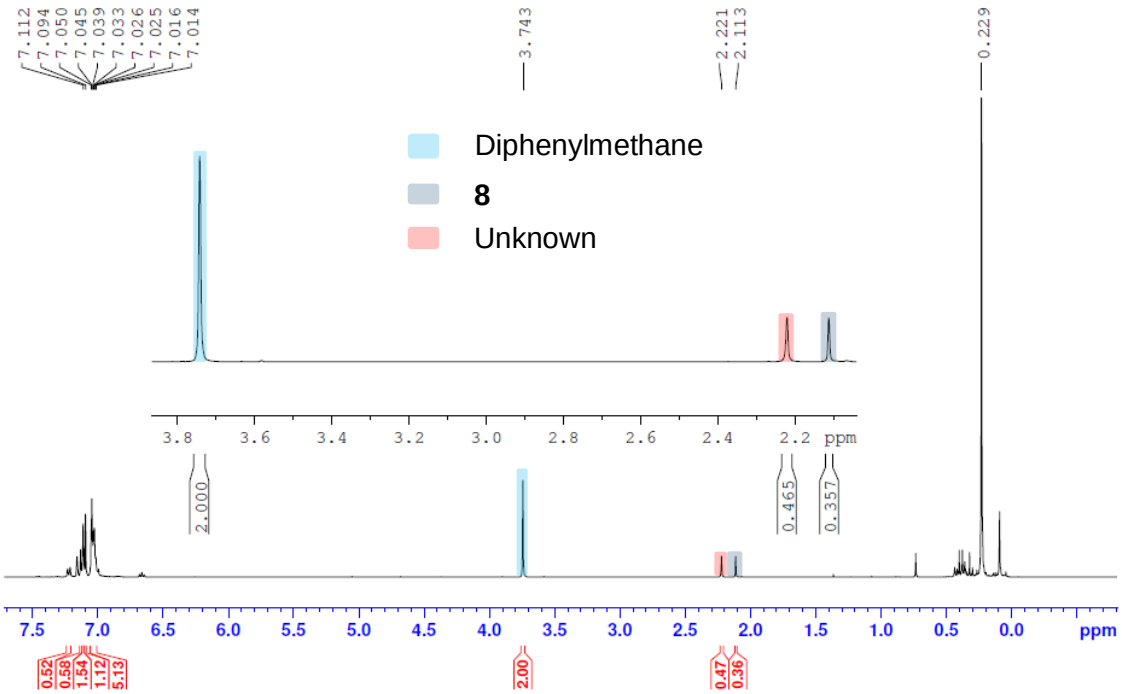

Figure 3.6 – ^{1}H NMR spectrum obtained in C_6D_6 from the reaction of **8** with CH_2Ph_2 after one night of heating

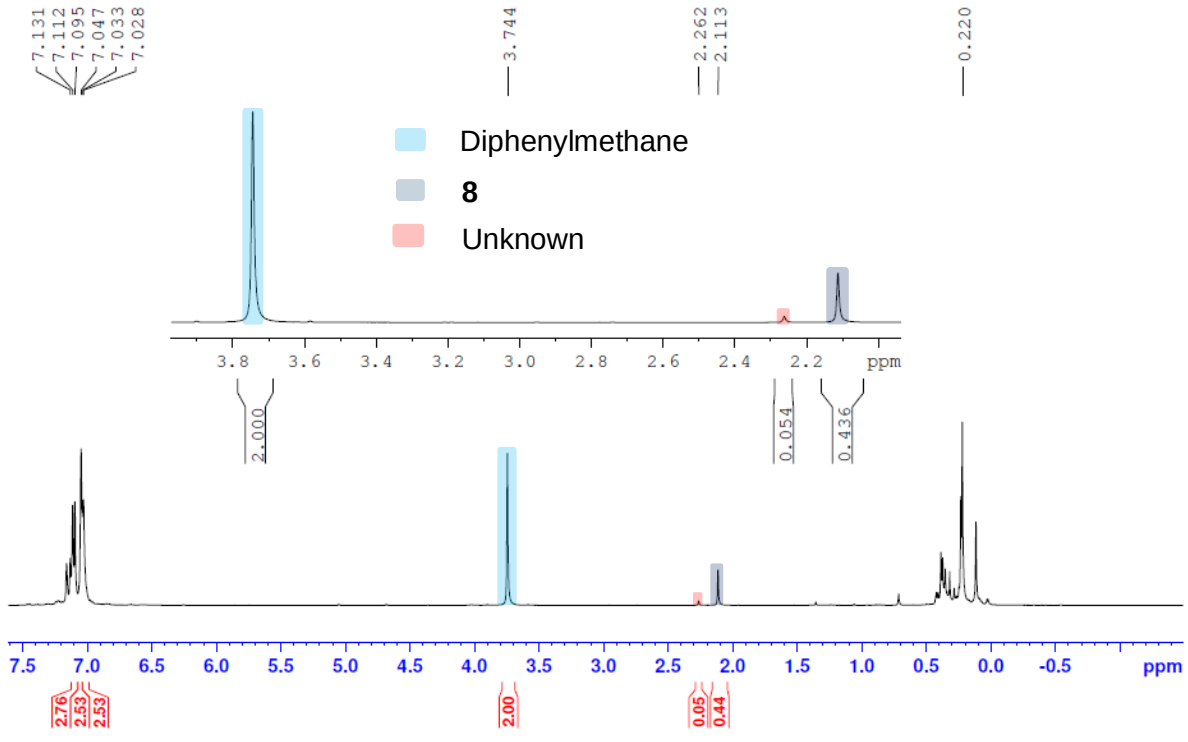

Figure 3.7 – ^{1}H NMR spectrum obtained in C_6D_6 from the reaction of **8** with CH_2Ph_2 after 48 h of heating

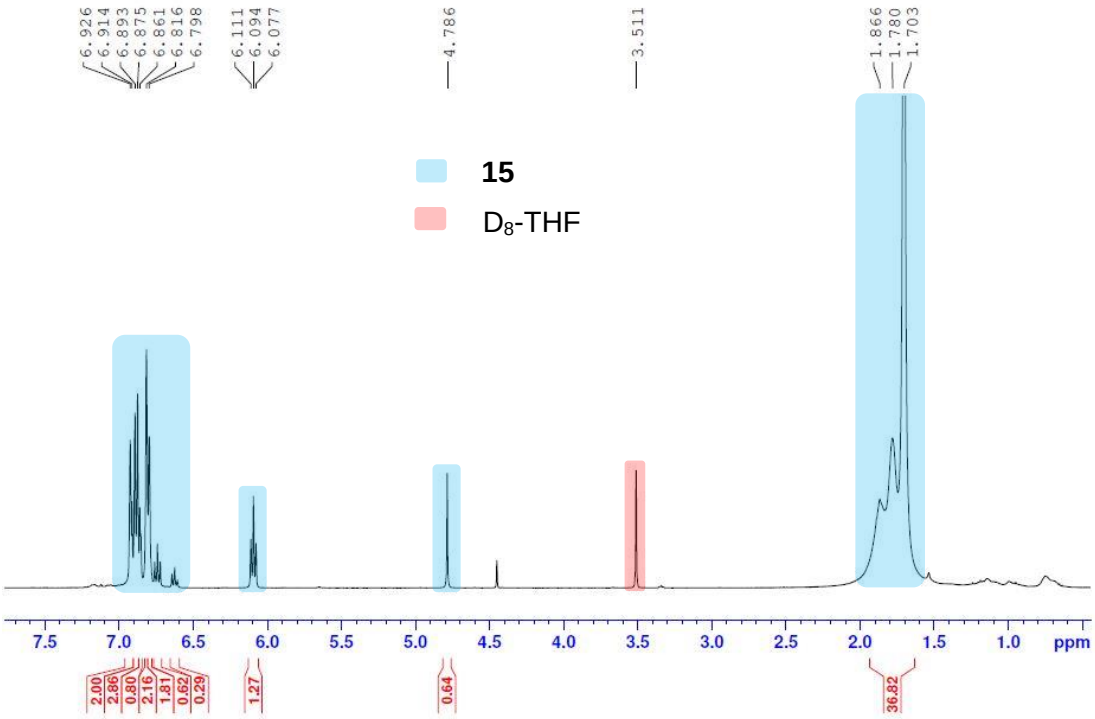

Figure 3.11 - ^{1}H NMR spectrum obtained in D_8-THF of **15**

3.5 X-Ray Data

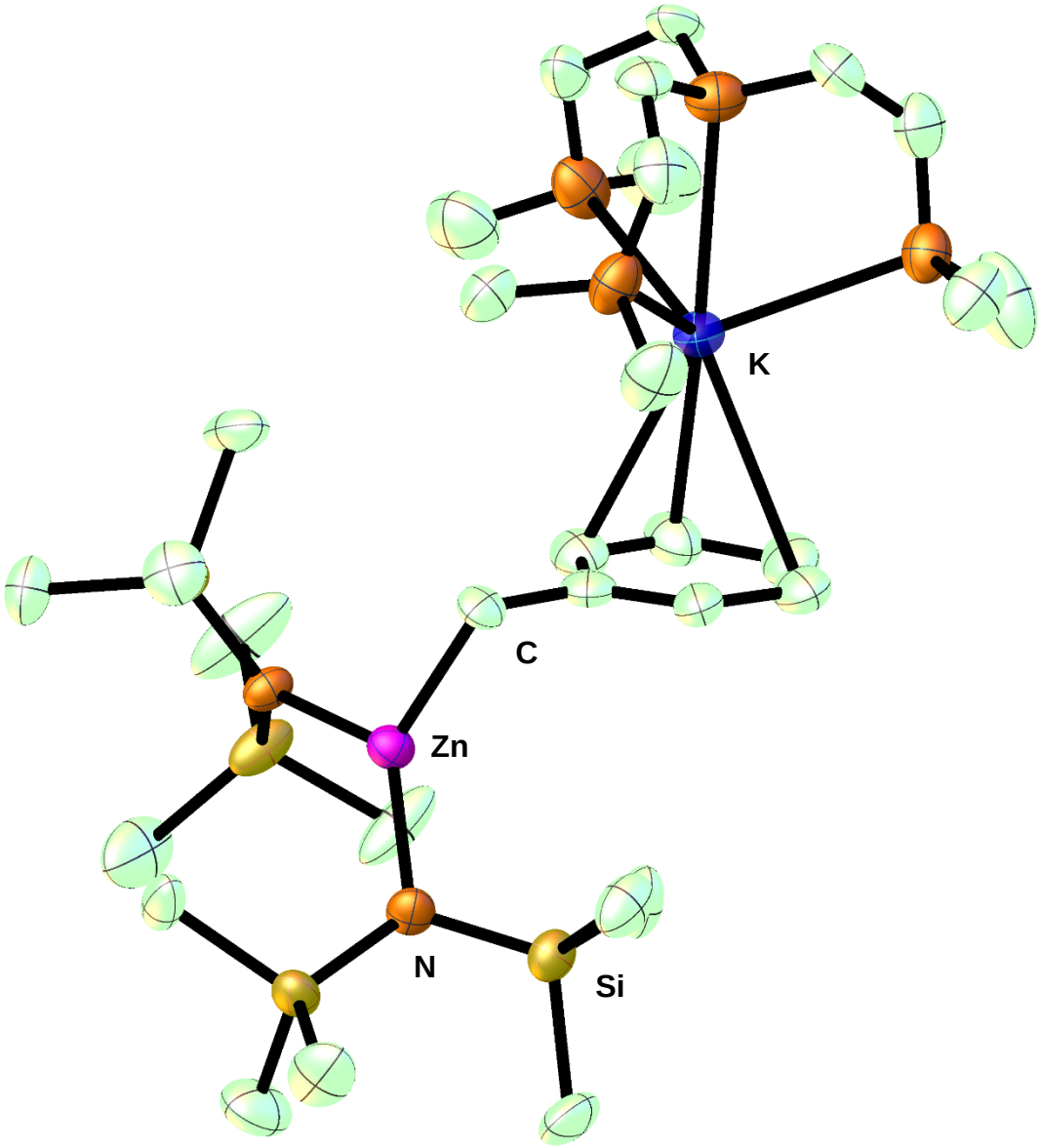

Figure 3.8 – Molecular structure of $(HMDS)_2ZnCH_2PhK{\cdot}Me_6TREN$ (**14**). Ellipsoids are shown at 50% probability and all hydrogen atoms and minor disordered components have been removed for clarity

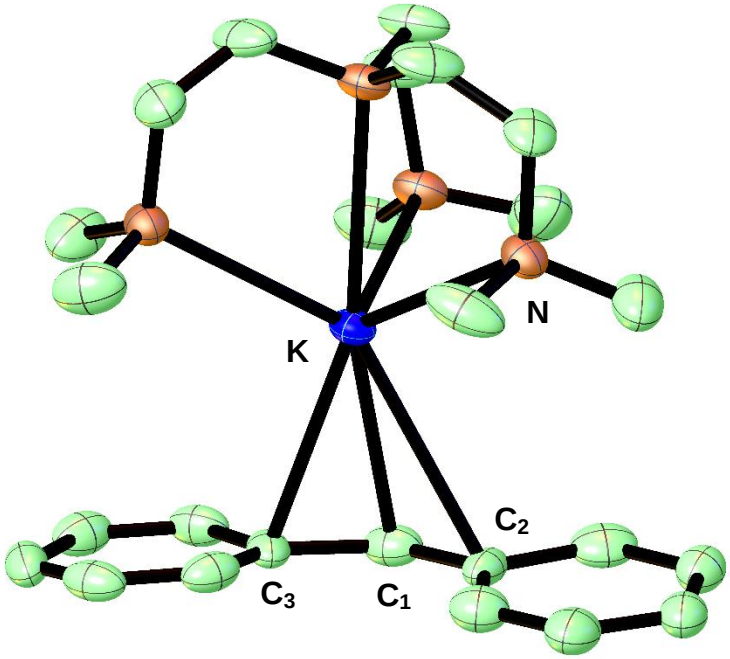

Figure 3.10 – Molecular structure of $Ph_2CHK \cdot Me_6TREN$ (**15**). Ellipsoids are shown at 50% probability and all hydrogen atoms and minor disordered components have been removed for clarity

3.4 Conclusions

One of the aims of this project was to isolate and characterise the polymeric potassium zincate [{K(HMDS)$_2$ZnCHPh$_2$}$_\infty$] - proposed to be the intermediate in the investigations performed by Guan *et al.* Despite there being promising signs of achieving this, due to time constraints, this ultimately was not achieved. During this project crystals had formed of a compound that could have been the desired potassium zincate complex. However, this sample had decomposed before analysis of this sample could be attempted.

The second main aim of this section was to investigate how the potassium atom in [{K(HMDS)$_2$ZnBn}$_\infty$] primarily interacts with the zincate component by disrupting its polymeric nature. This was achieved using the highly effective monomerizing agent Me$_6$TREN. This study confirms that when Me$_6$TREN is introduced to the system, the potassium atom preferentially coordinates to the delocalised charge within the aryl ring rather than the localised charge of the amido nitrogen centres of the HMDS ligands, clipping the potassium-nitrogen bonds and having the potassium cap the π-system. A slight degree of disorder is present on the benzyl ring. However, there is no disorder shown through the rest of the compound. The size of Me$_6$TREN allows for the complete saturation of the potassium atom. This saturation successfully deaggregates the polymeric material and prevents polymerisation of this molecule. It did also prove possible to prepare and crystallographically characterize a rare example of a diphenylmethylpotassium monomer, also solvated by Me$_6$TREN. With this material to hand, it is hoped that in the future an authentic crystalline sample of K(HMDS)$_2$ZnCHPh$_2$ will be obtained.

Chapter 4: Closing Reflections

Despite being known since the 19th Century and comprehensively studied during the 21st century, it is clear that bimetallic 'ate' bases in general (and sodium zincate bases in particular) will continue to conjure up new and exciting chemistry in both stoichiometric transformations and catalytic processes. This latter type of reactivity is particularly important going forward as the main group positions itself to take advantage of its abundance and cost advantage over the most popular and already well-established transition metals in catalysis. While only scratching the surface, the work contained within this thesis has attempted to shed some more light on our understanding of the synthesis and reactivity of sodium zincate bases. For example, it is sensible to consider the environmental impact of our actions and so developing safer and simpler processes such as the synthesis of *i*Bu_2Zn is worthy of attention, even if ultimately it proved to be less potent when incorporated into a sodium zincate base. Likewise, functionalized ferrocene molecules are potentially important precursors in materials chemistry and so understanding how we can take an inexpensive substrate like ferrocene and then metallate and functionalize it is an important endeavour.

Although the work performed within this thesis is small in the overall grand scheme of research, it has still advanced our understanding of the field as highlighted in the fact that this work has been included in two published articles in international journals, these being Chem. Sci. and ZAAC. This is key to research; a continued everlasting effort towards the advancement of our knowledge and understanding. The work in this thesis has been built upon previously investigated areas and activities, such as the two-step mechanism or the functionalisation of ferrocene. The work put forth in this thesis could hopefully be built upon in a similar manner to lead to new discoveries.

Chapter 5: General Experimental Techniques and Procedures

5.1 Schlenk Techniques

Organometallic reagents are generally reactive in open air, with the classical example of *t*BuLi being pyrophoric in air. Therefore, to circumvent the pyrophoric nature of certain reagents and the degradation of others, all synthetic work was carried out under the use of standard Schlenk techniques.

All synthetic work was performed using a Schlenk line. A Schlenk line is a glass manifold, shown in figure 5.1, which consists of a two-part manifold which is connected to a vacuum pump and a continuous inert gas flow. The use of a stopcock in the manifold can dictate whether a vacuum or an inert gas is applied to the Schlenk flask. There is also a trap located between the manifold and vacuum pump, which can be cooled to sub-ambient temperature using liquid-nitrogen to prevent any volatile materials entering the pump. The second part of the manifold is a continuous flow of inert gas, which is bubbled through oil to ensure that the flow can be observed by the user. This continuous flow exits the manifold via the outlet, preventing pressure build up.

A Schlenk flask is fitted with a stopper and a tap in the sidearm. The sidearm is connected by rubber tubbing to the manifold. The purpose of the tap is to allow for the control of the applied vacuum or gas to the Schlenk flask. The stopper and tap also had vacuum grease applied to them, to prevent any unwanted air or moisture entering the flask. The flow of nitrogen gas was maintained throughout all experiments. This included the addition of reactants and solvents and the purging of needles. The flow of nitrogen was increased when it was necessary for a piece of glassware to be removed, such as when adding a solid to the system via a solid addition tube, as this would minimise the amount of air that would enter upon the removal of the apparatus.

Figure 5.1 – A typical Schlenk line on the benchtop

Prior to the use of any Schlenk flask, the flask should be allowed to dry thoroughly in an oven. All air and moisture must then be removed. This is achieved by applying vacuum to the flask for ten minutes. The flask is then filled with nitrogen gas. This was repeated a further two times to ensure a dry and inert atmosphere is obtained. Whenever a liquid had to be added to the flask, this was done by use of a syringe and needle, which had been purged with nitrogen gas prior to their use.

5.1 Use of Glovebox

For the storage and manipulation of air and moisture sensitive materials, a glovebox was employed. A typical glovebox consists of three chambers. However, the glovebox used for this work, had two chambers. There is the main chamber, where the physical manipulations are carried out. This main chamber has a gas recirculation and purification system, which ensures that there is constantly minimal amounts of air and moisture present. Manipulation of the materials is achieved through the use of semi-permeable gloves. The second chamber is smaller, this is the port. The port is used for the transport of chemicals and materials into and out of the glovebox. This port consists of two doors, an inner door to the main chamber and an outer door, which allows access to the environment. The outer door is opened and materials are placed into the port. The outer door is then closed and the port is purged through repeated flushing with nitrogen and evacuation under vacuum. Once this is completed, the user can then open the inner door from the inside and remove the materials into the main chamber. This entire process ensures that minimal exposure of the main chamber to air and moisture is achieved.

Figure 5.2 – An image of the glove box used for this work

5.1 Solvent and Reagent Purification

In all reactions that involved the use of *t*BuLi, a 1.7 M solution of *t*BuLi in pentane was used. In all reactions that involved the use of *n*BuLi, a 1.6 M solution of *n*BuLi in hexane was used. In all reactions that involved the use of *s*BuLi, a 1.4 M solution of *s*BuLi in cyclohexane was used.

Standardisation of organolithium reagents was performed under the following conditions. To an oven-dried round bottom flask was added menthol (0.156 g, 1 mmol), followed by 1,10-phenanthroline (3 mg). The flask was then purged to yield a nitrogen atmosphere and then dry THF (2 ml) was added. To the yellow tinged solution was added RLi dropwise until a persistent red colour was obtained and the volume of RLi used was recorded. This was repeated a further two times and the average volume of RLi calculated. From knowing the amount of menthol and the volume of RLi, the molarity of the RLi reagent used can be calculated.

Due to the extreme air and moisture sensitivity of the reactants and products, dried and degassed solvents were required. The solvents diethyl ether, THF, hexane and toluene were all used from stills within the laboratory. These solvents are placed under reflux conditions over sodium metal and benzophenone under a nitrogen atmosphere.[126] The sodium metal will react with the benzophenone, giving a blue ketyl radical anion. Hence, this blue colour can be used as an indicator of the state of the still. If there are sufficiently low amounts of moisture present, then the blue radical will persist. However, once the levels of moisture rise in the stills, the ketyl radical will react and the blue colour will gradually disappear over time. Once this blue colour has disappeared, it must be assumed that there are high levels of water present and the solvent should not be used. In the case of pentane, this solvent had to be freshly distilled in the laboratory and was then stored over microwave activated 4 Å molecular sieves and under argon in a sealed Schlenk flask.

For the purification of NMR solvents, a freeze-pump-thaw cycle was employed to remove any oxygen that may have been present.[126] The solvent was placed into a J. Youngs ampule and the flask was then closed using the tap. The flask is then lowered into liquid nitrogen to freeze it. The flask is then placed under vacuum and allowed to slowly rise to room temperature. This process was then repeated a further two times and the resulting solution was then stored over 4 Å molecular sieves. Commercially available reagents were purchased from Sigma Aldrich, Alfa Aesar or Fluorochem. Tetramethylpiperidine (TMP(H)) was purchased from Acros Organics.

5.4 Methods of Analysis

5.4.1 NMR Spectroscopy

All NMR spectra that were obtained throughout this project were obtained using a Bruker AV400 MHz spectrometer that operates at 400.13 MHz for ^{1}H NMR, 100.62 MHz for ^{13}C NMR and 155.50 MHz for ^{7}Li NMR.

When a DOSY NMR was required, this was performed on a Bruker AV400 operating at 400.13 MHz for proton resonance under TopSpin whilst being equipped with a BBFO-z-atm probe.

5.4.2 X-Ray crystallography

Crystallographic data was obtained using either a $Mo_{K\alpha}$ or a $Cu_{K\alpha}$ Oxford Diffraction instrument. The $Mo_{K\alpha}$ instrument operates at a wavelength of 0.71073 Å, whilst the $Cu_{K\alpha}$ instrument operates at a wavelength of 1.5418 Å. The structures were solved using either the SHELXL-2014/7 [127,128] or OLEX2 while refinement was carried out on F^2 against all independent reflections by the full matrix least-squares method using the SHELXL-2014/7 program or by using the GaussNewton algorithm for OLEX2.[129]

5.4.3 Gas Chromatography-Mass Spectrometry (GC-MS)

GC-MS data was collected using an Agilent Technologies 5975C GC-MS detector.

Chapter 6 Experimental

6.1 Preparation of Chapter 2 Compounds

Synthesis of TMEDA·Na(*μ*-TMP)(*μ*-*t*Bu)Zn(*t*Bu), (1)

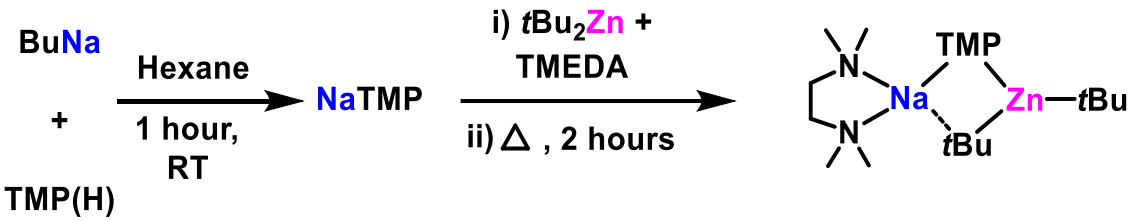

This compound was synthesised on a 4 mmol scale, using the described method in the referenced article.[73] Typical yield – 1.145 g, 63%

Synthesis of $Na_4(TMP)_4Zn_4(tBu)_4(C_5H_3)_2Fe$, (2)

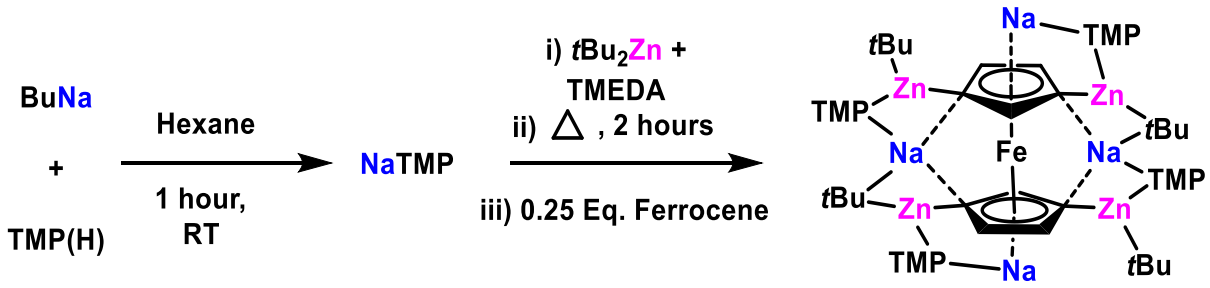

This compound was synthesised on a 0.5 mmol scale, using the described method in the referenced article.[110] Typical yield – 0.463 g, 70%

Synthesis of $Na_4(TMP)_4Zn_4(tBu)_2(CH_2Ph)_2[(C_5H_3)_2Fe]$ (3)

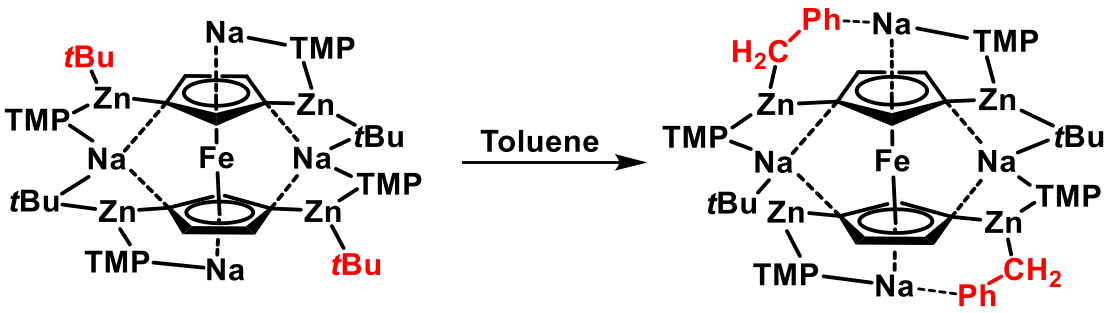

To a Schlenk flask was added *n*BuNa (0.16 g, 2 mmol). This Schlenk flask was then removed from the glovebox and hexane (15 ml) was added. The contents were allowed to stir for ten minutes before the addition of TMP(H) (0.34 ml, 2 mmol) was made. This resulted in the formation of a white suspension, which was left to stir for one hour. To the white suspension was added tBu_2Zn (2 ml of a 1M solution in hexane, 2 mmol), which was quickly followed by the addition of ferrocene (0.09 g, 0.5 mmol). The contents of the flask were then left to stir for two hours, which resulted in the formation of a red suspension.

The hexane was then removed *in vacuo* and the remaining contents were then dissolved in toluene (4 ml) before being placed in the freezer (-33°C). This resulted in the precipitation of a red solid. The resulting red solid was then filtered, dried *in vacuo* and isolated within the glovebox. Typical yield – 0.249 g, 36%

Synthesis of [(pyr)$_5$Na(μ-pyr)Zn(pyr)(*t*Bu)]$_\infty$, (4)

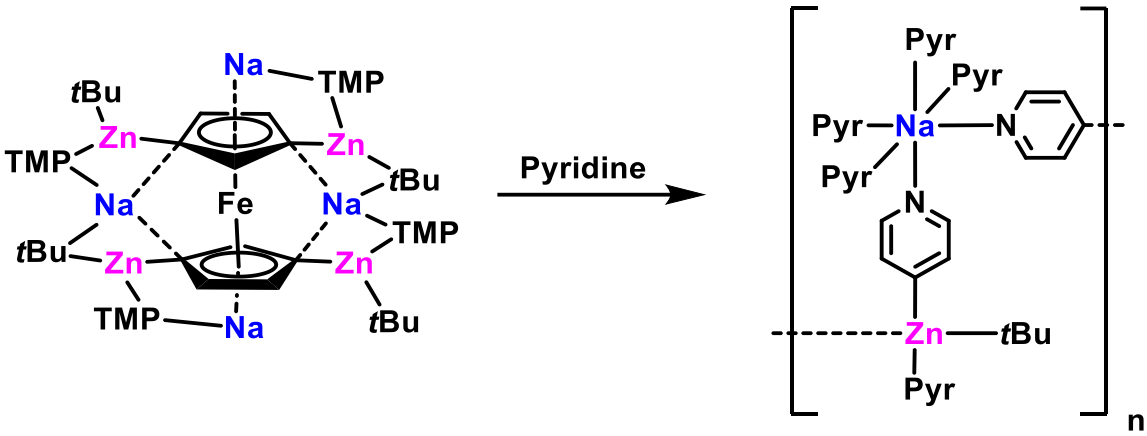

Complex **2** was prepared as above. The hexane was then removed *in vacuo* and the remaining contents were then dissolved in pyridine (4 ml) before being placed in the fridge (4°C). The resulting crystalline material was then filtered and collected. The crystals were then dried *in vacuo* and isolated within the glovebox. Typical yield – 0.128 g, 9%

Synthesis of TMEDA·Na(μ-TMP)(μ-C$_5$H$_4$)$_2$Fe(C$_5$H$_5$)Zn(*t*Bu), (5)

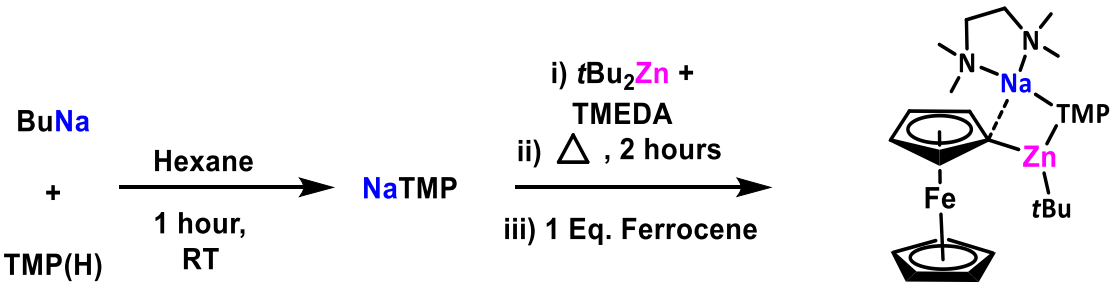

This compound was synthesised on a 0.5 mmol scale, using the described method in the referenced article.[110] Typical yield – 0.540 g (No absolute yield due to presence of small amount of dizincated compound **6**)

Synthesis of [TMEDA·Na(*μ*-TMP)Zn(*t*Bu)]$_2$(C$_5$H$_4$)$_2$Fe, (6)

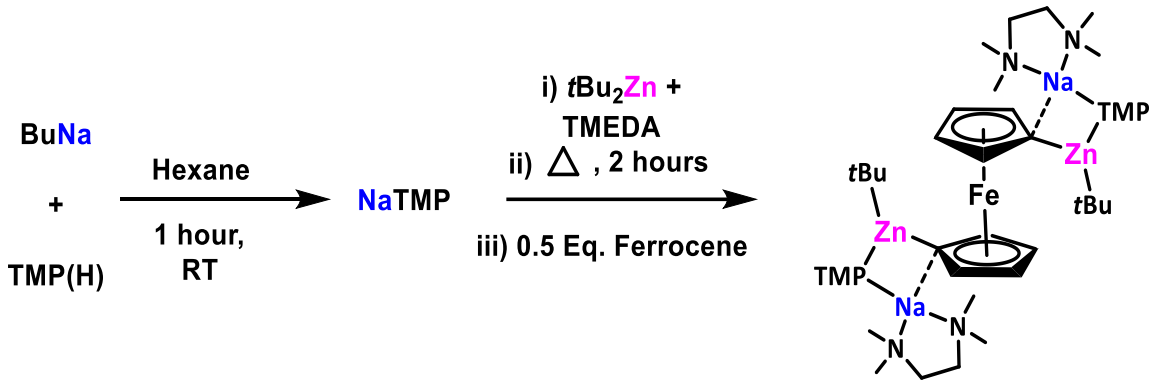

This compound was synthesised on a 0.5 mmol scale, using the described method in the referenced article.[110] Typical yield – 0.504 g (No absolute yield due to presence of monozincated compound)

Synthesis of [TMEDA·Na(*μ*-TMP)Zn(*t*Bu)]$_2$(C$_5$H$_4$)$_2$Fe·C$_7$H$_8$, (6')

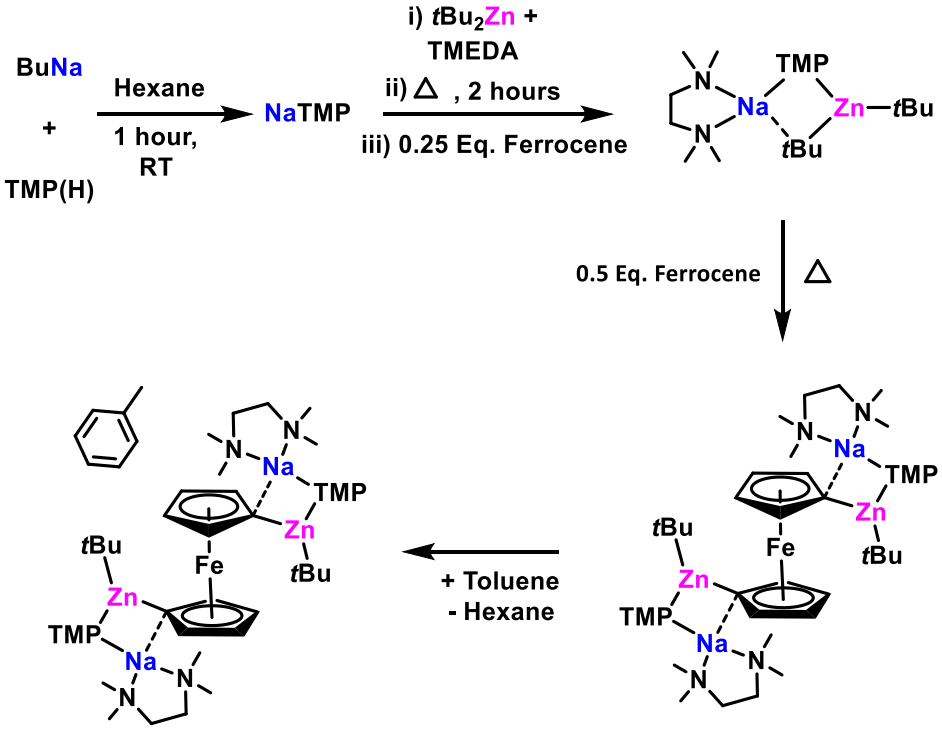

To a Schlenk flask was added *n*BuNa (0.16 g, 2 mmol). This Schlenk was then removed from the glovebox and hexane (15 ml) was added. The contents were

allowed to stir for ten minutes before the addition of TMP(H) (0.34 ml, 2 mmol) was made. This resulted in the formation of a white suspension, which was left to stir for one hour. To the white suspension was added *t*Bu_2Zn (2 ml of a 1M solution in hexane, 2 mmol), which was quickly followed by the addition of TMEDA (0.30 ml, 2 mmol). The contents were then heated gently until a yellow solution is observed. Upon cooling to ambient temperature, ferrocene (0.18 g, 2 mmol) was then added. The contents of the flask were then left to stir for two hours, which resulted in the formation of an orange suspension. The hexane was removed *in vacuo* and replaced with toluene (10 ml). The contents of the flask were then left to stir overnight whilst being refluxed, resulting in a red solution. The Schlenk flask was then placed in the freezer (-33°C) and a crop of red crystals were obtained. Typical yield – 0.221 g, 20%.

Iodine quench of *in-situ* generated 4

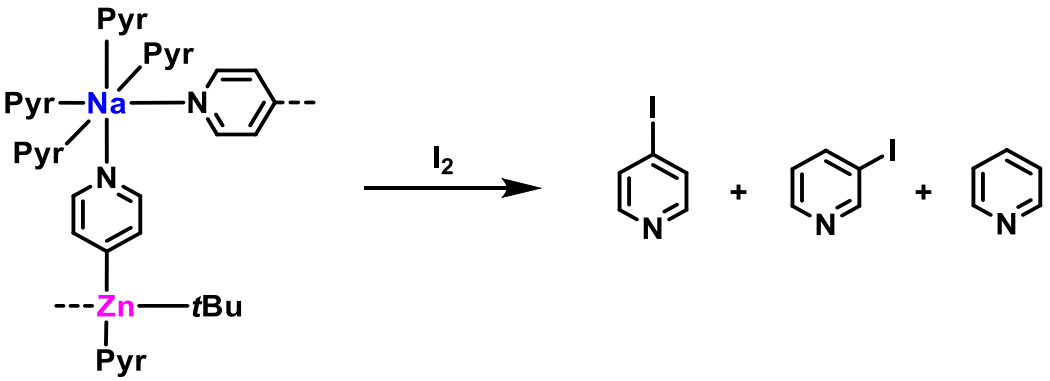

To a Schlenk flask was added *n*BuNa (0.16 g, 2 mmol). This Schlenk flask was then removed from the glovebox and hexane (15 ml) was added. The contents were allowed to stir for ten minutes before the addition of TMP(H) (0.34 ml, 2 mmol) was made. This resulted in the formation of a white suspension, which was left to stir for one hour. To the white suspension was added *t*Bu_2Zn (2 ml of a 1M solution in hexane, 2 mmol), which was quickly followed by the addition of ferrocene (0.09 g, 0.5 mmol). The contents of the flask were then left to stir for two hours, which resulted in the formation of a red suspension. The hexane

was then removed *in vacuo* and the remaining contents were then dissolved in pyridine (4 ml) before being placed in the fridge (4°C).

To a separate Schlenk flask was added I_2 (6.345 g, 25 mmol), followed by the addition of THF (25 ml) to make a 1M solution. Both flasks were then cooled to sub-ambient temperatures (-78°C) and the metallated compound was transferred to the I_2 solution via canula. The reaction was then left to stir overnight and rise to ambient temperature slowly.

At this point, NH_4Cl was added to the Schlenk flask, followed by the addition of $Na_2S_2O_3$ (30 ml). The resulting mixture was then extracted using EtOAc (3 x 10 ml). The organic layer was then dried over $MgSO_4$ and filtered, before the solvent was removed in *vacuo*.

Deuterium quench of $Na_4(TMP)_4Zn_4(tBu)_4(C_5H_3)_2Fe$

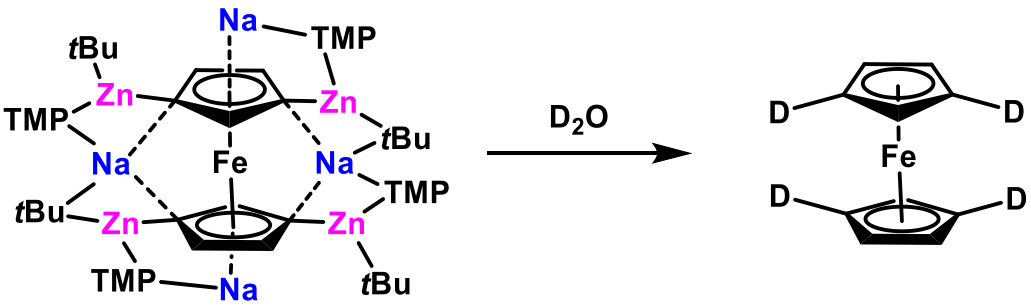

To a Schlenk flask was added $Na_4(TMP)_4Zn_4(tBu)_4(C_5H_3)_2Fe$ (0.026 g, 0.02 mmol), followed by the addition of D_2O (1 ml). This was allowed to stir for 10 minutes resulting in the formation of an orange suspension. To this suspension was added C_6D_6 (1 ml) and this resulted in the dissolution of the suspension, giving two distinct layers.

The organic layer was then removed from the Schlenk flask via needle and syringe. It was then washed with D_2O (3 x 1 ml) before being dried over $MgSO_4$ and then filtered. ^1H NMR (C_6D_6) – δ 4.01 (10H, s, Fer. CH), 1.51 (2H, m, TMP CH_2), 1.25 (4H, t, TMP CH_2), 1.05 ppm (12H, s, CH_3)

CO_2 quench of $Na_4(TMP)_4Zn_4(tBu)_4(C_5H_3)_2Fe$

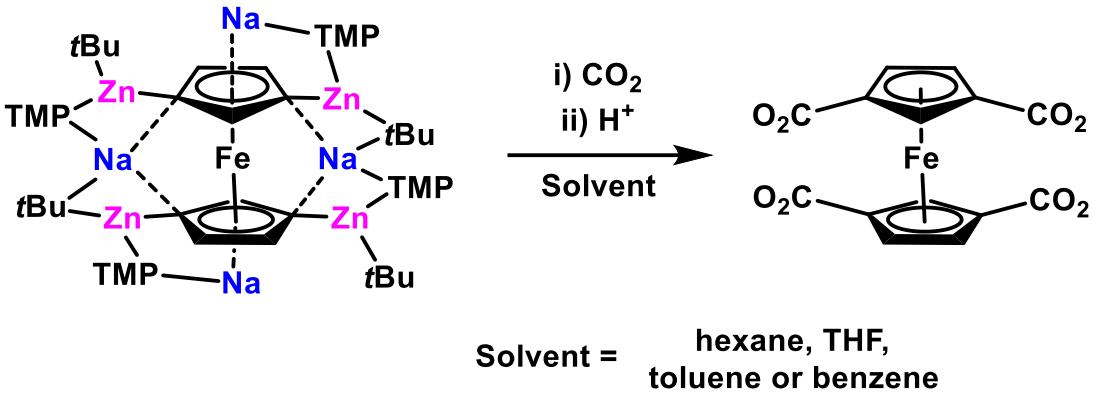

Solvent = hexane, THF, toluene or benzene

Complex **2** was prepared as described previously.

To a Schlenk flask was added $Na_4(TMP)_4Zn_4(tBu)_4(C_5H_3)_2Fe$ (0.136 g, 0.1 mmol), followed by the addition of solvent (10 ml). The contents of the flask were then left to stir for two hours, which resulted in the formation of a red suspension. To a separate Schlenk flask was added CO_2 pellets. A canula was then inserted to join the two flasks and the CO_2 was allowed to bubble through the red suspension for an hour. A noticeable colour change could be observed, going from red to orange.

At this point, 1M HCl (20 ml) was added to the flask. This resulted in the formation of two layers. DCM (10 ml) was then added to the flask and the two layers were then separated. The organic layer was washed with water (3 x 10 ml). The organic layer was then dried over $MgSO_4$ before being filtered. The hexane and DCM were then removed *in vacuo*, yielding an orange powder.

Synthesis of *i*Bu_2Zn

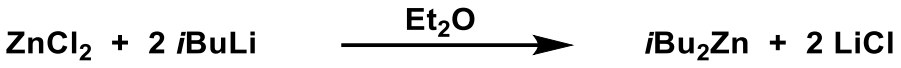

To a suspension of anhydrous $ZnCl_2$ (5.45 g, 40 mmol) in 80 ml of diethyl ether, at 0 ^oC, *i*BuLi (47.1 ml of a 1.7 M heptane solution, 80 mmol) was then added. The resulting suspension was then protected from light to prevent decomposition by covering the Schlenk tube with a black bag and allowing to stir for 2-3 hours. The suspension was then filtered through celite and glass wool to remove the formed LiCl. The colourless solution is then placed under vacuum to remove the diethyl ether and the cloudy liquid was then isolated and characterised (typical yield: 6.842 g, 95%).

^1H NMR (C_6D_6) – δ 2.03 (1H, m, $^3J_{H,H}$ = 37.79 Hz, CH), 0.99 (6H, d, $^3J_{H,H}$ = 7.00 Hz, CH_3), 0.40 ppm (2H, d, $^3J_{H,H}$ = 6.53 Hz, CH_2)

^{13}C NMR (C_6D_6) – δ 31.9 (CH), 28.7 (CH_3), 27.2 (CH_2)

Synthesis of *i*Bu_2Zn·TMEDA

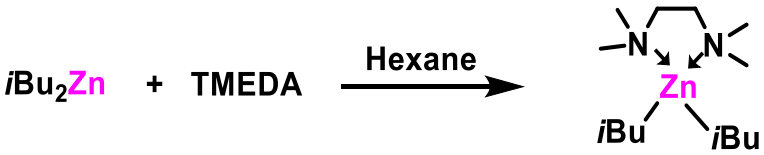

To a Schlenk flask was added *i*Bu_2Zn (0.180 g, 1 mmol), followed by the addition of hexane (4 ml). This was allowed to stir for 10 minutes resulting in the formation of a clear solution. At this point, TMEDA (0.15 ml, 1 mmol) was added slowly, resulting in the formation of a slightly yellow tinged solution. This was allowed to stir for 15 minutes before being placed into the freezer (-33 ^oC). After a period of 1 week had passed with no signs of crystallisation being observed, the solvent was then removed *in vacuo* where a yellow coloured oil was isolated. Yield – 0.078 g, 27%

^{1}H NMR (C_6D_6) – δ 2.39 (2H, m, $^{3}J_{H,H}$ = 39.83 Hz, *i*Bu_2Zn CH), 1.88 (6H, s, TMEDA CH_3), 1.74 (2H, s, TMEDA CH_2), 1.37 (12H, d, $^{3}J_{H,H}$ = 6.21 Hz, *i*Bu_2Zn CH_3), 0.27 ppm (2H, d, $^{3}J_{H,H}$ = 15.79 Hz, *i*Bu_2Zn CH)

Synthesis of *i*Bu_2Zn·PMDETA

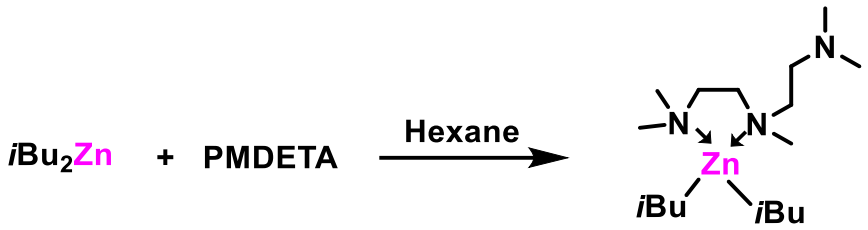

To a Schlenk flask was added *i*Bu_2Zn (0.180 g, 1 mmol), followed by the addition of hexane (4 ml). This was allowed to stir for 10 minutes before resulting in the formation of a clear solution. At this point, PMDETA (0.21 ml, 1 mmol) was added slowly, resulting in the formation of a slightly yellow tinged solution. This was allowed to stir for 15 minutes before being placed into the freezer (-33 ^{o}C). After a period of 1 week had passed with no signs of crystallisation being observed, the solvent was then removed *in vacuo* where a yellow coloured oil was isolated. Yield - 0.224 g, 64%

^{1}H NMR (C_6D_6) – δ 2.38 (2H, m, $^{3}J_{H,H}$ = 26.51 Hz *i*Bu_2Zn CH), 2.33 (4H, t, $^{3}J_{H,H}$ = 12.38 Hz, PMDETA CH_2), 2.20 (4H, t, $^{3}J_{H,H}$ = 13.03 Hz, PMDETA CH_2), 2.08 (3H, s, PMDETA CH_3), 2.04 (12H, s, PMDETA CH_3), 1.40 (12H, d, $^{3}J_{H,H}$ = 6.45 Hz, *i*Bu_2Zn CH_3), 0.30 ppm (2H, d, $^{3}J_{H,H}$ = 7.32 Hz, *i*Bu_2Zn CH)

Synthesis of *i*Bu$_2$Zn·Me$_6$TREN

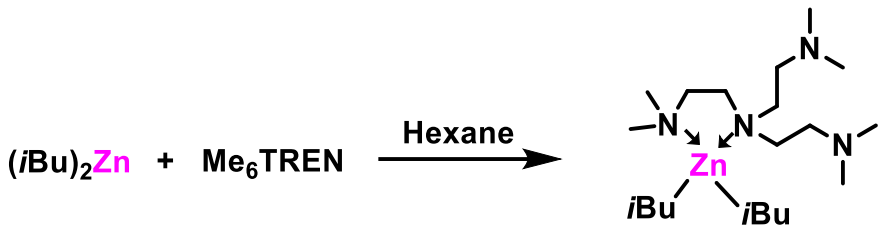

To a Schlenk flask was added *i*Bu$_2$Zn (0.180 g, 1 mmol), followed by the addition of hexane (4 ml). This was allowed to stir for 10 minutes resulting in the formation of a clear solution. At this point, Me$_6$TREN (0.26 ml, 1 mmol) was added slowly, resulting in the formation of a slightly yellow tinged solution. This was allowed to stir for 15 minutes before being placed into the freezer (-33 ^{o}C). After a period of 1 week had passed with no signs of crystallisation being observed, the solvent was then removed *in vacuo* before a yellow coloured oil was isolated. Yield - 0.290 g, 71%

^{1}H NMR (C_6D_6) – δ 2.55 (6H, t, $^{3}J_{H,H}$ = 26.25 Hz, Me$_6$TREN CH_2), 2.34 (2H, m, $^{3}J_{H,H}$ = 13.03 Hz, *i*Bu$_2$Zn CH), 2.23 (6H, t, $^{3}J_{H,H}$ = 13.39 Hz, Me$_6$TREN CH_2), 2.03 (18H, s, Me$_6$TREN CH_3), 1.34 (12H, d, $^{3}J_{H,H}$ = 15.72 Hz, *i*Bu$_2$Zn CH_3), 0.33 ppm (4H, d, $^{3}J_{H,H}$ = 7.29 Hz, *i*Bu$_2$Zn CH_2)

Synthesis of TMEDA·Na(*μ*-TMP)(*μ*-*i*Bu)Zn(*i*Bu), (7)

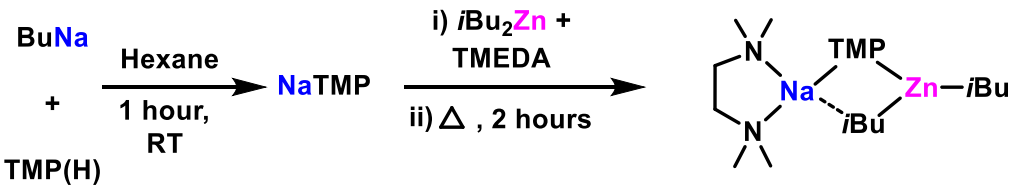

This complex was prepared on a 2 mmol scale by a modification of the literature procedure for the preparation of **1** with the exception that *i*Bu$_2$Zn was used instead of *t*Bu$_2$Zn. Yield 0.516 g, 56%.

^{1}H NMR (C_6D_6) – δ 2.65 (2H, m, $^{3}J_{H,H}$ = 25.62 Hz, *i*Bu_2Zn CH), 2.04 (2H, m, TMP CH_2), 1.86 (4H, t, TMP CH_2), 1.75 (12H, s, TMEDA CH_3), 1.63 (4H, s, TMEDA CH_2), 1.48 (6H, s, TMP CH_3), 1.46 (12H, d, $^{3}J_{H,H}$ = 6.54 Hz, *i*Bu_2Zn CH_3), 1.11 (6H, s, TMP CH_3), 0.34 ppm (4H, d, $^{3}J_{H,H}$ = 7.05 Hz, *i*Bu_2Zn CH_2)

6.2 Preparation of Chapter 3 Compounds

Synthesis of $Me_6TREN{\cdot}K(PhCH_2)Zn(HMDS)_2$, 13

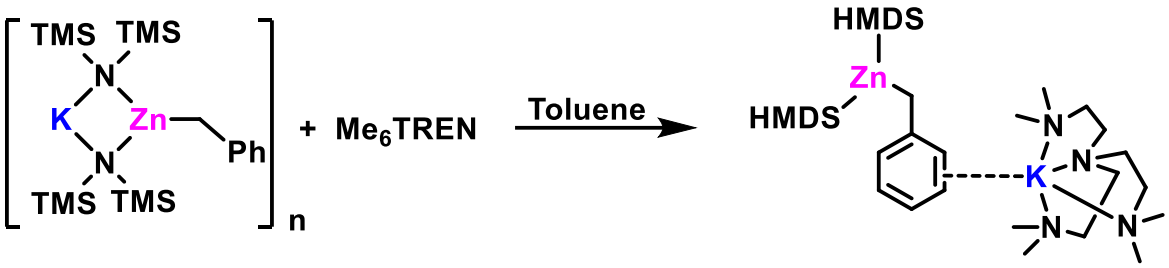

To a Schlenk flask was added [{$KZn(HMDS)_2(CH_2Ph)$}$_\infty$] (0.476 g, 1 mmol) and toluene (4 ml) was added. The contents were allowed to stir for 10 minutes, which resulted in the formation of a white suspension, before the addition of Me_6TREN (0.26 ml, 1 mmol), which led to the alteration from a white suspension to a dark (almost black) solution. The flask was then placed in the freezer (-33 ^{O}C). A crystalline material was then observed in the flask. Accurate yield unavailable as of now, due to efforts made at X-ray being detrimental to mass obtained. Typical yield – 0.382 g, 50%

^{1}H NMR (C_6D_6) – δ 7.22 (2H, d, $^{3}J_{H,H}$ = 8.27 Hz, C_6H_5 CH), 6.92 (2H, t, $^{3}J_{H,H}$ = 15.12 Hz, C_6H_5 CH), 6.48 (1H, t, $^{3}J_{H,H}$ = 14.17 Hz, C_6H_5 CH), 2.04 (6H, t, $^{3}J_{H,H}$ = 14.22 Hz, Me_6TREN CH_2), 1.95 (6H, t, $^{3}J_{H,H}$ = 13.95 Hz, Me_6TREN CH_2), 1.88 (18H, s, Me_6TREN CH_3), 1.68 (2H, s, benzyl CH_2), 0.62 ppm (36H, s, HMDS CH_3)

Synthesis of diphenylmethyl potassium

This compound was synthesised on a 10 mmol scale, using the described method in the referenced article.[118] Typical yield – 1.832 g, 89 %

6.3 Preparation of Common Starting Materials

6.3.1 Preparation of *n*BuNa [130]

To a suspension of NaO*t*Bu (3.84 g, 40 mmol) in 50 ml of *n*-hexane, *n*BuLi (25 ml of a 1.6 M heptane solution, 40 mmol) was added slowly at 0 °C. The white suspension was left to stir overnight before filtering to collect the white solid (typical yield: 2.4 g, 75%).

6.3.2 Preparation of *t*Bu$_2$Zn [73]

To a suspension of anhydrous $ZnCl_2$ (5.45 g, 40 mmol) in 80 ml of diethyl ether, at 0 °C, *t*BuLi (48 ml of a 1.7 M heptane solution, 80 mmol) was then added. The resulting suspension was then protected from light to prevent decomposition by covering the Schlenk tube with a black bag and allowing to stir for 2-3 hours. The suspension was then filtered through celite and glass wool. The colourless solution was then placed under vacuum to remove the majority of the diethyl ether. The remaining solution was then transferred to sublimation apparatus via cannula. The remaining solvent was then removed under vacuum. Chilled *i*propanol (-30 °C) was then placed in the cool finger and continually maintained whilst the *t*Bu$_2$Zn is subliming. Once complete the sublimation apparatus is transferred to a glovebox to collect the purified *t*Bu$_2$Zn (typical yield: 5.0 g, 69%). This is then stored in a Schlenk tube as a 1M hexane solution at -30 °C.

6.3.3 Preparation of $(HMDS)_2Zn$ [131]

To a Schlenk flask was added Et_2O (80 ml), followed by the addition of HMDS(H) (6.3 ml, 30 mmol). This was allowed to stir for 5 minutes before the flask was cooled to 0 ^oC, for the addition of *n*BuLi (18.75 ml, 30 mmol. This mixture was allowed to warm up to room temperature and then stir for one hour. At this point, anhydrous $ZnCl_2$ (2.04 g, 15 mmol) was added to the flask at 0 ^oC and the mixture was allowed to stir at room temperature, overnight.

Volatiles were then removed *in vacuo* and hexane (15 ml) was added. The mixture was then filtered through celite and glass wool, to remove the LiCl and then the filtrate was reduced *in vacuo*. The resulting brown liquid was then distilled and the light brown liquid was identified to be the desired $Zn(HMDS)_2$ (typical yield: 4.490 g, 78%).

6.3.4 Preparation of Me_6TREN [132]

To a solution of tris(2-aminoethyl)amine (TREN) (5 ml, 19.9 mmol) in acetic acid (135 ml) in a 1 L round bottom flask, was added formaldehyde (49 ml, 660 mmol). To this was added acetonitrile (500 ml) and this was allowed to stir for one hour. At this point, the round bottom flask was cooled to 0 ^oC and sodium borohydride (10 g, 13.4 mmol) was added slowly. After the full addition of the sodium borohydride, the contents of the flask were left to stir for forty-eight hours.

All solvents were then removed *in vacuo* and the resulting residue was made strongly basic using 3 M sodium hydroxide. A separation was then performed and the organic layer was extracted using dichloromethane (DCM). Any residual water was removed by the use of magnesium sulphate and this was then filtered off, before the removal of the DCM. This resulted in the mixture of a solid present with an oil. This mixture was then dissolved in pentane and filtered. The pentane was then removed *in vacuo* to yield the desired Me_6TREN (typical yield: 6.058 g, 79%).

Chapter 7 References

1 W. Schlenk and J. Holtz, *Ber. Dtsch. Chem. Ges.*, 1917, **50**, 262–274.

2 T. T. Tidwell, *Angew. Chem. Int. Ed.*, 2001, **40**, 331–337.

3 V. H. Gessner, C. Däschlein and C. Strohmann, *Chem. Eur. J.*, 2009, **15**, 3320–3334.

4 G. Wu and M. Huang, *Chem. Rev.*, 2006, **106**, 2596–2616.

5 M. Pérez, M. Fañanás-Mastral, P. H. Bos, A. Rudolph, S. R. Harutyunyan and B. L. Feringa, *Nat. Chem.*, 2011, **3**, 377–381.

6 J. Clayden, in *Organolithiums: Selectivity for Synthesis*, Pergamon, Elsevier Science, 2002, vol. 23.

7 M. Schlosser, in *Organometallics in Synthesis*, Wiley: Chichester, 2nd edn., 2002.

8 D. B. Collum, *Acc. Chem. Res.*, 1993, **26**, 227–234.

9 E. Karl and D. Stalke, in *Lithium Compounds in Organic Synthesis*, Wiley-VCH, 2014, pp. 1–32.

10 M. Weiner, G. Vogel and R. West, *Inorg. Chem.*, 1962, **1**, 654–658.

11 H. L. Lewis and T. L. Brown, *J. Am. Chem. Soc.*, 1970, **92**, 4664–4670.

12 H. Dietrich, *Acta Crystallogr.*, 1963, **16**, 681–689.

13 H. Dietrich, *J. Organomet. Chem.*, 1981, **205**, 291–299.

14 T. Kottke and D. Stalke, *Angew. Chem. Int. Ed.*, 1993, **32**, 580–582.

15 R. E. Dinnebier, U. Behrens and F. Olbrich, *J. Am. Chem. Soc.*, 1998, **120**, 1430–1433.

16 E. Weiss and E. A. C. Lucken, *J. Organomet. Chem.*, 1964, **2**, 197–205.

17 M. A. Nichols and P. G. Williard, *J. Am. Chem. Soc.*, 1993, **115**, 1568–1572.

18 J. A. Garden, D. R. Armstrong, W. Clegg, J. García-Alvarez, E. Hevia, A. R. Kennedy, R. E. Mulvey, S. D. Robertson and L. Russo, *Organometallics*, 2013, **32**, 5481–5490.

19 D. W. Slocum, T. K. Reinscheld, C. B. White, M. D. Timmons, P. A.

Shelton, M. G. Slocum, R. D. Sandlin, E. G. Holland, D. Kusmic, J. A. Jennings, K. C. Tekin, Q. Nguyen, S. J. Bush, J. M. Keller and P. E. Whitley, *Organometallics*, 2013, **32**, 1674–1686.

20 D. R. Armstrong, P. García-Álvarez, A. R. Kennedy, R. E. Mulvey and S. D. Robertson, *Chem. Eur. J.*, 2011, **17**, 6725–6730.

21 T. Niklas, D. Stalke and M. John, *Chem. Commun.*, 2015, **51**, 1275–1277.

22 S. Bachmann, B. Gernert and D. Stalke, *Chem. Commun.*, 2016, **52**, 12861–12864.

23 M. Schlosser, *Angew. Chem. Int. Ed.*, 1964, **3**, 287–306.

24 L. Orzechowski, G. Jansen and S. Harder, *Angew. Chem. Int. Ed.*, 2009, **48**, 3825–3829.

25 J. Barluenga, F. J. Fañanás and M. Yus, *J. Org. Chem.*, 1981, **46**, 1281–1283.

26 P. Beak and V. Snieckus, *Acc. Chem. Res.*, 1982, **15**, 306–312.

27 V. Snieckus, *Chem. Rev.*, 1990, **90**, 879–933.

28 M. C. Whisler, S. MacNeil, V. Snieckus and P. Beak, *Angew. Chem. Int. Ed.*, 2004, **43**, 2206–2225.

29 H. Gilman and R. L. Bebb, *J. Am. Chem. Soc.*, 1939, **61**, 109–112.

30 G. Wittig and G. Fuhrmann, *Ber. Dtsch. Chem. Ges.*, 1940, **73**, 1197–1218.

31 D. E. Applequist and D. F. O. Brien, *J. Am. Chem. Soc.*, 1963, **85**, 743–748.

32 P. Knochel and G. A. Molander, in *Comprehensive Organic Synthesis*, Elsevier, 2nd edn., 2014.

33 R. E. Mulvey and S. D. Robertson, *Angew. Chem. Int. Ed.*, 2013, **52**, 11470–11487.

34 R. E. Mulvey, *Chem. Soc. Rev.*, 1998, **27**, 339–346.

35 R. E. Mulvey, *Chem. Soc. Rev.*, 1991, **20**, 167–209.

36 K. Gregory, P. v. R. Schleyer and R. Snaith, *Adv. Inorg. Chem.*, 1991, **37**, 47–142.

37 W. S. Rees, O. Just, H. Schumann and R. Weimann, *Polyhedron*, 1998, **17**, 1001–1004.

38 T. Güngör, F. Marsais and G. Queguiner, *J. Organomet. Chem.*, 1981, **215**, 139–150.

39 F. Marsais, P. Granger and G. Quéguiner, *J. Org. Chem.*, 1981, **46**, 4494–4497.

40 H. Gilman and B. J. Gaj, *J. Org. Chem.*, 1957, **22**, 1165–1168.

41 S. C. Honeycutt, *J. Organomet. Chem.*, 1971, **29**, 1–5.

42 R. B. Bates, L. M. Kroposki and D. E. Potter, *J. Org. Chem.*, 1972, **37**, 560–562.

43 R. E. Mulvey and S. D. Robertson, *Angew. Chem. Int. Ed.*, 2013, **52**, 11470–11487.

44 D. Mootz, A. Zinnius and B. Böttcher, *Angew. Chem Int. Ed.*, 1969, **8**, 378–379.

45 L. M. Engelhardt, B. S. Jolly, P. C. Junk, C. L. Raston, B. W. Skelton and A. H. White, *Aust. J. Chem.*, 1986, **39**, 1337–1345.

46 K. W. Henderson, A. E. Dorigo, Q. Y. Liu and P. G. Williard, *J. Am. Chem. Soc.*, 1997, **119**, 11855–11863.

47 B. Gehrhus, P. H. Hitchcock, A. R. Kennedy, M. F. Lappert, R. E. Mulvey and P. J. a Rodger, *J. Organomet. Chem.*, 1999, **587**, 88–92.

48 D. R. Armstrong, P. García-ÃÁlvarez, A. R. Kennedy, R. E. Mulvey and S. D. Robertson, *Chem. Eur. J.*, 2011, **17**, 6725–6730.

49 D. R. Armstrong, D. V. Graham, A. R. Kennedy, R. E. Mulvey and C. T. O'Hara, *Chem. Eur. J.*, 2008, **14**, 8025–8034.

50 B. Y. Kimura and T. L. Brown, *J. Organomet. Chem.*, 1971, **26**, 57–67.

51 M. Schlosser, *Pure Appl. Chem.*, 1988, **60**, 1627–1634.

52 M. Schlosser, *J. Organomet. Chem.*, 1967, **8**, 9–16.

53 L. Lochmann, J. Pospíšil and D. Lím, *Tetrahedron Lett.*, 1966, **7**, 257–262.

54 M. Schlosser, H. C. Jung and S. Takagishi, *Tetrahedron*, 1990, **46**, 5633–5648.

55 W. Clegg, S. T. Liddle, A. M. Drummond, R. E. Mulvey and A. Robertson, *Chem. Commun.*, 1999, 1569–1570.

56 M. Marsch, K. Harms, L. Lochmann and G. Boche, *Angew. Chem. Int. Ed.*, 1990, **29**, 308–309.

57 A. R. Kennedy, J. G. MacLellan and R. E. Mulvey, *Angew. Chem. Int. Ed.*, 2001, **40**, 3245–3247.

58 C. Unkelbach, D. F. O'Shea and C. Strohmann, *Angew. Chem. Int. Ed.*, 2014, **53**, 553–556.

59 P. Benrath, M. Kaiser, T. Limbach, M. Mondeshki and J. Klett, *Angew. Chem. Int. Ed.*, 2016, **55**, 10886–10889.

60 P. Fleming and D. F. O'shea, *J. Am. Chem. Soc.*, 2011, **133**, 1698–1701.

61 A. Manvar, P. Fleming and D. F. O'Shea, *J. Org. Chem.*, 2015, **80**, 8727–8738.

62 J. Wanklyn, *Proc. R. Soc.*, 1858, 341–345.

63 G. Wittig, F. J. Meyer and G. Lange, *Justus Liebigs Ann. Chem.*, 1951, **571**, 167–201.

64 R. E. Mulvey and S. D. Robertson, *Top. Organomet. Chem.*, 2014, **47**, 129–158.

65 L. Pauling, in *General Chemistry An Introduction to Descriptive Chemistry and Modern Chemical Theory*, ed. C. W. H. Freeman, San Francisco, 1947.

66 C. D. Broaddus, *J. Org. Chem.*, 1970, **35**, 10–15.

67 A. J. Chalk and T. J. Hoogeboom, *J. Organomet. Chem.*, 1968, **11**, 615–618.

68 C. D. Broaddus, *J. Am. Chem. Soc.*, 1966, **88**, 4174–4178.

69 P. C. Andrikopoulos, D. R. Armstrong, D. V. Graham, E. Hevia, A. R. Kennedy, R. E. Mulvey, C. T. O'Hara and C. Talmard, *Angew. Chem. Int. Ed.*, 2005, **44**, 3459–3462.

70 A. R. Kennedy, J. Klett, R. E. Mulvey and D. S. Wright, *Science*, 2009, **706**, 706–709.

71 J. Francos, A. R. Kennedy and C. T. O'Hara, *Dalton. Trans.*, 2016, **45**, 6222–6233.

72 D. R. Armstrong, V. L. Blair, W. Clegg, S. H. Dale, J. Garcia-Alvarez, G. W. Honeyman, E. Hevia, R. E. Mulvey and L. Russo, *J. Am. Chem. Soc.*, 2010, **132**, 9480–9487.

73 P. C. Andrikopoulos, D. R. Armstrong, H. R. L. Barley, W. Clegg, S. H. Dale, E. Hevia, G. W. Honeyman, A. R. Kennedy and R. E. Mulvey, *J. Am. Chem. Soc.*, 2005, **127**, 6184–6185.

74 D. R. Armstrong, W. Clegg, S. H. Dale, D. V Graham, E. Hevia, L. M. Hogg, G. W. Honeyman, A. R. Kennedy and R. E. Mulvey, *Chem. Commun.*, 2007, 598–600.

75 R. E. Mulvey, *Dalton. Trans.*, 2013, **42**, 6676–6693.

76 R. E. Mulvey, *Acc. Chem. Res.*, 2009, **42**, 743–755.

77 R. E. Mulvey and S. D. Robertson, *Top. Organomet. Chem.*, 2013, **45**, 103–139.

78 M. Hatano, T. Matsumura and K. Ishihara, *Org. Lett.*, 2005, **7**, 573–576.

79 E. Weiss and R. Wolfrum, *Ber. Dtsch. Chem. Ges.*, 1968, **101**, 35–40.

80 E. Weiss, *Angew. Chem. Int. Ed.*, 1993, **32**, 1501–1523.

81 Y. Kondo, M. Shilai, M. Uchiyama and T. Sakamoto, *J. Am. Chem. Soc.*, 1999, **121**, 3539–3540.

82 M. Uchiyama, Y. Matsumoto, D. Nobuto, T. Furuyama, K. Yamaguchi and K. Morokuma, *J. Am. Chem. Soc.*, 2006, **128**, 8748–8750.

83 W. Clegg, S. H. Dale, E. Hevia, G. W. Honeyman and R. E. Mulvey, *Angew. Chem. Int. Ed.*, 2006, **45**, 2370–2374.

84 W. Clegg, S. H. Dale, E. Hevia, L. M. Hogg, G. W. Honeyman, R. E. Mulvey and C. T. O'Hara, *Angew. Chem. Int. Ed.*, 2006, **45**, 6548–6550.

85 W. Clegg, S. H. Dale, R. W. Harrington, E. Hevia, G. W. Honeyman and R. E. Mulvey, *Angew. Chem. Int. Ed.*, 2006, **45**, 2374–2377.

86 B. Conway, E. Hevia, A. R. Kennedy and R. E. Mulvey, *Chem.*

Commun., 2007, 2864–2866.

87 L. Balloch, A. R. Kennedy, R. E. Mulvey, T. Rantanen, S. D. Robertson and V. Snieckus, *Organometallics*, 2011, **30**, 145–152.

88 E. Hevia, G. W. Honeyman, A. R. Kennedy and R. E. Mulvey, *J. Am. Chem. Soc.*, 2005, **127**, 13106–13107.

89 J. J. Crawford, B. J. Fleming, A. R. Kennedy, J. Klett, C. T. O'Hara and S. A. Orr, *Chem. Commun.*, 2011, **47**, 3772–3774.

90 D. R. Armstrong, L. Balloch, J. J. Crawford, B. J. Fleming, L. M. Hogg, A. R. Kennedy, J. Klett, R. E. Mulvey, C. T. O'Hara, S. A. Orr and S. D. Robertson, *Chem. Commun.*, 2012, **48**, 1541–1543.

91 R. E. Mulvey, V. L. Blair, W. Clegg, A. R. Kennedy, J. Klett and L. Russo, *Nat. Chem.*, 2010, **2**, 588–591.

92 D. Nobuto and M. Uchiyama, *J. Org. Chem.*, 2008, **73**, 1117–1120.

93 D. R. Armstrong, L. Balloch, E. Hevia, A. R. Kennedy, R. E. Mulvey, C. T. O'Hara and S. D. Robertson, *Beilstein J. Org. Chem.*, 2011, **7**, 1234–1248.

94 A. J. Martínez-Martínez, A. R. Kennedy, R. E. Mulvey and C. T. O'Hara, *Science*, 2014, **346**, 834–837.

95 M. Uchiyama, H. Naka, Y. Matsumoto and T. Ohwada, *J. Am. Chem. Soc.*, 2004, **126**, 10526–10527.

96 H. Naka, M. Uchiyama, Y. Matsumoto, A. E. H. Wheatley, M. McPartlin, J. V. Morey and Y. Kondo, *J. Am. Chem. Soc.*, 2007, **129**, 1921–1930.

97 H. Naka, J. V. Morey, J. Haywood, D. J. Eisler, M. McPartlin, F. García, H. Kudo, Y. Kondo, M. Uchiyama and A. E. H. Wheatley, *J. Am. Chem. Soc.*, 2008, **130**, 16193–16200.

98 R. E. Mulvey, D. R. Armstrong, B. Conway, E. Crosbie, A. R. Kennedy and S. D. Robertson, *Inorg. Chem.*, 2011, **50**, 12241–12251.

99 D. R. Armstrong, E. Crosbie, E. Hevia, R. E. Mulvey, D. L. Ramsay and S. D. Robertson, *Chem. Sci.*, 2013, **5**, 3031–3045.

100 M. Uzelac, A. R. Kennedy, E. Hevia and R. E. Mulvey, *Angew. Chem. Int. Ed.*, 2016, **55**, 13147–13150.

101 D. R. Armstrong, E. Brammer, T. Cadenbach, E. Hevia and A. R. Kennedy, *Organometallics*, 2013, **32**, 480–489.

102 R. A. Benkeser, D. Goggin and G. Schroll, *J. Am. Chem. Soc.*, 1954, **76**, 4025–4026.

103 F. Rebiere, O. Samuel and H. B. Kagan, *Tetrahedron Lett.*, 1990, **31**, 3121–3124.

104 I. R. Butler, W. R. Cullen, J. Ni and S. J. Rettig, *Organometallics*, 1985, **4**, 2196–2201.

105 M. Walczak, K. Walczak, R. Mink, G. Stucky and M. D. Rausch, *J. Am. Chem. Soc.*, 1978, **100**, 6382–6388.

106 A. F. Halasa and D. P. Tate, *J. Organomet. Chem.*, 1970, **24**, 769–773.

107 A. G. Osborne and R. H. Whiteley, *J. Organomet. Chem.*, 1978, **162**, 79–81.

108 W. Clegg, K. W. Henderson, A. R. Kennedy, R. E. Mulvey, C. T. O'Hara, R. B. Rowlings and D. M. Tooke, *Angew. Chem Int. Ed.*, 2001, **40**, 3902–3905.

109 P. C. Andrikopoulos, D. R. Armstrong, W. Clegg, C. J. Gilfillan, E. Hevia, A. R. Kennedy, R. E. Mulvey, C. T. O'Hara, J. A. Parkinson and D. M. Tooke, *J. Am. Chem. Soc.*, 2004, **126**, 11612–11620.

110 W. Clegg, E. Crosbie, S. H. Dale-Black, E. Hevia, G. W. Honeyman, A. R. Kennedy, R. E. Mulvey, D. L. Ramsay and S. D. Robertson, *Organometallics*, 2015, **34**, 2580–2589.

111 D. R. Armstrong, W. Clegg, E. Hevia, G. W. Honeyman, A. R. Kennedy, R. McLellan, S. A. Orr, J. A. Parkinson, D. L. Ramsay, S. D. Robertson and R. E. Mulvey, *Unpublished Results*.

112 B. Jennewein, S. Kimpel, D. Thalheim and J. Klett, *Chem. Eur. J.*, 2018, **24**, 7605–7609.

113 T. Cadenbach, E. Hevia, A. R. Kennedy, R. E. Mulvey, J. A. Pickrell and S. D. Robertson, *Dalton Trans.*, 2012, **41**, 10141–10144.

114 J. A. Garden, A. R. Kennedy, R. E. Mulvey and S. D. Robertson, *Chem. Commun.*, 2012, **48**, 5265–5267.

115 Y.-F. Liu, D.-D. Zhai, X.-Y. Zhang and B.-T. Guan, *Angew. Chem. Int. Ed.*, 2018, **57**, 8245–8249.

116 D. O. Khristolyubov, D. M. Lyubov, A. V. Cherkasov, G. K. Fukin, A. S. Shavyrin and A. A. Trifonov, *Organometallics*, 2018, **37**, 1627–1634.

117 H. Viebrock, U. Behrens and E. Weiss, *Ber. Dtsch. Chem. Ges.*, 1994, **127**, 1399–1400.

118 H. Schumann, D. M. M. Freckmann and S. Dechert, *Organometallics*, 2006, **25**, 2696–2699.

119 B. Fischer, J. Boersma, G. Van Koten, W. J. J. Smeets and A. L. Spek, *Organometallics*, 1989, **8**, 667–672.

120 W. Clegg, G. C. Forbes, A. R. Kennedy, R. E. Mulvey and S. T. Liddle, *Chem. Commun.*, 2003, 406–407.

121 M. G. Davidson, D. Garcia-Vivo, A. R. Kennedy, R. E. Mulvey and S. D. Robertson, *Chem. Eur. J.*, 2011, **17**, 3364–3369.

122 G. Ferguson and M. Parvez, *Acta Crystallogr.*, 1979, **640**, 2207–2210.

123 A. G. Blackman, *Polyhedron*, 2005, **24**, 1–39.

124 C. Slugovc, C. Gemel, J. Y. Shen, D. Doberer, R. Schmid, K. Kirchner and K. Mereiter, *Monatsh. Chem.*, 1999, **130**, 363–375.

125 D. R. Armstrong, M. G. Davidson, D. Garcia-Vivo, A. R. Kennedy, R. E. Mulvey and S. D. Robertson, *Inorg. Chem.*, 2013, **52**, 12023–12032.

126 D. F. Shriver and M. A. Drezdon, in *The Manipulation of Air-Sensitive Compounds*, ed. N. Y. Wiley, 2nd edn., 1986.

127 G. M. Sheldrick, *Acta Crystallogr. Sect. A Found. Crystallogr.*, 2008, **64**, 112–122.

128 G. M. Sheldrick, *Acta Crystallogr. Sect. C Struct. Chem.*, 2015, **71**, 3–8.

129 O. V Dolomanov, L. J. Bourhis, R. J. Gildea, J. A. K. Howard and H. Puschmann, *J. Appl. Crystallogr.*, 2009, **42**, 339–341.

130 C. Schade, W. Bauer and P. v. R. Schleyer, *J. Organomet. Chem.*, 1985, **295**, 25–28.

131 H. Bürger, W. Sawodny and U. Wannagat, *J. Organomet. Chem.*,

1965, **3**, 113–120.

132 G. J. P. Britovsek, J. England and A. J. P. White, *Inorg. Chem.*, 2005, **44**, 8125–8134.